COO-1569-14

ION TRAPPING IN ROTATING SUPERFLUID LIQUID HELIUM UNDER PRESSURE

A THESIS

SUBMITTED TO THE FACULTY OF THE GRADUATE SCHOOL

OF THE UNIVERSITY OF MINNESOTA

By

WILLIAM PORTER PRATT, JR.

IN PARTIAL FULFILLMENT OF THE REQUIREMENTS

FOR THE DEGREE OF

DOCTOR OF PHILOSOPHY

DECEMBER, 1967

DISCLAIMER

ION TRAPPING IN ROTATING SUPERFLUID LIQUID HELIUM UNDER PRESSURE

A THESIS

SUBMITTED TO THE FACULTY OF THE GRADUATE SCHOOL

OF THE UNIVERSITY OF MINNESOTA

By

WILLIAM PORTER PRATT, JR.

IN PARTIAL FULFILLMENT OF THE REQUIREMENTS

FOR THE DEGREE OF

DOCTOR OF PHILOSOPHY

DECEMBER, 1967

ABSTRACT

ION TRAPPING IN ROTATING SUPERFLUID LIQUID HELIUM UNDER PRESSURE

Measurements of the lifetime of negative ions trapped in rotating superfluid liquid helium have been made in the range 10 to 1000 seconds as a function of temperature and applied electric field at the saturated vapor pressure of the liquid. Measurements of the lifetime of trapped negative ions have also been made in the range 20 to 400 seconds as a function of temperature and pressure from the vaporization pressure to the solidification pressure of liquid helium.

The experiment involves observing the amount of trapped charge released by the liquid upon cessation of rotation. A reproducible amount of charge is initially trapped in the liquid rotating at 6 rad sec^{-1} and held in rotation for a variable waiting period before release. The decay in the amount of the trapped charge in the rotating liquid has been observed by this method to be exponential in time.

The data are interpreted in terms of models which have recently been proposed in the literature for ion-trapping in the rotating liquid. There are two models involved: First, the negative ion is assumed to be an electron contained in a hollow cavity in the liquid of approximately 20 Å radius. Of particular interest is the prediction of this "bubble model" that the size of the negative ion decreases as pressure is applied to the liquid. Second, the rotating liquid is thought to consist

of a uniform array of singly quantized vortices. The ions are assumed to be trapped by hydrodynamic forces on these vortex lines in the rotating liquid and to escape from these vortex lines by thermal activation.

The activation energy for escape of an ion from a vortex line can be determined from the temperature dependence of the lifetime of the trapped ion. The radius of the ion can in turn be determined from this activation energy. At saturated vapor pressure such analysis of the data indicates that the radius of the negative ion is between 18.9 Å and 20.6 Å. As the pressure is raised from saturated vapor pressure to 24 atm, the radius of the negative ion decreases by 38%. This decrease compares favorably with the prediction of a simple form of the "bubble model" that the radius of the negative ion decreases by 35% over the same pressure range. The dependence of the lifetime of the trapped negative ion upon the applied electric field can also be understood in terms of these models.

In addition, studies have been made in which trapped ions are used to probe certain properties of the rotating state of the liquid. Such studies include observations of the growth and decay of vorticity in the superfluid brought about by the starting and stopping of rotation of the vessel containing the liquid helium.

Over the full range of pressures and temperatures covered in this experiment, no positive ion trapping was observed.

CONTENTS

CONTENTS (continued)

LIST OF FIGURES

I. INTRODUCTION

1. Two-Fluid Model of Superfluid Liquid Helium

Helium (He^4) becomes a liquid at 4.18°K under one atmosphere pressure.[1-5] The liquid state is thought to exist down to absolute zero as long as the pressure is kept less than 25 atmospheres. It is only by an application of pressures in excess of 25 atmospheres that helium solidifies. This behavior is a consequence of the large quantum-mechanical zero-point energy of the helium atoms and the weak interparticle forces between the atoms.

At T_λ=2.172°K, the so-called "lambda point", the liquid undergoes a phase transition. This phase transition is characterized by a logarithmic singularity in the specific heat of the liquid. Below this transition temperature the liquid exhibits rather strange "superfluid" properties, which appear to be quantum-mechanical effects on a macroscopic scale. For example, below T_λ the liquid will flow readily through very small channels even if above T_λ the liquid flows very slowly through these channels. Below T_λ the liquid also has an anomalously large ability to conduct heat while above T_λ the liquid conducts heat about as well as air at room temperature.

In 1938 London suggested that the transition of liquid helium from a normal liquid to a "super" liquid at T_λ might be

related to the condensation in momentum space of an ideal Bose-Einstein gas.[6] For the ideal Bose gas the condensate consists of atoms in their ground states.

Around 1940 in a series of papers Tisza developed a "two-fluid model" to describe the observed mechanical superfluid effects.[7] In this model the liquid is considered to be a combination of two interpenetrating fluids, a normal fluid and a superfluid. Each component is assigned a separate velocity and density: $\vec{v}_n$ and ρ_n for the normal fluid, and $\vec{v}_s$ and ρ_s for the superfluid. The total density of the fluid and the densities of the two components are related by the expression $\rho = \rho_n + \rho_s$. Similarly, the total mass current $\vec{j}$ is given by the relationship $\vec{j} = \rho_n\vec{v}_n + \rho_s\vec{v}_s$. The superfluid flows at small velocities with no dissipation and carries no entropy. The normal fluid is viscous and carries all of the entropy. The densities ρ_n and ρ_s are temperature dependent, and at T_λ the fluid is entirely normal fluid while at T=0°K the liquid is entirely superfluid.

Landau developed a quantum-mechanical theory of superfluid helium which reflects the two-fluid model.[8] In this theory the liquid is in its ground state at T=0°K. For temperatures slightly above 0°K the liquid is considered to be weakly excited. The weakly excited states of the liquid are regarded as being sets of separate elementary excitations of the liquid as a whole. These elementary excitations form

a gas of "quasi-particles" moving through the liquid, each having a definite energy and momentum. These quasi-particles can collide with each other and with the walls of the container giving the appearance that there is a second fluid present in the background fluid. The normal fluid is identified with this gas of excitations; the superfluid, with the background fluid in which these excitations move.

Landau, in an attempt to treat the density and the mass current of the liquid at 0°K as quantum-mechanical operators, arrived at the conclusion that the curl of the superfluid velocity field is zero (curl $\vec{v}_s = 0$) for the lowest state of the fluid. This led him to postulate the existence of a localized excitation (curl $\vec{v}_s \neq 0$) of the liquid which subsequently became known as a "roton". The other excitation postulated was a low energy soundlike excitation, the "phonon". Landau was able to make certain plausibility arguments to obtain a form for the dispersion curve of these two excitations. From the form of these dispersion curves and from considerations of the conservation of momentum and energy in the creation of these excitations by superfluid flow along a boundary, Landau was able to account for the ability of the superfluid to flow without dissipation below a certain critical velocity.

2. Superfluid Flow

In 1949 Onsager proposed a further restriction upon the

superfluid motion: the circulation of the superfluid should be quantized according to the relation

$$\oint \vec{v}_s \, d\vec{l} = n \frac{h}{m} \tag{1}$$

where n is an integer, h is Planck's constant, and m is the mass of the helium atom.[9] Feynman later presented a more thorough discussion of this quantization condition.[10] Both Onsager and Feynman suggested by analogy with the wave mechanics of single particles that the superfluid velocity could be expressed in the form

$$\vec{v}_s = \frac{\hbar}{m} \text{ grad } \phi \tag{2}$$

where ϕ is the phase of a single-valued complex quantum-mechanical wave function characterizing the flow of the liquid. Since $\vec{v}_s$ is a gradient of a scalar, Landau's criterion that curl $\vec{v}_s = 0$ is automatically satisfied. For the wave function to be single valued the phase, ϕ, of the wave function must change by integral multiples of 2π around any closed path. This condition implies quantization of circulation as stated by Equation (1).

The condition curl $\vec{v}_s = 0$ requires that $n = 0$ in Equation (1) if the closed path of integration does not enclose an internal boundary of the liquid. However, around boundaries which make the liquid multiply connected n need not be zero. Vinen performed an experiment to check this quantization of

circulation condition around an internal boundary in liquid helium.[11] The apparatus consisted of a fine wire stretched in the liquid. When plucked, this wire had degenerate circularly polarized modes of vibration. With circulation present around the wire the degeneracy was lifted. The resulting frequency splitting was proportional to the circulation. There was some evidence for stable circulations at n = 0 and n = 1. More recently, Whitmore and Zimmermann have repeated the Vinen wire experiment and have observed n = 0,1,2, and 3 levels.[12]

Also proposed in the Onsager-Feynman theory is the existence of line singularities in the superfluid velocity field which make the liquid effectively multiply connected. These so-called "vortex lines" would have quantized circulation. A straight line vortex would have the following cylindrically symmetric velocity field

$$\vec{v}_s(r) = \frac{nh}{2\pi mr}\,\hat{\theta} \tag{3}$$

expressed in terms of cylindrical coordinates r, θ, z with the z axis coinciding with the vortex core. A vortex line either will end on itself in the form of a ring or will end at the boundaries of the fluid.

The kinetic energy density E near a straight line vortex is given by the expression

$$E = \frac{n^2}{8\pi^2}\left[\frac{h}{m}\right]^2 \frac{\rho_s(r)}{r^2} \tag{4}$$

The superfluid density must go to zero as r approaches zero in order that the kinetic energy density not become singular. The problem of vortices in the condensate of a dilute interacting Bose gas has been considered by Fetter.[13] A good approximation to the density of the condensate n(r) near a vortex line found by Fetter is

$$n(r) = n(\infty) \frac{r^2}{r^2 + d^2} \tag{5}$$

where "d" is a parameter characterizing the size of the "core" of the vortex line. Not well understood at the present time is the relationship between the condensate of this Bose gas model of liquid helium and the superfluid density of the two-fluid model. However, for the analyses presented in this thesis the superfluid density is assumed to obey Equation (5) near a vortex line as a first approximation.

Except for the quantization condition the velocity fields of these vortex lines are identical to the velocity fields of vortex lines in the ideal fluids of classical hydrodynamics. Thus vortex lines in superfluid liquid helium will have the same dynamical properties as vortex lines in ideal fluids. In particular, vortex lines in ideal fluids must move with the fluid if there are no forces acting on these lines. However, if there are forces acting on these vortex lines, these lines must drift relative to the fluid. In liquid helium such forces might arise from the scattering of the microscopic

excitations which comprise the normal fluid by the vortex lines and from the pinning of the ends of the vortex lines to the walls surrounding the fluid.

There is experimental evidence for quantized vortex rings (n = 1) in liquid helium at 0.3°K. Rayfield and Reif observed the creation of vortex rings by energetic ions in the liquid at these temperatures.[14] They observed the characteristic property of a classical vortex ring: the energy of the ring is very nearly inversely proportional to its propagation velocity. Using ions in the same temperature region, Gamota and Sanders have observed another property of a classical ring vortex: the energy of the ring is very nearly proportional to the size of the ring.[15]

Feynman's discussion of vortex rings also sheds some light on the problem of critical velocities for superfluid flow in fine channels. From Landau's theory the superfluid should be able to flow without dissipation up to 60 meters/second. However, critical velocities are observed at velocities several orders of magnitude smaller. Feynman pointed out that vortex line and ring creation at the walls of a channel could produce a much lower critical velocity. His estimates are in better agreement with the observed critical velocities.

There is other evidence for the existence of vortex lines in liquid helium. In particular the rotating state of the superfluid is thought to involve vortex lines. This topic

will be considered in the next section of this chapter.

In summary, the flow properties of superfluid liquid helium can be described in terms of a two-fluid model. Landau's excitation theory leads naturally to the two-fluid model and accounts well for the thermodynamic properties of liquid helium near T=0°K. The Onsager-Feynman theory requires that the circulation of the superfluid be quantized and adds another excitation of the liquid, the vortex line.

3. Rotating Liquid Helium

Landau considered in his theory the rotating state of the liquid. He pointed out that the condition curl $\vec{v}_s = 0$ implies that in a rotating cylindrically-symmetric simply-connected container, the superfluid must remain at rest. Osborne in 1950 tested this prediction by observing the meniscus of the rotating liquid.[16] If the superfluid were not participating in the rotation, then only the normal fluid could contribute to the parabolic meniscus expected for a uniformly rotating liquid. The relevant equation is

$$h = \frac{\rho_n}{\rho} \frac{\omega_o^2 R^2}{2g} \tag{6}$$

where h is the depth of the meniscus, ρ_n the normal fluid density, ρ the total fluid density, ω_o the angular velocity, R the radius of the rotating bucket, and g the gravitational acceleration. The normal fluid density is temperature dependent. Then h, the depth of the meniscus, should be temperature

dependent also. Osborne found that the depth of the meniscus was not temperature dependent and thus that the whole liquid appeared to rotate like a solid body. This observation appeared to contradict Landau's prediction that the superfluid component would not rotate.

In 1955 Hall and Vinen propagated thermal waves called "second sound" in a rotating bucket of superfluid helium.[17] These thermal waves are propagating fluctuations in the relative densities of normal and superfluid components. These fluctuations are accompanied by counter motion of normal and superfluid components. They found that attenuation of the second sound waves increased when rotation was started. This attenuation was anisotropic, taking on its maximum value for waves propagated perpendicular to the axis of rotation. Attenuation of waves propagated parallel to the axis of rotation did not change with rotation. The fact that Hall and Vinen were able to see second sound propagating in the liquid meant that the rotation did not destroy the superfluid character of the liquid.

The Onsager-Feynman vortex-line model provided a description of how the superfluid component could appear to rotate as a solid body without losing its "superfluidity". In this model the velocity field of the superfluid component in steady rotation consists of an array of vortex lines with one quantum unit of circulation for each line. The axes of

these vortex lines are parallel to the axis of rotation. For a uniform dense array of vortex lines the macroscopic velocity field resembles that of solid body rotation.

Let us construct a circular closed line integral of the superfluid velocity in a plane perpendicular to the axis of the rotating liquid. Assume in steady-state rotation that the velocity field has cylindrical symmetry on the average. Then, we have the relation

$$\oint \vec{v}_s \cdot d\vec{l} = 2\pi r \, v_s(r) \tag{7}$$

where r is the radius of the circular path. Since curl $\vec{v}_s = 0$, everywhere except at the vortex cores, Stokes theorem states that the closed line integral executed in Equation (7) is equal to the sum of the circulations around each vortex line contained within this closed line integral. Since the array is uniform, we can define a uniform vortex line density (per unit area), N. Therefore,

$$\oint \vec{v}_s \cdot d\vec{l} = \frac{Nh\pi r^2}{m}. \tag{8}$$

Equations (7) and (8) combine to give

$$v_s(r) = \frac{Nhr}{2m} = \omega r \tag{9}$$

This is the velocity field of solid body rotation where

$$\omega = \frac{Nh}{2m}. \tag{10}$$

For rotating speeds relevant to the experiment discussed in this thesis, $\omega = 6$ radian sec^{-1} which implies $N = 10^4$ vortex-lines cm^{-2}.

Feynman showed for a bucket of 1 cm radius rotating at 1 radian sec^{-1} that the energy necessary to create this uniform array of vortex lines is only 2% higher than the energy of a rigidly rotating body. More recently Fetter has considered the case of an array of vortex lines in a rotating annulus.[18] He found in the limit of high rotation speeds where there is a dense array of vortex lines that the free energy of the rotating liquid was a minimum for a uniform array. Fetter has pointed out also that the array of vortex lines probably exists in the form of a stable triangular lattice.[19]

Hall and Vinen interpreted their second sound results in terms of the Feynman-Onsager theory. The vortex lines provide a "mutual friction" force between the superfluid and the normal fluid components which attenuates the second sound wave. The alignment of the vortices parallel to the axis of rotation will produce a larger attenuation of the second sound waves propagating perpendicular to the axis of rotation.

Not well understood at the present time is how the vorticity is created in the first place. It is assumed that when a bucket is set into rotation, vortex lines appear at the walls of the bucket and move into the liquid. During this build-up of vorticity, the normal fluid is accelerating and

applying forces to the vortices if they are moving relative to the normal fluid. There is evidence that the state of the liquid is quite turbulent during acceleration and deceleration of the liquid. Second sound attenuation experiments indicate that during approximately the first 50 seconds after sudden acceleration or deceleration of a rotating bucket containing liquid helium, the attenuation of second sound reaches a maximum and then decays to a value consistent with the final rotation speed.[20] This excess attenuation is observed for waves propagating perpendicular and parallel to the axis of rotation. This implies that the vortex lines are not, on the average, parallel to the axis of rotation during these transient periods. These vortex lines probably form a tangled array during acceleration and deceleration. The density of this tangled array appears to be higher during these periods of acceleration and deceleration than the density of the stable array of vortex lines eventually formed during steady rotation.

Observed also in various rotation experiments is a time for creation of a stable rotating state of the liquid which is on the order of 100 seconds.[21] The time required for the liquid to slow down is observed to be on the order of one fourth of the time necessary for the creation of the stable rotating state.

4. Ions in Liquid Helium

Both positive and negative ions in liquid helium have

been used as microscopic probes of some of the properties of superfluid liquid helium.[22-24] The mobility, defined as the drift velocity of the ions under an applied electric field divided by the strength of that field, of both species has been interpreted quite successfully in terms of the Landau excitation theory of liquid helium. What is of interest for the purposes of this thesis are the structures of the ions.

Atkins has proposed an electrostriction model for the structure of the positive ion.[25] In this model a He^+ or He_2^+ ion is surrounded by polarized helium atoms. The electrostriction pressure is calculated to produce a sphere of solid helium around the ion of approximately 6 Å radius. Atkins discusses the possibility of the ion growing larger if the external pressure is raised to a value close to the solidification pressure. Whether or not the ion will grow depends upon the assumed magnitude of the surface energy of the ion.

The so-called "bubble model" seems to account best for the observed behavior of the negative ion. This model was first proposed by Ferrel[26] and developed further by Kuper[27] and others.[28-31]. This model has recently received strong confirmation in an experiment performed by Northby and Sanders.[32] This model depends upon the phenomenon that in effect a repulsive "hard core" interaction exists between an electron and a neutral helium atom.[33] The wave function of the electron, then, has a nodal surface at each atom.

Because of the high zero-point energy involved in confining the electron to a cavity of atomic dimensions, it requires an energy of approximately one electron-volt to place the electron in undisturbed liquid helium.[34,35] With additional kinetic energy above 1 eV, the electron can propagate in the liquid as a quasi-free particle. However, it proves to be energetically favorable for a small bubble devoid of helium atoms to form around the electron. The bubble will expand until the surface-tension pressure of the bubble and the pressure externally applied to the liquid overcome the zero-point pressure of the confined electron. An energy of 0.2 eV is required to introduce the electron into liquid helium in the bubble state.

Experiments conducted by Northby and Sanders consist of measuring the cross section for photo-ejection of an electron out of the bubble state into the quasi-free state. The radius at saturated vapor pressure determined from this experiment is 21.2 ± 0.5 Å.

Several bubble models have been proposed which give a negative ion radius ranging from 12 Å to 20 Å. Presented below is a very simple model.

Assume that the total free energy of the bubble plus the liquid is the following:

$$F_t = \frac{h^2}{2m}\left[\frac{\pi}{R}\right]^2 + \sigma 4\pi R^2 + P\frac{4\pi R^3}{3} . \qquad (11)$$

The first term is the zero-point energy of an electron confined to a bubble of radius R with an infinite potential wall at the surface of the bubble. The second term is the surface energy where σ is the surface tension. The third term is the work done against external pressure P in forming the bubble. At saturated vapor pressure and T=1.65°K in liquid helium $\sigma \cong 0.34$ ergs cm^{-2}.[36]

Minimizing F_t with respect to R,

$$\frac{\partial F_t}{\partial R} = 0, \tag{12}$$

we get R = 19.3 Å. This model predicts that the radius of the negative ion will decrease as the external pressure is increased.

A more complete model of the negative ion should include the following: First, forces due to electrostatic polarization by the electron of the helium atoms surrounding the bubble will tend to make the radius of the negative ion smaller than the radius calculated above. Second, since the well depth for the electron is not infinite but rather is approximately 1 eV, penetration of the wave function into the liquid must be taken into account. Third, the density of the liquid probably does not go to zero discontinuously at the surface of the bubble but rather goes to zero over some finite distance. Finally, the bulk surface tension is probably inapplicable to a bubble of atomic dimensions.

The effective mass of this bubble model ion is probably very nearly equal to its hydrodynamic mass. This hydrodynamic mass is associated with the energy of "backflow" of the fluid as the ion moves through the fluid. For a sphere, Lamb, ignoring viscosity effects, obtains[37]

$$M_{eff} = \frac{1}{2}(\text{volume of sphere})(\text{fluid density}).$$

At 1.6°K and saturated vapor pressure the model above yields the result

$$M_{eff} \cong 330\, M_{He}$$

where M_{He} is the mass of the helium atom.

5. Experiments Concerning Interaction of Ions and Vortex Lines

Careri *et al.* have performed experiments studying ions in rotating liquid helium above 1°K.[38] Under the condition of space-charge-limited current flow they observed that the negative ion current perpendicular to the axis of rotation in a cylindrical electrode system was attenuated when the apparatus was rotating. For a negative ion current parallel to the axis of rotation no attenuation was observed. No attenuation of the positive ion current was seen for either orientation of the current relative to the axis of rotation.

Careri *et al.* suggested that some of the electrons were trapped in the hollow cores of the vortex lines, the cross section being larger for electrons travelling perpendicular to the vortex lines. These trapped electrons would tend to reduce the applied electric field. A smaller applied electric

field in the region of the source of ions (ions were produced by alpha particle bombardment) would result in a reduced current.

More recently Donnelly and his students have conducted a series of experiments to measure the cross section for capture of an ion by a vortex line.[39-42] An ion beam was propagated across a rotating vessel perpendicular to the axis of rotation. The current in this beam was not space charge limited. They observed an attenuation of the negative ion current from the lowest temperature they could reach, 0.98°K, up to approximately 1.7°K. From these observations they were able to infer a cross section for capture of negative ions by vortices. These cross sections were generally on the order of 10^{-5}cm. Above 1.7°K no attenuation of the negative ion current was seen. No attenuation of the positive ion current was observed from 0.98 to 1.7°K.

Douglass has performed an experiment measuring the lifetime of trapped negative ions on vortex lines as a function of temperature at the saturated vapor pressure.[43] The measurement of the lifetime consisted of observing the exponential decay in time of a population of trapped charge. He observed that the lifetime rose from 1 second at 1.72°K to 1000 seconds at 1.59°K. No positive ion trapping was seen.

The previously mentioned vortex ring experiments should also be included here. Both positive and negative ion trapping on vortex rings was seen between 0.3 and 0.6°K.

In summary, negative ion trapping has been seen in the experimental regions covered, 0.3 to 0.6°K and 0.98 to 1.7°K. Positive ion trapping has been seen unambiguously only in the lower temperature region, 0.3 to 0.6°K.

6. Outline of Thesis: Experimental Measurements Made and Analyses Conducted

The present experiment was undertaken for the purpose of improving our understanding of the interaction between ions and vortex lines. The following measurements and analyses represent the accomplishments of this thesis project.

1. Measurement of the lifetime of negative ions trapped on vortex lines in rotating liquid helium at saturated vapor pressure as a function of temperature and applied electric field to an accuracy greater than the accuracy of the data of R. L. Douglass.
2. Measurement of the lifetime of trapped negative ions as a function of temperature for various pressures between the vaporization curve and the solidification curve.
3. Search for positive ion trapping at elevated pressures.
4. Use of negative ion trapping to probe some of the properties of the vortex line structure of rotating liquid helium.

The rest of the thesis, except for a chapter in which the experimental apparatus is discussed, is devoted to analyses of the measurements listed above. The measurements mentioned in

Item #1 are used to give an estimate of the radius of the negative ion at saturated vapor pressure. The dependence of the lifetime upon applied electric field at saturated vapor pressure is discussed. From the measurements contained in Item #2 a determination of the pressure dependence of the negative ion radius is made. These results are compared with the pressure dependence of the radius of the negative ion predicted by our simple bubble model. Observations included in Item #3 are used to place certain limitations on the radius of the positive ion. In connection with Item #4 the analysis includes observations based on ion behavior of the growth and decay of the vorticity in the superfluid brought about by the starting and stopping of rotation of the vessel containing the liquid helium.

II. INTERACTION OF IONS AND VORTEX LINES

1. Mechanism for Ion-Vortex Line Attraction

In this chapter a series of calculations will be presented concerning the trapping of an ion by a vortex line and the eventual escape of the ion from the vortex line. Such calculations are necessary for the analysis of the lifetime data.

Let us assume that a spherical ion in liquid helium places the following boundary conditions on the liquid: the superfluid density equals zero on the surface of the ion, and the superfluid velocity normal to the surface of the ion is zero.

As pointed out before, vortex lines in superfluid helium are in most respects identical to vortex lines of classical hydrodynamics. It is then most interesting that Sir William Thomson (Lord Kelvin) in 1873 suggested the existence of an attractive interaction between a classical vortex and a solid sphere in the liquid:[44]

> By taking an infinite straight line for the core a simple but very important example is afforded. In this case the undisturbed motion of the fluid is in circles having their centers in the core (or axis as we may now call it) and their planes perpendicular to it. As is well known, the velocity of irrotational revolution around a straight axis is inversely proportional to distance from the axis. Hence the potential function W for the force experienced by an infinitesimal solid sphere in the fluid is inversely as the square of the distance of its centre from the axis; and therefore the force is inversely as the cube of the distance, and is towards the nearest point of the axis...

We present below a calculation of the effective potential

energy of interaction at long range between a vortex line and a sphere satisfying the boundary conditions stated above. Our calculation is a modernization of the original calculation published by Thomson in 1873.

Assume that the vortex line is fixed along the axis of a cylindrical vessel (C) of infinite length and large diameter as shown in Figure 1. Let ϕ be the velocity potential for this vortex when sphere Σ is not present. The velocity potential is defined by the following: $\vec{v} = -\nabla\phi$ where $\vec{v}$ is the velocity of the fluid. For incompressible flow ϕ satisfies the equation $\nabla^2\phi = 0$. Because of the vortex, the velocity field is singular at the vortex line and the velocity potential is not single valued. However, a cylindrical barrier σ of infinite length and small diameter whose axis coincides with the vortex line may be placed in the fluid to remove the singularity in the velocity field. Also, barrier σ' may be placed in the fluid between barrier σ and vessel C to make ϕ single valued. From Lamb,[45] Green's theorem for multiply connected regions is used to obtain the following expression for the kinetic energy T of the fluid

$$2T = -\rho_s \kappa \iint_{\sigma'} \frac{\partial\phi}{\partial n}\, dS \qquad (13)$$

where the integral is taken over one side of σ' and $\frac{\partial\phi}{\partial n}$ is the derivative of ϕ normal to σ' taken in the same direction as "dS" in Figure 1. κ is the circulation around the vortex; the

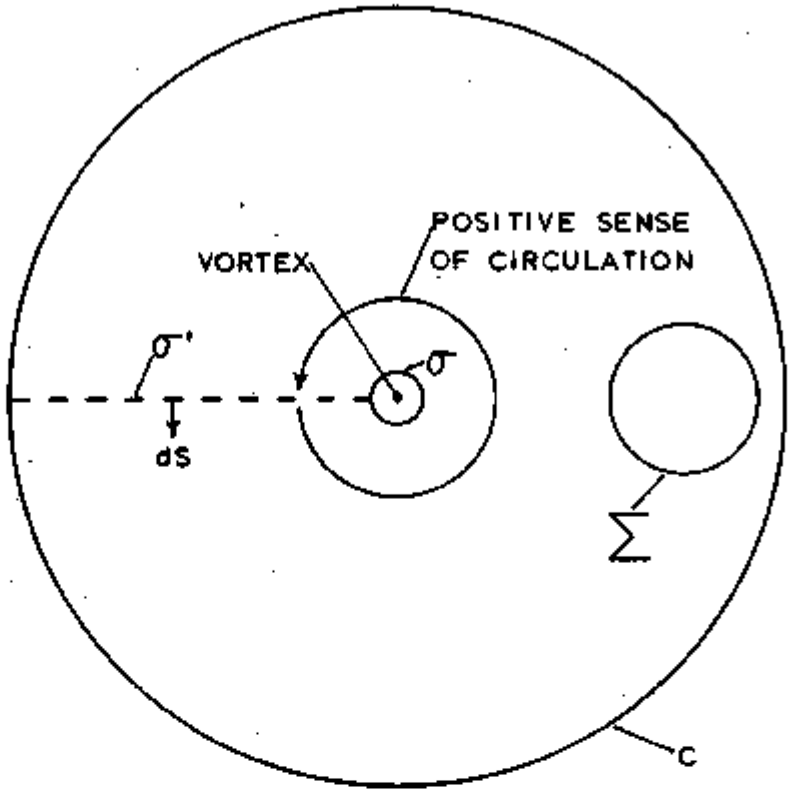

Figure 1: Vortex Line and Sphere in a Cylindrical Vessel

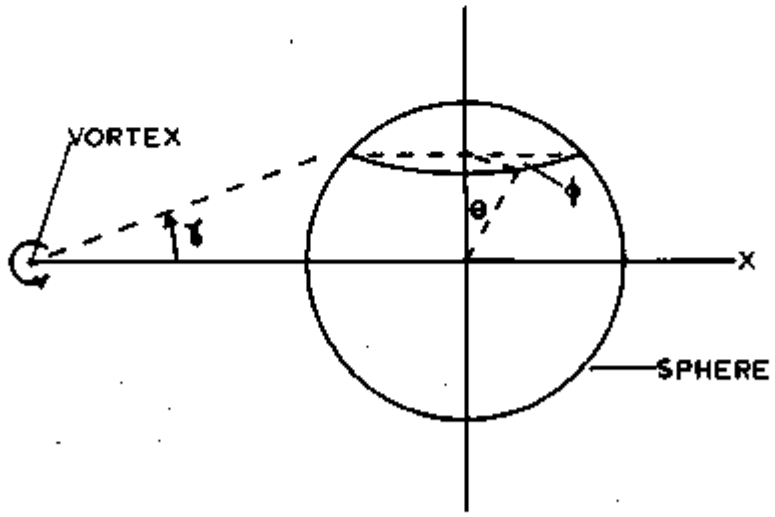

Figure 2: Coordinate System for Velocity Potentials

positive sense of κ is shown in Figure 1. Now place sphere Σ in the fluid. Let ϕ_t be the new velocity potential. Again we have $\nabla^2\phi_t = 0$. We also require the derivative of this new velocity potential normal to sphere Σ to be zero,

$$\left.\frac{\partial\phi_t}{\partial n}\right|_{\substack{\text{on}\\ \Sigma}} = 0. \tag{14}$$

Again using Green's theorem, we get

$$2T_t = -\rho_s\kappa\iint_{\sigma'}\frac{\partial\phi_t}{\partial n}\,dS \tag{15}$$

where T_t is the new kinetic energy of flow. Also by Green's theorem for ϕ_t and ϕ we have

$$\kappa\iint_{\sigma'}\frac{\partial\phi_t}{\partial n}\,dS = \iint_{\Sigma}\phi_t\,\frac{\partial\phi}{\partial n}\,dS + \kappa\iint_{\sigma'}\frac{\partial\phi}{\partial n}\,dS. \tag{16}$$

Therefore, the effective potential energy of interaction U between sphere Σ and the vortex line is given by the expression

$$U = T_t - T = -\frac{1}{2}\rho_s\iint_{\Sigma}\phi_t\,\frac{\partial\phi}{\partial n}\,dS \tag{17}$$

where dS and the normal derivative are taken in the direction of the "outward normal" to sphere Σ. We now pass to the limit in which the diameter of vessel C approaches infinity. Equation (17) remains unchanged.

Expressed in terms of cylindrical coordinates based on the vortex we have $\phi = -\frac{\kappa\gamma}{2\pi}$ (see Figure 2). Let us expand ϕ in spherical harmonics about x, the position of the center of the

sphere. For r<x we have

$$\Phi(r,\theta,\phi) = \sum_{\ell=0}^{\infty} \sum_{m=-\ell}^{m=+\ell} C_{\ell m}\, Y_{\ell m}(\theta,\phi) \left[\frac{r}{R}\right]^{\ell} \tag{18}$$

where R is the radius of the sphere, r is the distance between the center of the sphere and a field point, and

$$C_{\ell m} = \iint \sin\theta \; d\theta \; d\phi \; Y^{*}_{\ell m}(\theta,\phi) \; \Phi(R,\theta,\phi). \tag{19}$$

Let $\Psi = \Phi_t - \Phi$. We expand Ψ in spherical harmonics and obtain

$$\Psi(r,\theta,\phi) = \sum_{\ell=0}^{\infty} \sum_{m=-\ell}^{m=+\ell} Y_{\ell m}(\theta,\phi) \; B_{\ell m} \left[\frac{R}{r}\right]^{\ell+1} . \tag{20}$$

Using the boundary condition expressed in Equation (14), we get

$$\Phi_t(R,\theta,\phi) = \sum_{\ell=1}^{\infty} \sum_{m=-\ell}^{m=+\ell} \frac{2\ell + 1}{\ell + 1} C_{\ell m} \; Y_{\ell m}(\theta,\phi). \tag{21}$$

Making use of the orthogonality relations of the spherical harmonics, we obtain

$$U(x) = -\frac{1}{2}\rho_s R \sum_{\ell=1}^{\infty} \sum_{m=-\ell}^{m=+\ell} C_{\ell m}\, C_{\ell -m} (-1)^m \frac{\ell(2\ell + 1)}{\ell + 1} . \tag{22}$$

It can be seen that

$$\Phi(R,\theta,\phi) = -\frac{\kappa}{2\pi} \arctan\left[\frac{R\cos\theta}{x + R\sin\theta\cos\phi}\right]. \tag{23}$$

The $C_{\ell m}$ may be obtained by expanding this expression for

$\Phi(R,\theta,\phi)$ in powers of $\frac{R}{x}$ and by making use of Equation (19). Then to second order in $\frac{R}{x}$

$$U(x) = -\frac{1}{2}\rho_s\left[\frac{\kappa}{2\pi x}\right]^2\left[\frac{4\pi R^3}{3}\right]\left[\frac{3}{2}\right]\left[1 + \frac{4}{9}\left[\frac{R}{x}\right]^2 + 0\left[\frac{R}{x}\right]^4\right] \quad . \tag{24}$$

For $\frac{R}{x} << 1$, $U(x)$ is indeed inversely proportional to the square of the distance from the sphere to the vortex line. In the same limit we can write $U(x)$ in the form

$$U(x) = -\frac{3}{2}\rho_s\left[\begin{matrix}\text{vol. of}\\ \text{sphere}\end{matrix}\right]\frac{\left[\begin{matrix}\text{vel. at x}\\ \text{due to vortex}\end{matrix}\right]^2}{2} \quad . \tag{25}$$

In a recent paper Parks and Donnelly have estimated this attractive potential between a vortex line and a spherical ion.[46] They assumed that the introduction of an ion into the moving superfluid reduces the energy of the system by an amount equal to the superfluid kinetic energy contained in a volume of fluid equal to the volume of the ion. In the limit of large distances from the vortex line, this assumption would give

$$U(x) = -\rho_s\left[\begin{matrix}\text{vol. of}\\ \text{sphere}\end{matrix}\right]\frac{\left[\begin{matrix}\text{vel. at x}\\ \text{due to vortex}\end{matrix}\right]^2}{2} \tag{26}$$

Equations (25) and (26) differ by a factor of 3/2 because Parks and Donnelly did not consider in their estimation of this potential the energy associated with superfluid flow around the ion. However, in the limit that the ion is situated at $x = 0$, the calculation of Parks and Donnelly is correct and is reproduced below.

The lowest energy state of the ion-vortex system is represented in Figure 3. With the ion placed symmetrically on the vortex line, no distortion of the superfluid flow around the vortex occurs. The binding energy of the ion to the vortex line, then, is just the kinetic energy of flow removed by the ion. This change in kinetic energy is

$$U(x=0) = -\frac{1}{2}\int\int\int \rho_s v_s^2 dV \qquad (27)$$

where $v_s = \frac{\kappa}{2\pi r'}$, r' is the perpendicular distance from the vortex to the field point, and the integral is carried out over the volume of the ion. The superfluid density is assumed to go to zero in the core of the vortex line in the manner proposed by Fetter in Equation (5) (replace r by r' in this equation). The "healing length" d has been determined by Parks and Donnelly from the vortex ring experiments; their result is $d = 1.46 \pm 0.14$ Å. The solution to Equation (27) is

$$U(0) = 2\pi\rho_s\left[\frac{\kappa}{2\pi}\right]^2 R\left[1 - \left[1 + \frac{d^2}{R^2}\right]^{\frac{1}{2}} \sinh^{-1}\left[\frac{R}{d}\right]\right]. \qquad (28)$$

For a negative ion of 20 Å radius, we obtain $-\frac{U(0)}{k} \approx 60°K$; and for a positive ion of 6 Å radius, we have $-\frac{U(0)}{k} \approx 18°K$ where k is Boltzmann's constant.

Not taken into account so far is the healing length associated with the superfluid density going to zero at the surface of the ion. The effect of such a healing length is to make the effective volume of excluded superfluid flow

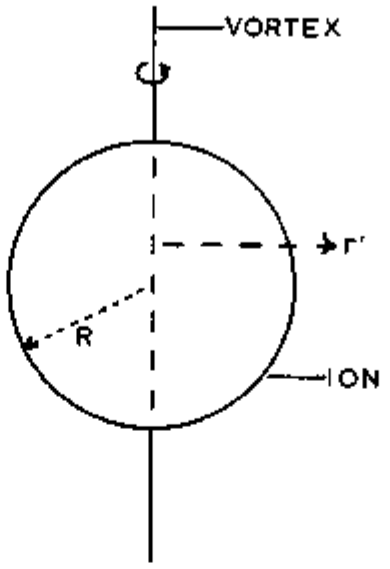

Figure 3: Representation of the Lowest Energy State of the Ion-Vortex System

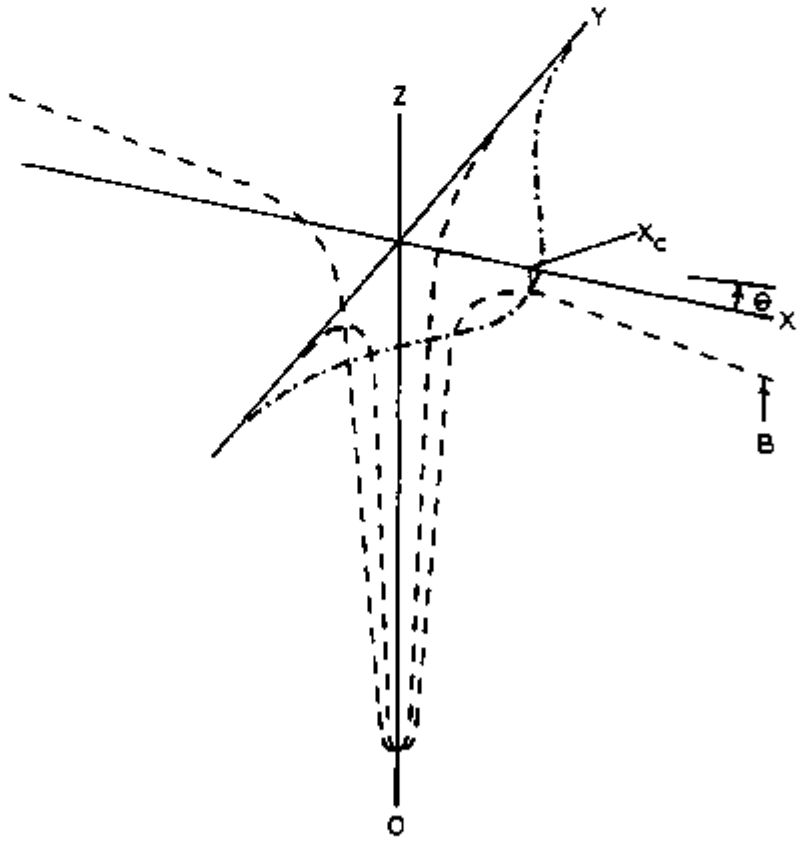

Figure 4: Perspective Drawing of Ion-Vortex Line Trapping Potential

larger than the actual volume of the ion. Although the healing length for the superfluid density near an ion is not known, it is probably not much different from d. Analysis of the lifetime data will result in a value for U(0), the binding energy of an ion to a vortex line. Substitution of this value of U(0) into Equation (28) will determine an effective hydrodynamic radius for the ion which may be on the order of d larger than the actual radius of the ion. Unless stated to the contrary, statements in this thesis about "the radius of the ion" determined from the experimentally measured binding energy will refer to the effective hydrodynamic radius of the ion.

Presented in Figure 4 is a perspective drawing of the ion trapping potential with an applied electric field in the x direction. The total trapping potential can be expressed in the following way:

$$U_t(r,\theta) = U(r) - eE r\cos\theta \qquad (29)$$

where U_t is the total potential, U(r) the trapping potential, E the applied electric field, and e the electronic charge. Notice that the potential in the region $r = x_c$ and $\theta \approx 0$ has the shape of a "pouring spout".

Certain parameters which characterize this potential are useful in the calculation of the escape mechanism for the ion out of the well. They are

$$\left.\frac{\partial U_t(r,0)}{\partial r}\right|_{r=x_c} = 0, \tag{30a}$$

$$\omega_c^2 = -\frac{1}{M}\left.\frac{\partial^2 U_t(r,0)}{\partial r^2}\right|_{r=x_c}, \tag{30b}$$

$$\omega_o^2 = \frac{1}{M}\left.\frac{\partial^2 U_t(r,0)}{\partial r^2}\right|_{r=0}, \tag{30c}$$

$$S_o^2 = \frac{1}{M}\left.\frac{\partial^2 U_t(r,\pi/2)}{\partial r^2}\right|_{r=0}, \tag{30d}$$

and

$$S_c^2 = \frac{1}{M}\left.\frac{\partial^2 U_t(x_c,\theta)}{x_c^2\,\partial\theta^2}\right|_{\theta=0} \tag{30e}$$

where M is the effective mass of the ion. These parameters are essentially the same as those introduced by Parks and Donnelly. In the limit of large distances from the vortex [see Equation (24)] we have

$$U_t(r,\theta) \cong -\frac{1}{2}\rho_s\left[\frac{4\pi R^3}{3}\right]\left[\frac{3}{2}\right]\left[\frac{\kappa}{2\pi r}\right]^2\left[1 + \frac{4}{9}\left[\frac{R}{r}\right]^2\right] - eEr\cos\theta. \tag{31}$$

From Equations (30a) and (31) we obtain

$$x_c \cong R\left[\frac{\rho_s\kappa^2}{2\pi eE}\right]^{\frac{1}{3}}\left[1 - \frac{8}{9}\left[\frac{2\pi eE}{\rho_s\kappa^2}\right]^{\frac{2}{3}}\right] - \frac{1}{3} \tag{32}$$

Also we have

$$\omega_c^2 = \frac{3}{2}\left[\frac{\rho_s \kappa^2}{R\pi M}\right]\left[\left[\frac{R}{x_c}\right]^4 + \frac{40}{27}\left[\frac{R}{x_c}\right]^6\right] , \tag{33a}$$

and

$$S_c^2 = \frac{\omega_c^2}{3} . \tag{33b}$$

The remaining important quantity to evaluate is ω_o. Parks and Donnelly were able to calculate ω_o using their model for the trapping potential. To repeat, in their model they assume that the trapping potential is just the kinetic energy of the superfluid flow contained in a volume equal to the volume of the ion. No account was taken of the energy of flow around the ion which is thought to be the source of the discrepancy of 3/2 for the ion at large distances from the vortex line. An analysis of the actual flow pattern for an ion slightly off-center on the vortex line will be rather complicated. For an estimate of ω_o we adopt the model of Parks and Donnelly where no departures of the vortex from a straight line are considered. Their results are

$$\omega_o^2 = S_o^2 = \frac{\rho_s \kappa^2}{4\pi M}\left[-1 + \left[2 + \frac{d^2}{R^2}\right]\left[1 + \frac{d^2}{R^2}\right]^{-\frac{1}{2}} \times \sinh^{-1}\left[\frac{R}{d}\right]\right]\left[R\left[1 + \frac{d^2}{R^2}\right]\right]^{-1} \tag{34}$$

where d is the healing length.

At 1.6°K and at saturated vapor pressure where $\rho_s = 0.12$ gm cm^{-3} and μ_- (negative ion mobility) = 0.18 cm (volt-sec)$^{-1}$,

these parameters are evaluated under the assumptions that $R = 19.5$ Å, $M \cong 300M_{He}$, $E = 40$ volts cm^{-1}, and $d = 1.46$ Å:

$$x_c = 129 \text{ Å} ,$$

$$\omega_c = 2.8\times10^{8} \text{ sec}^{-1} ,$$

$$\omega_o = 1.2\times10^{10} \text{sec}^{-1} ,$$

and

$$\frac{U_t(x_c,0)}{k} = - 0.90°K.$$

For other values of applied electric field,

$$x_c = 102 \text{ Å at } E = 80 \text{ volts cm}^{-1},$$

and

$$x_c = 441 \text{ Å at } E = 1 \text{ volt cm}^{-1},$$

Another important parameter that will be useful later is β, the reciprocal of the "current relaxation time" of the ion, which is expressed as

$$\beta = \frac{e}{\mu M} . \tag{35}$$

For the negative ion at 1.6°K and at saturated vapor pressure

$$\beta = 4.0\times10^{9} \text{ sec}^{-1}.$$

2. Escape of an Ion from a Vortex Line

Parks and Donnelly have proposed that the ion behaves like a Brownian particle and escapes from the vortex line by thermal activation. So far only the final results of their calculation have been published. Since their results are quite important for our analysis of the data presented in this thesis, a complete derivation is given below.

Parks and Donnelly indicated that their derivation

commenced with the two-dimensional Fokker-Planck equation, and they cited a review article by S. Chandrasekhar.[47] According to Chandrasekhar, the derivation can begin with the simpler stationary-state Smoluchowski equation if the following conditions are satisfied:

1. The trapping well should be deep with respect to kT. A deep trapping well results in a slow diffusion of the ion out of the well. This system, then, is considered to be "quasi-stationary" which makes the steady-state Smoluchowski equation applicable.
2. Grad $U_t(r,\theta)$ should not change appreciably over distances on the order of the mean stopping length of the ion λ, given by the expression

$$\lambda = \frac{1}{\beta}\frac{kT}{M} .$$

Another way of stating this condition is that λ must be small compared to space intervals of interest.

3. $\beta^2 >> \omega_c^2$. Implicit in the use of the Smoluchowski equation is the assumption that β^{-1} must be small compared to time intervals of interest. According to Chandrasekhar ω_c^{-1} is the shortest time interval of interest--hence the above inequality.

For the negative ion Items #1 and #2 are satisfied since the well is approximately 60°K deep in comparison to T≅1°K and is approximately 200 Å wide in comparison to $\lambda \cong 4$ Å at 1.6°K. For Item #3 at 1.6°K and at saturated vapor pressure, we

have for the negative ion

$$\frac{\beta^2}{\omega_c^2} \simeq 200.$$

With a pressure of 25 atm at 1.1°K we obtain

$$\frac{\beta^2}{\omega_c^2} = 10 \ .$$

Thus this condition is reasonably satisfied over the range that data has been taken in the experiment reported in this thesis.

The steady-state diffusion current derived from the Smoluchowski equation is

$$\vec{J} = - D \text{ grad } f - \frac{D}{kT} f \text{ grad } U_t(r,\theta) \qquad (36a)$$

$$= - D e^{-\frac{U_t(r,\theta)}{kT}} \text{ grad } \left[f e^{\frac{U_t(r,\theta)}{kT}} \right] \qquad (36b)$$

where D is the diffusion coefficient, which satisfies the Einstein relationship

$$D = \frac{kT}{M\beta} \ , \qquad (37)$$

and where f is the two-dimensional particle density.

The first term in the steady-state diffusion equation [Equation (36a)] is the normal diffusion of particles due to a concentration gradient. The second term represents the drift of particles under an applied force, - grad $U_t(r,\theta)$.

Assume that at time t=0 an ion is trapped in the well. We shall use Equation (36b) to determine the probablity of

escape per unit time of this ion out of the well. The ion density f is assumed to be small beyond the lip of the well.

Let us integrate the radial component of

$$\vec{j}\, e^{\frac{U_t(r,\theta)}{kT}}$$

along $\theta \doteq 0$ from $r = 0$ at the bottom of the well to some point $r = B$ beyond $r = x_c$. Then, using Equation (36b), we have

$$\int_0^B j_r\, e^{\frac{U_t(r,\theta)}{kT}}\, dr = D\, f\, e^{\frac{U_t(r,\theta)}{kT}} \Bigg|_B^0 . \qquad (38)$$

The ion density f is assumed to be small at B; the right-hand side of this equation reduces to

$$= D\, f_o\, e^{\frac{U(0)}{kT}} \qquad (39)$$

where $U_t(0,\theta) = U(0)$, the binding energy of the ion to the vortex line. A sharp peak in the value of the integrand on the left-hand side of Equation (38) occurs at $r = x_c$ since U_t has a maximum there for $\theta \doteq 0$. We can, then, approximate the integral by the expression

$$\doteq j_r(x_c,\theta) \int_0^B e^{\frac{U_t(r,\theta)}{kT}}\, dr \qquad (40)$$

for θ close to zero. In this region we may approximate the potential by

$$U_t(r,\theta) \doteq U(x_c,\theta) - \tfrac{1}{2}M\omega_c^2(r - x_c)^2. \qquad (41)$$

To a sufficient degree of accuracy Equation (40) becomes

$$\approx j_r(x_c,\theta)\, e^{\frac{U(x_c,\theta)}{kT}} \int_0^\infty e^{-\frac{M\omega_c^2(r-x_c)^2}{2kT}}\, dr \tag{42a}$$

$$= j_r(x_c,\theta) \left[\frac{2\pi kT}{M\omega_c^2}\right]^{\frac{1}{2}} e^{\frac{U(x_c,\theta)}{kT}} . \tag{42b}$$

Therefore,

$$j_r(x_c,\theta) \approx D\, f_o \left[\frac{M\omega_c^2}{2\pi kT}\right]^{\frac{1}{2}} e^{\frac{U(0)-U(x_c,\theta)}{kT}} . \tag{43}$$

We wish to calculate the total ion current per unit length out of the well:

$$I = \int_{-\pi}^{+\pi} j_r(x_c,\theta) r d\theta . \tag{44}$$

So far, however, we have only considered the value of $j_r(x_c,\theta)$ for θ near zero. Let us define $r_c(\theta)$ to be the position of the maximum of U_t for a given value of θ where $r_c(0) = x_c$. Equation (43) will be correct for any value of θ if x_c is replaced by $r_c(\theta)$ and if we make ω_c a function of θ. For those values of θ where $x<0$, there is no maximum for U_t; there will be little contribution to the current I in this region because of the e^{-U} factor in Equation (43). For $x>0$ $r_c(\theta)$ is an even function of θ which approaches ∞ as θ approaches $\pm\pi/2$. $\omega_c(\theta)$ is also an even function of θ satisfying $\omega_c(\theta) \approx r_c(\theta)^{-2}$. Finally, $U[r_c(\theta),\theta]$ has its minimum value at $\theta = 0$. All these

effects contribute to make the integrand of Equation (44) a maximum at $\theta = 0$. We approximate $U(r_c,\theta)$, then, in the following way:

$$U(r_c,\theta) \cong U_c + \tfrac{1}{2}MS_c^2(x_c\theta)^2. \tag{45}$$

Therefore,

$$I \cong D\, f_o\left[\frac{M\omega_c^2}{2\pi kT}\right]^{\frac{1}{2}} e^{\frac{U(0) - U_c}{kT}} \int_{-\pi/2}^{+\pi/2} e^{-\frac{1}{2}MS_c^2(x_c\theta)^2} x_c d\theta. \tag{46}$$

As an approximation to the above integral, we extend the limits of integration to infinity; and we obtain

$$I \cong D\, f_o \frac{\omega_c}{S_c} e^{\frac{U(0) - U_c}{kT}}. \tag{47}$$

Let d^2N_o be the number of ions in the region $d\theta dr dr$ near $r = 0$. Then

$$d^2N_o = f_o\, e^{\frac{U_t(r,\theta) - U(0)}{kT}} r dr d\theta. \tag{48}$$

Let us approximate $U_t(r)$ in the following way:

$$U_t(r,\theta) \cong U(0) + \tfrac{1}{2}M\omega_o^2 r^2. \tag{49}$$

Taking the integral of Equation (48), we obtain

$$N_o = f_o \int_{\substack{\text{near} \\ r=0}} e^{-\frac{M\omega_o^2 r^2}{2kT}} 2\pi r dr. \tag{50}$$

Again extending the limits of integration to infinity as an approximation to this integral, we have

$$N_o \simeq f_o 2\pi \frac{kT}{M\omega_o^2} \quad . \tag{51}$$

Finally, the probability of escape per second is given by the expression

$$P = \frac{I}{N_o} = \frac{\omega_o^2}{2\pi\beta} \frac{\omega_c}{S_c} e^{\frac{U(0) - U_c}{kT}} \quad , \tag{52}$$

Let τ equal the lifetime of the trapped ion. Then,

$$\tau = \frac{1}{P} = \frac{2\pi\beta}{\omega_o^2} \frac{S_c}{\omega_c} e^{\frac{U_c - U(0)}{kT}} \quad . \tag{53}$$

This last equation now provides an explanation of why only negative ion trapping is seen at temperatures above 1.0°K. At 1.6°K and at saturated vapor pressure the negative ion lifetime is measured to be on the order of 10^3 seconds where $-\frac{U(0)}{kT} \simeq 37$. For the positive ion at the same temperature $-\frac{U(0)}{kT} \simeq 11$. Therefore, at 1.6°K the positive ion lifetime is smaller than the negative ion lifetime by the multiplicative factor of e^{-26}--a very small number. For the positive ion $-\frac{U(0)}{k} \simeq 18$°K. Hence, for the positive ion lifetime to be on the order of one second, the temperature must be 0.65°K in reasonably good agreement with the experimental observation that positive ion trapping disappears between 0.6 and 1.0°K.

The final aspect of Equation (53) to consider is what

temperature dependence is expected for the lifetime at saturated vapor pressure. Experimentally the mobility of the negative ion at saturated vapor pressure obeys

$$\mu_- \propto e^{\frac{\Delta}{T}}$$

where $\Delta \cong 8.1°K$.[48] This behavior can be understood in terms of kinetic theory arguments about ions colliding with roton excitations in the liquid. U(0), the binding energy of the ion to the vortex line, is proportional to ρ_s; it is temperature dependent. U_c is very small compared to U(0) and has the following temperature dependence:

$$U_c \propto (\rho_s)^{\frac{1}{3}} .$$

This is negligible compared to the temperature dependence of U(0). Finally, we have $\omega_o^2 \propto \rho_s$. Then the temperature dependence of the lifetime is

$$\tau = \frac{F_o}{\rho_s(T)} e^{-\frac{\Delta}{T}} e^{\frac{f(R)\rho_s(T)}{T}} \qquad (54)$$

where we define $f(R)\rho_s(T) = [U_c - U(0)]/k$ and where F_o is a constant. The function f(R) represents the dependence of the depth of the trapping well upon the size of the ion where R is the radius of the ion.

In summary, the models presented in this chapter appear to explain in a qualitative way the observed difference between

positive and negative ion trapping. These models will be used to analyze the experimental results presented in this thesis. In particular, we shall attempt to fit Equation (54) to the experimental data.

III. EXPERIMENTAL APPARATUS AND PROCEDURES

1. Introduction

A series of preliminary experiments were conducted with another apparatus and have been reported elsewhere.[49] During the execution of these experiments, the following phenomenon was observed: Charges trapped on vortex lines in rotating liquid helium were released from the liquid when the rotation of the vessel which contained the liquid helium was suddenly stopped. The length of time over which the release of the trapped charge occurred was on the order of 15 seconds.

A new apparatus which would make use of this charge release effect was designed to make measurements of the lifetime of trapped ions. This new apparatus was constructed so that pressures up to the solidification pressure could be applied to the rotating liquid.

2. Overall Apparatus

An overall drawing of the apparatus is presented in Figure 5. The two glass Dewars are supported by a stand made from welded sections of 2" by 2" hollow aluminum tubing. The aluminum turntable rides on a 5" diameter aircraft ball bearing. Inside the ball bearing a commercial oil seal provides a vacuum seal between the turntable and the inner Dewar.[50] The "apparatus flange" to which the pressure vessel is connected is sealed to the turntable with a rubber "O"

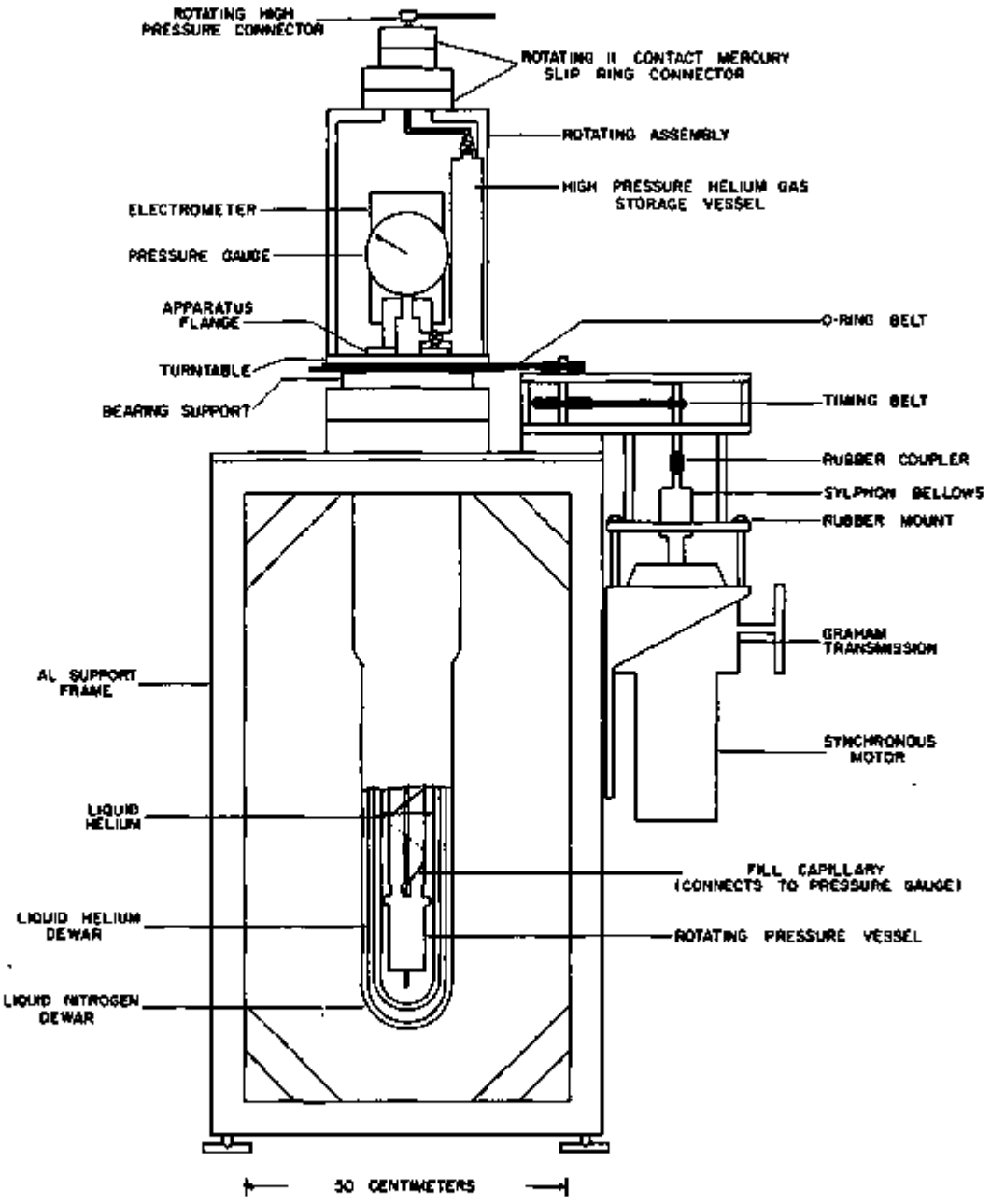

Figure 5: Diagram of Overall Apparatus

ring. The turntable is driven by a continuously variable speed (0 to 1750 rpm) transmission which is suspended from rubber mounts for vibration isolation.[51] A bellows and rubber coupling remove most of the vibrations associated with improper alignment of the transmission with respect to the shaft to which the small timing-belt pulley is attached. A long rubber "O" ring of 1/4" cross section is used as a belt to drive the turntable. The "O" ring isolates the remaining torsional vibrations which come through the rubber coupling. The turntable speed ranges from 0 to 102 rpm.

Various electrical leads are brought through a mercury slip ring connector, details of which are shown in Figure 6a. For control of the pressure in the apparatus during rotation, a rotating high-pressure seal is provided. Details of this seal are shown in Figure 6b.

For pressurization of the liquid in the low-temperature portion of the apparatus, the following system is used: A 2000 psi storage tank of helium gas is connected to a pressure regulator. The output of the regulator is fed through an activated-charcoal trap which is immersed in liquid nitrogen. In this way all impurities except neon and hydrogen are removed from the helium gas. The purified helium gas then passes through the rotating seal to a pressure manifold on the turntable. A 0 to 600 psi (gauge pressure) pressure gauge[52] with an accuracy of ±1/4% of its full scale value,

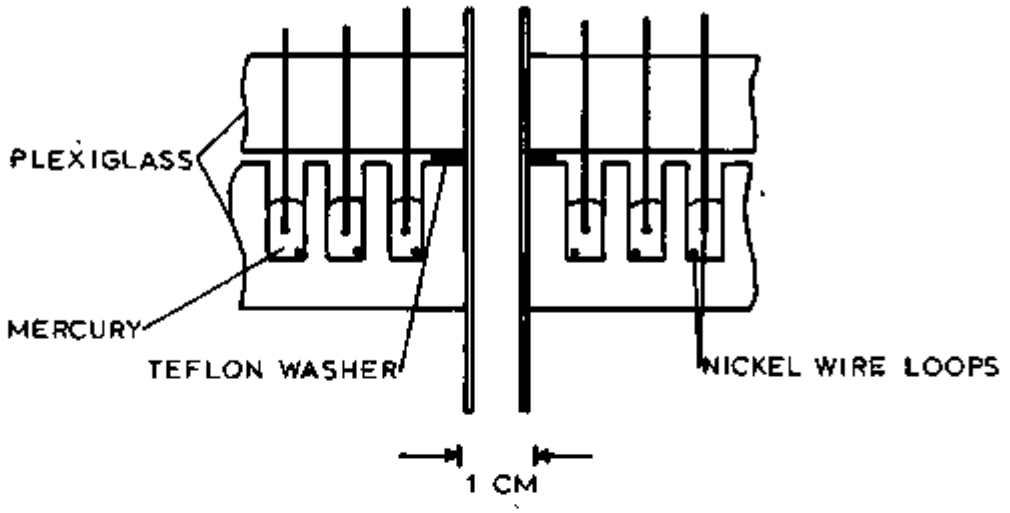

Figure 6a: Mercury Slip-Ring Connector

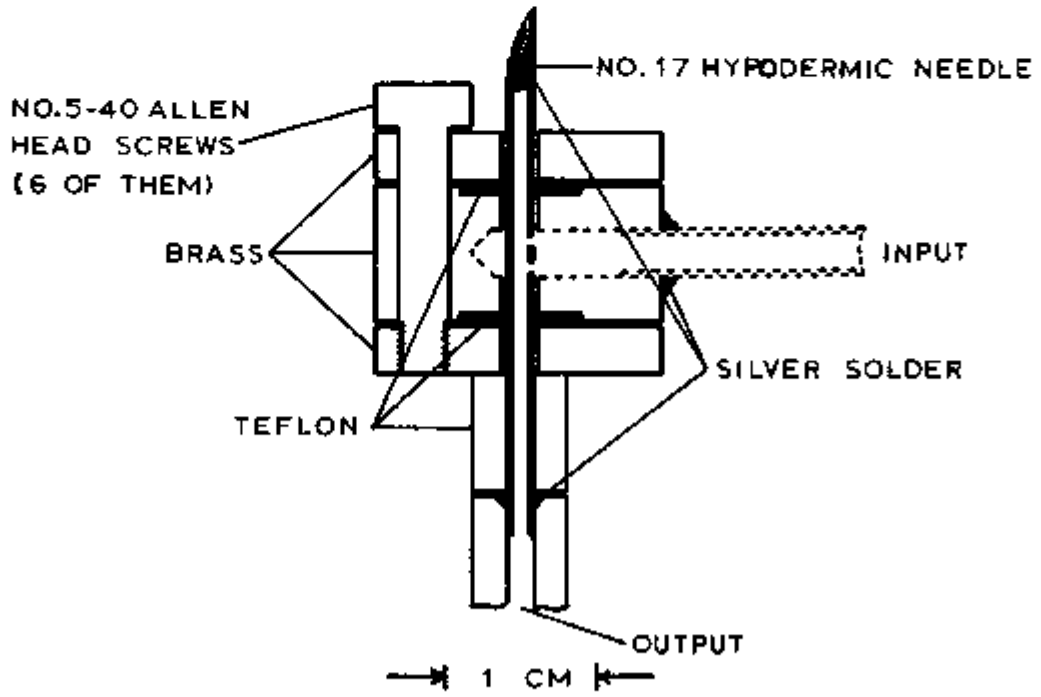

Figure 6b: Rotating High-Pressure Seal

a 1/2 liter storage vessel, and assorted valves[53] constitute this pressure manifold. The output of this manifold is fed through a 0.010" i.d. by 0.010" thick wall stainless steel capillary to the pressure vessel at the low-temperature end of the apparatus. For low-pressure measurements two mercury manometers in series can be connected to the pressurization system between the rotating seal and the charcoal trap. In the intermediate range a 0 to 200 psi gauge[54] rated at ±1/4% of its full scale value can be connected to the system in the same place as the mercury manometers. For the high-pressure range the 600 psi gauge on the turntable is used. The 200 psi and the 600 psi gauges agree within their stated accuracies. No attempt has been made to calibrate these gauges against an accurate standard gauge.

A high-speed vacuum pump is connected to the top of the inner Dewar via a 4" diameter rubber hose.[55] The lowest pressure which can be reached with liquid helium in the Dewar is approximately 300 microns of mercury (T=1.1°K). The evaporation rate of the liquid is equivalent to a heat input of approximately 0.1 watts.

3. Pressure Vessel

In Figure 7 a more detailed drawing of the pressure vessel and its contents is shown. In the drawing of the top view of the apparatus, the dotted lines marked "A" and "B" illustrate that the side view of the pressure vessel is a

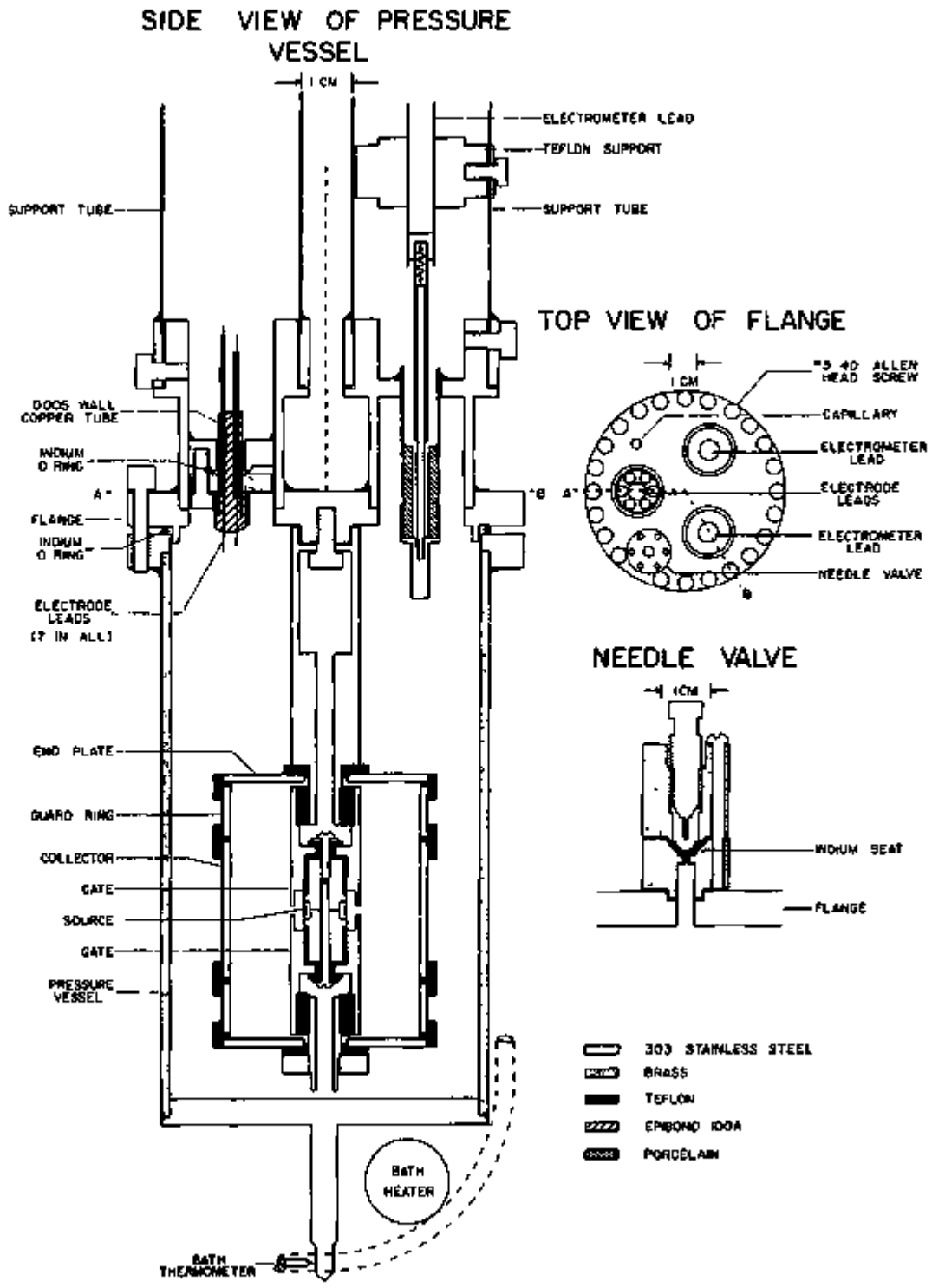

Figure 7: Diagram of Pressure Vessel

120 degree sectional view.

The pressure vessel is attached to the "apparatus flange" on the turntable via three 1" o.d. by 0.010" wall stainless steel tubes. Two of these tubes contain a carefully insulated lead to the electrometer. The lead in each 1" tube consists of a 3/16" o.d. by 0.005" wall stainless steel tube which is supported every 12.5 cm by teflon plugs. At each end of this lead a vacuum-tight, well insulated feed-through is used.[56] The electrometer, which is mounted directly on the apparatus flange, can be connected to either or both of the two electrometer leads. If only one electrometer lead is connected to the electrometer, the other lead can be connected to an external potential via the mercury slip ring connector. The seven remaining electrical leads pass through the third 1" support tube. These leads enter the pressure vessel via a leak-tight, demountable polymer seal.[57] This seal consists of seven #30 copper wires which have been sealed inside a thinwall copper tube which in turn is silver soldered into a small brass flange. The brass flange is sealed to the top of the pressure vessel with an indium "O" ring. Teflon tubes (1/32" o.d.) provide insulation for the seven leads from the pressure vessel to the apparatus flange. One has to be careful about the insulation of these leads since there is danger of electrical discharge between the leads through the low-pressure helium gas above the liquid.

The indium-seal needle valve is used for two reasons: First, it makes possible the filling of the pressure vessel from the surrounding helium bath. Second, it provides a way of venting the pressure vessel should the capillary ever become clogged. Also, it is much easier to evacuate the pressure vessel through the needle valve than through the capillary.

The temperature of the bath surrounding the pressure vessel is regulated. A germanium resistance thermometer which is connected to an A.C. Wheatstone bridge is used as a temperature sensor.[58] The output of the bridge is amplified and fed into a phase-sensitive detector. The output of the detector is fed into a 5 KΩ heater in the liquid. In the temperature range covered by this experiment the temperature regulation is better than $\pm 5\times10^{-5}$°K.

4. Electrode Assembly

Also shown in Figure 7 are details concerning the electrode system which is used to measure the lifetimes. These electrodes, made of #303 stainless steel, were electropolished in a solution of 60% glycerine and 40% phosphoric acid. The insulators are made of teflon. The alpha-particle source consists of small glass beads 40 microns in size which are impregnated with Po^{210}.[59] These beads were glued into a groove on the surface of the ring-shaped "source" electrode and then were covered with a vacuum-deposited layer of gold 2000 Å thick. The collector is connected to one of the electrometer leads. The guard rings are

grounded. The gate electrode is generally set at a potential of -40 volts. The potential between the gate and source electrodes is adjustable. The end plates are normally set at -80 volts in order to provide a confining field to keep trapped charge from leaking out the ends of the vortex lines.

It should be pointed out that electrodes are normally gold plated in order to minimize the formation of insulating surfaces on the electrodes. The charge build-up on such insulating surfaces could produce unwanted distortions in the electric fields. It has already been mentioned that the stainless steel electrodes used in this experiment were electropolished but not gold plated. However, we believe that gold plating of these electrodes was not necessary for the following reasons: Long term drifts in the ion current between electrodes are indicative of the charging of insulating surfaces on the electrodes, but no such drifts were ever observed in the experiments performed with this apparatus. The observed reproducibility of lifetime measurements, which depend upon the applied electric field, made several months apart is another indication that insulating surfaces were not forming on the stainless steel electrodes. It should be emphasized that great care was taken between low temperature runs to make sure that only helium gas of high purity ever came into contact with the electrodes.

The electrodes were designed to have cylindrical symmetry. In this way it was hoped that some information about the

mechanisms involved in the release of the trapped charge could be obtained. A non-cylindrical system would, upon cessation of rotation, have secondary flow patterns generated which would further complicate the analysis.

For a gate potential of -40 volts the potential difference between the gate and the source is adjusted to be *57 volts. This particular value of the potential difference was chosen to minimize the distortion of the field lines in the region between the gate and the collector near the gap in the gate when negative ions are travelling from the gate to the collector. The determination of this particular value of the potential difference was made with a mock-up of the electrode system in an electrolytic tank and is discussed elsewhere.[60] The current transmitted by the gap in the gate under these conditions is 25% of the source to gate current.

The potential between two concentric cylinders with end plates can be expressed in terms of a Fourier series which is a solution of the Laplace equation. The solution and its evaluation are discussed in Appendix I. We shall only present the results here.

Representative field lines in the upper half of the region between the gate and the collector are shown in Figure 8a. Let a be the radius of the gate where a = 0.635±0.002 cm, and let b be the radius of the collector where b = 1.747±0.005 cm. The boundary conditions are the following: the gate

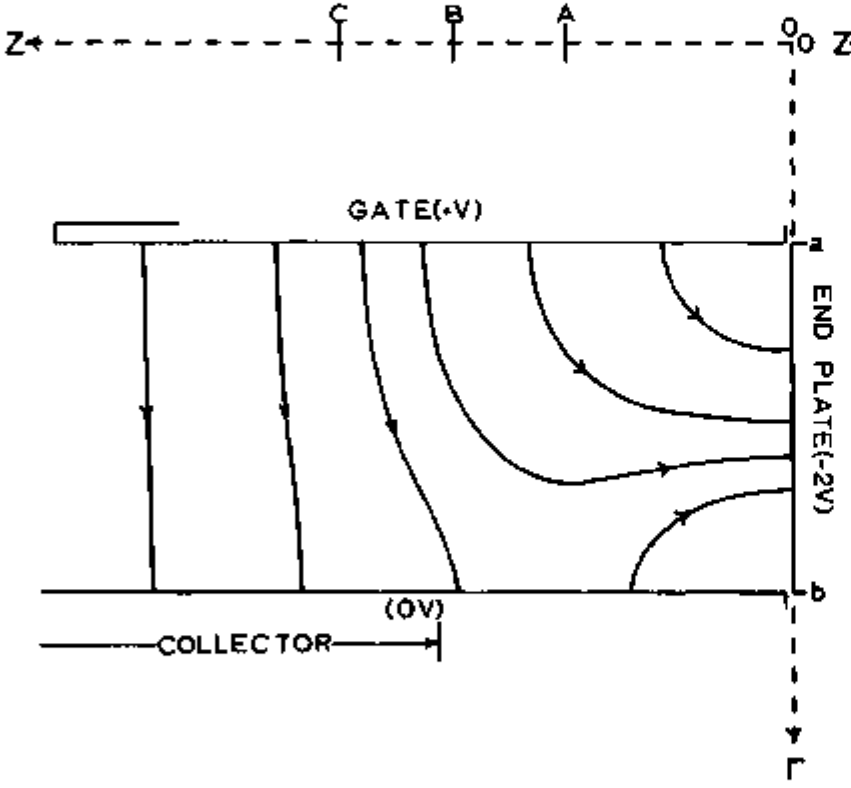

Figure 8b: Representative Electric Field Lines for a Positive Gate Potential

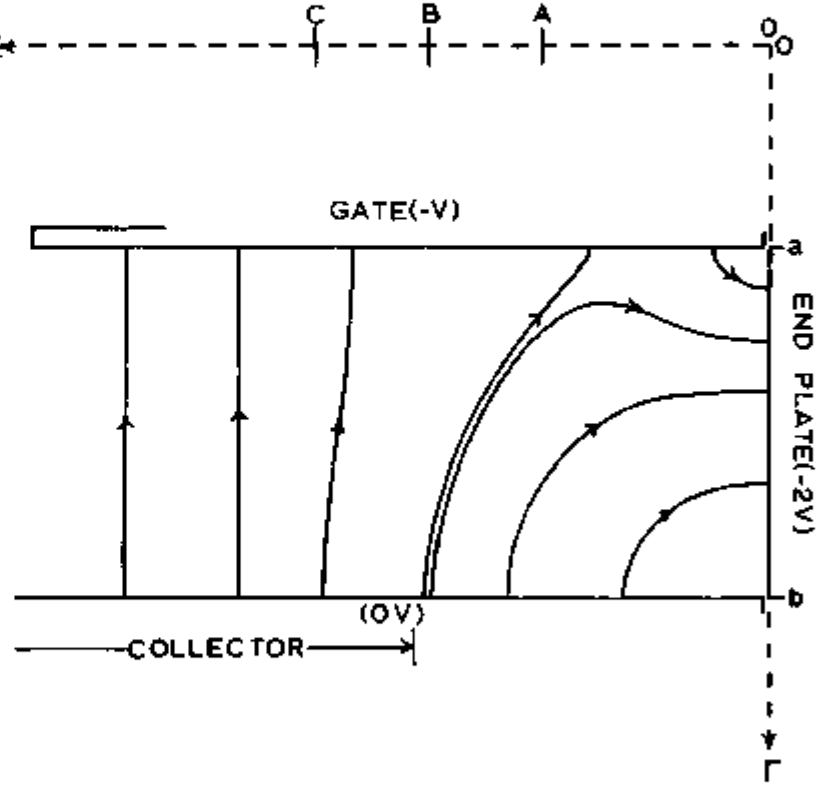

Figure 8a: Representative Electric Field Lines for a Negative Gate Potential

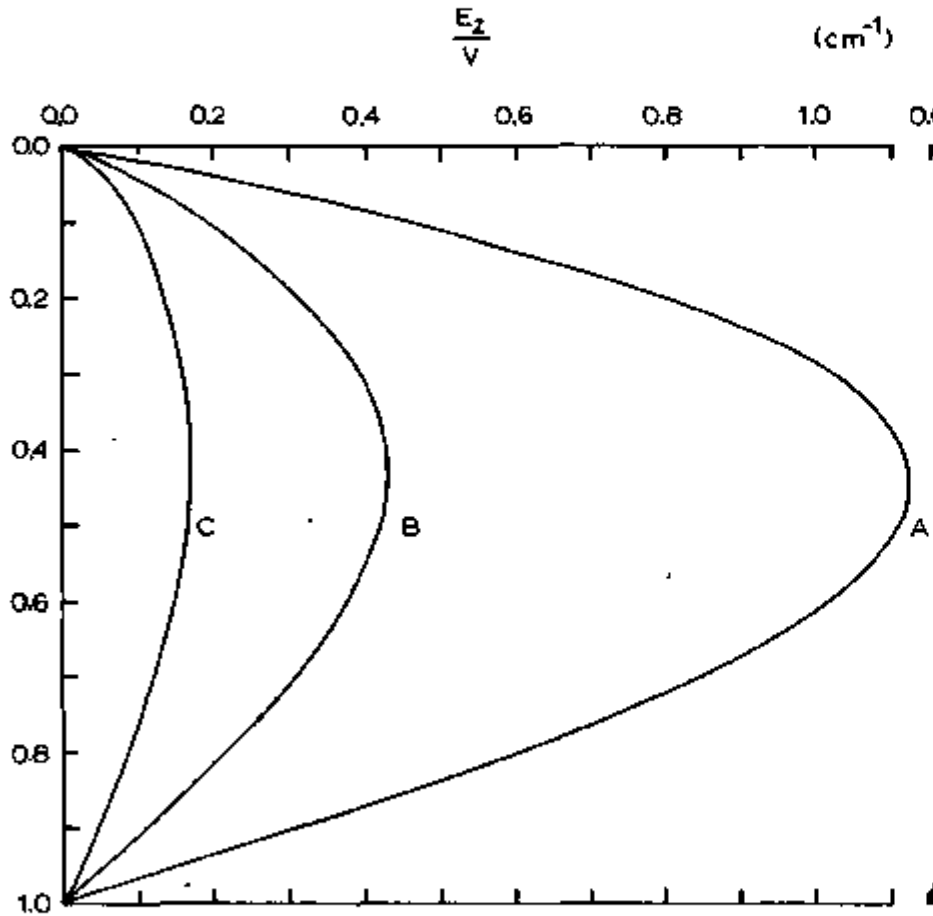

Figure 9b: Z Component of the Electric Field for Positive Gate Potential

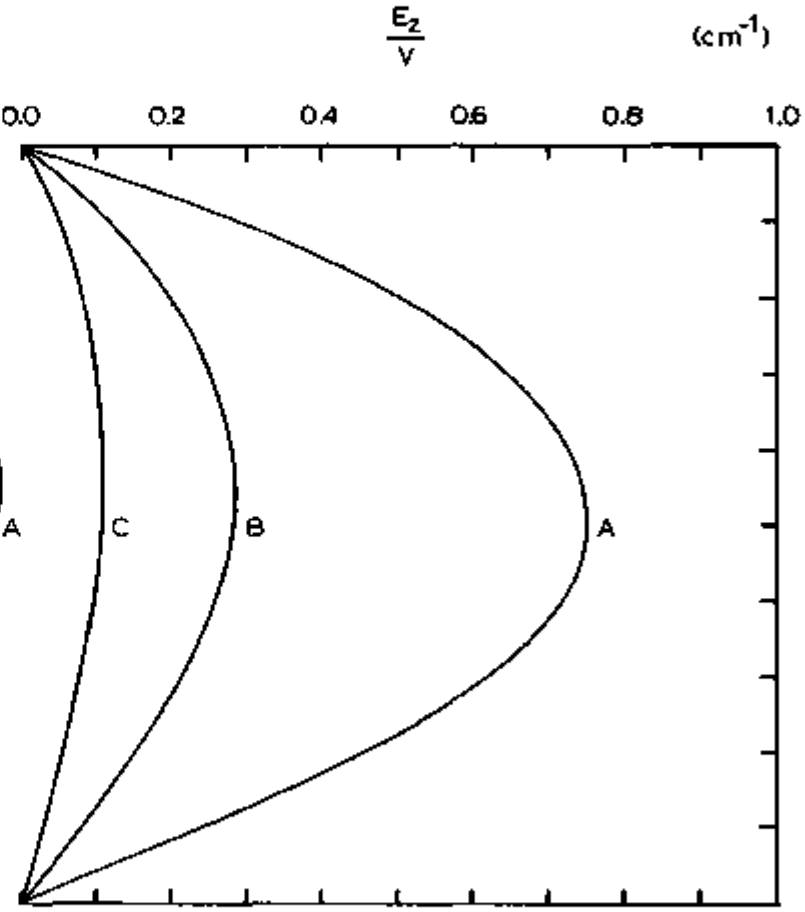

Figure 9a: Z Component of the Electric Field for Negative Gate Potential

potential equals -V, the end plate potential is -2V, and the guard rings and the collector potentials are at 0 volts. The confining nature of the field is quite evident. Presented in Figure 9a are plots of the z component of the confining field at the position "A", "B", and "C" shown in Figure 8a. We see that near the upper edge of the collector the average value of the z component of the confining field for a gate potential of -40 volts is 6 to 8 volts cm^{-1}.

In Figures 8b and 9b the case where the gate potential has been changed to +V is presented. This case represents the experimental situation in which the release of trapped charge occurs with the electrical forces on the negative ions directed toward the gate. The magnitude of the z component of the confining field is approximately 60% larger than in the first case.

It is important, particularly for the first set of boundary conditions presented, to estimate the field developed by the trapped charge in comparison to the confining field. In those experiments performed for this thesis in which a lifetime was actually determined, the largest amount of trapped charge was approximately 5×10^{-12} coulombs.

Consider a cylinder of length ℓ and radius r which contains a uniform density of charge ρ. The field at the center of either end of this cylinder is

$$E = 2\pi\rho[r + \ell - (r^2 + \ell^2)^{\frac{1}{2}}]. \qquad (55)$$

Let us use this expression to estimate the z component of the electric field generated by a uniform density of charge contained between the gate and the collector. We let the total charge be 5×10^{-12} coulombs in this region. Let the length of this cylinder be equal to the length of the collector in the z direction. The relevant effective radius of our hypothetical cylinder ranges from half the distance between the gate and the collector to the radius of the collector. The former distance gives $E_z = 0.7$ volts cm^{-1}; the latter case gives $E_z = 1.9$ volts cm^{-1}. The actual value of E_z is probably in between these two values. The larger value is still rather small compared to the average confining field of 6 to 8 volts cm^{-1}. It is only in the region very close to the collector and the gate that the z component of the confining field is small. Thus the potentials which have been chosen for the various electrodes appear to provide a sufficient confining field.

The remaining characteristic of the cylindrical-electrode system to consider is the amount of charge which actually passes through the electrometer when trapped charge is released and moves toward the collector. Effectively, the gate and the collector are connected by a series combination of a battery and a resistor. The battery provides the potential at which the gate is sitting. The resistor represents the effective input impedance of the electrometer. For the

currents measured in this experiment the potential difference across the input of the electrometer is negligible compared to the gate potential. When some negative charge $-Q$ is trapped in the liquid, a total charge $+Q$ is induced on the electrodes. The distribution of induced charge is such as to keep the potential difference between the gate and collector equal to the battery potential. Let there be $y(+Q)$ induced charge on the gate and $(1-y)(+Q)$ on the collector, neglecting the charge induced on the other electrodes. When the trapped charge is released, it moves to the collector. However, the amount of charge which passes through the electrometer is just yQ. Thus the amount of charge one measures upon the release of the trapped charge is generally not the total charge in the liquid.

We approximate our cylindrical electrodes with end plates by two concentric cylinders of infinite length. Assuming a uniform charge distribution between the cylinders (not necessarily of infinite extent in the z direction) and making use of Gauss' law, we obtain

$$y = \frac{1}{2\ln\left[\frac{b}{a}\right]} - \frac{1}{\left[\frac{b}{a}\right]^2 - 1} \qquad (56)$$

where a is the radius of the gate and b is the radius of the collector. Putting in the appropriate values of a and b, we have $y = 0.34$. This correction was used in arriving at the

estimate of 5×10^{-12} coulombs for the largest amount of trapped charge.

5. Electrical Systems

In Figure 10 is shown an overall block diagram of the electrical systems involved in the experiment. The electrometer and its power supply are on the turntable. The 12-volt battery power for this power supply and the output of the electrometer pass through the rotating connector. The heater and the germanium thermometer rotate with the pressure vessel. The potentials of the gate, source, and end plates can be adjusted during rotation and are measured with a vacuum-tube voltmeter to an accuracy of ±1%.[61] The output of the electrometer is connected to the integrating circuit through a D.C. amplifier so that the total charge passing through the electrometer as a function of time can be measured.[62] The electrometer voltage divider (1% resistors) matches the electrometer output to the 10 millivolt input of the low-speed chart recorder.[63] This low-speed chart recorder can be connected to either the voltage divider or the output of the integrating circuit. The high-speed chart recorder is connected to the output of the electrometer only when the low-speed chart recorder is connected to the output of the integrating circuit.[64] The actual sequence of operations involved when the amount of charge trapped in the liquid is measured will be discussed later.

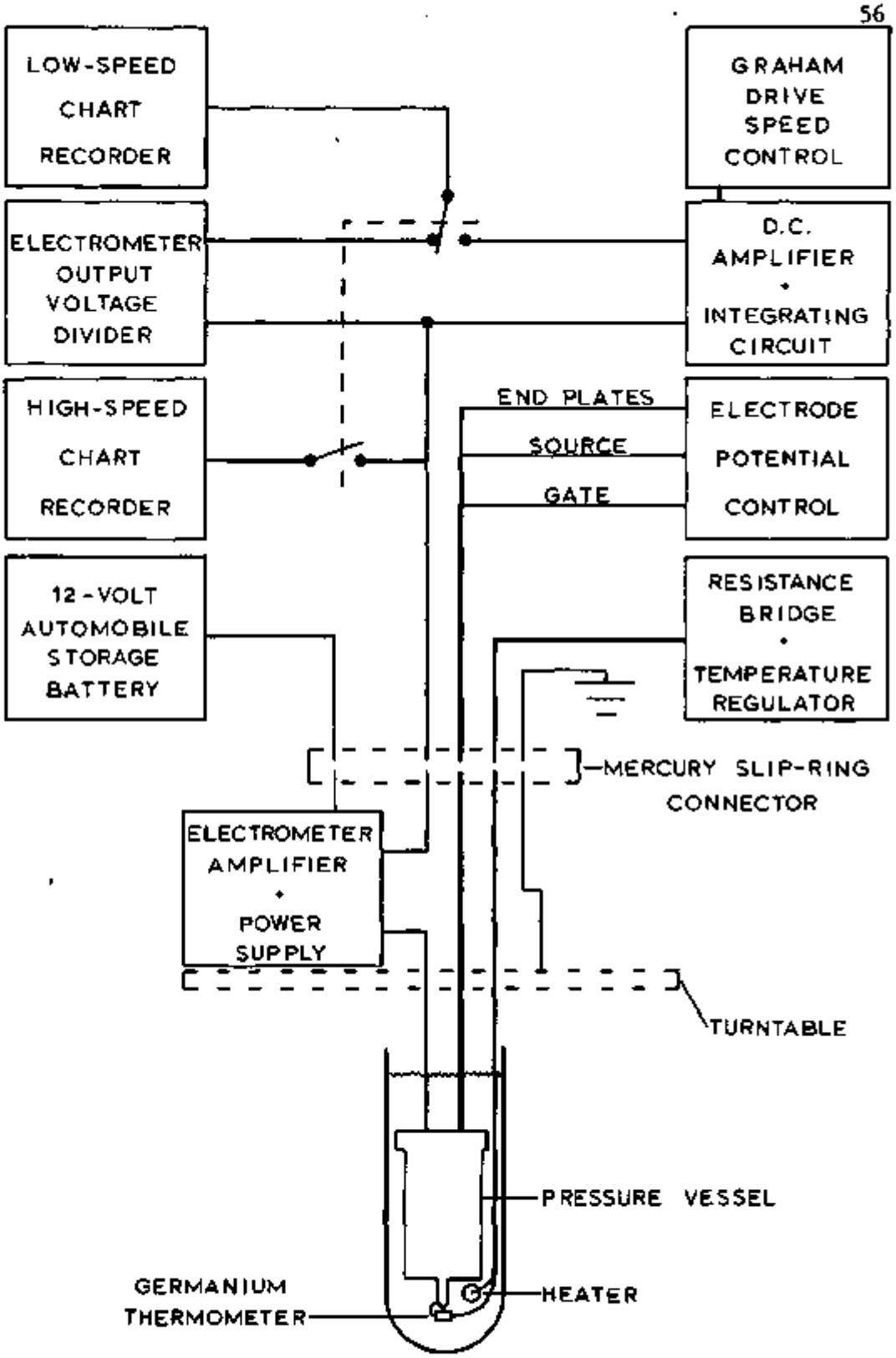

Figure 10: Overall Diagram of Electrical Systems

A more detailed diagram of the electrometer and integrating circuits is shown in Figure 11. Both circuits use an amplifier of high gain and of very high input impedance. The amplifiers contain two matched CK5889 electrometer-tubes. The grid of one tube is grounded; the grid of the other is the input of the amplifier. A transistor amplifier with a gain on the order of 10^4 amplifies the voltage difference between the plates of the two tubes. Provision is made for balancing this potential difference to zero by an adjustment of the screen grid of one of the vacuum-tubes. Both circuits have what is commonly referred to as "operational feedback".

The feedback loop for the electrometer consists of a $10^{11}(\pm 10\%)\Omega$ resistor shunted by an adjustable 1 to 5 picofarad capacitor. The capacitor controls the response time of the electrometer; a response time of 1/2 second is generally used. If I is the average current into the electrometer, the average output voltage e_o of this equation satisfies

$$e_o = - IR \tag{57}$$

where R is the feedback resistor and where the gain of the amplifier is large and negative.[65] The averaging mentioned above occurs over times which are long compared to the 1/2 second response time of the circuit. It is estimated that the input voltage remains within 10^{-3} volts of ground potential over the full range of currents measured.

The integrating circuit has a 0.01 ($\pm 10\%$) mfd capacitor

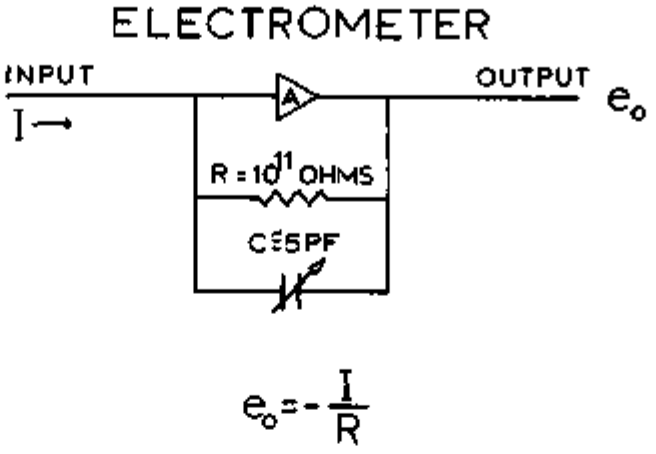

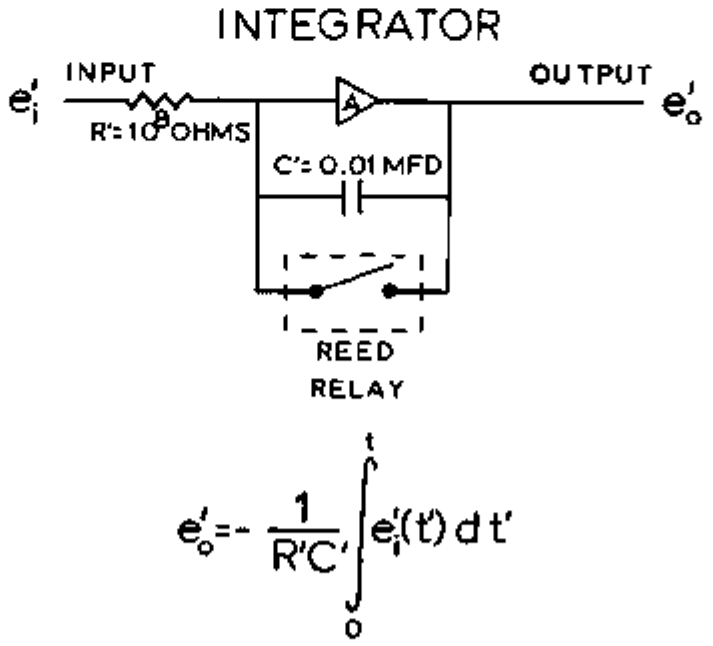

Figure 11: Diagram of Electrometer and Integrator Circuits

in the feedback loop which is shunted by a reed relay. The input resistor has a resistance of $10^8(\pm 10\%)$ ohms. The circuit obeys the equation

$$e_o'(t) = -\frac{1}{R'C'}\int_0^t e_i'(t')dt' \qquad (58)$$

where e_i' is the input voltage, e_o' is the output voltage, and again the gain of the amplifier is large and negative.[66] This integrating circuit has been calibrated, and R'C' was found to be 0.98 sec. The reed relay is operated by the speed control on the transmission which drives the turntable. The relay is normally closed. It opens when the turntable speed reaches zero at which point integration of the output of the electrometer begins.

6. Temperature Measurements

The vapor pressure of the liquid is measured with a 1/2" bore manometer containing Octoil-S.[67] The manometer is connected to the top of the inner Dewar by a one meter length of 3/4" o.d. copper refrigerator tubing. One side of the manometer is evacuated to pressures less than 1 micron of mercury by a vacuum pump.[68] The oil levels are measured with a cathetometer and can be measured to an accuracy of from ± 0.01 mm. to ± 0.02 mm.[69]

The lambda transition in liquid helium is easy to detect with the temperature regulating bridge. If the temperature of the liquid is rising slowly from below the lambda point,

the resistance of the germanium thermometer will be dropping smoothly. At T_λ the thermal conductivity of the liquid becomes very poor. The small amount of current passing through the germanium resistor heats the resistor above the temperature of the liquid helium, and the resistance suddenly drops. The regulator can be adjusted here so that when the resistance suddenly drops, the regulator will "over regulate" and put too little power into the heater in the bath. The high-speed vacuum pump, which has been pumping on the bath all along, then pulls the temperature of the liquid below the lambda point again before the regulator can react. The throttle valve between the vacuum pump and the inner Dewar is adjusted so that when the regulator has recovered, the temperature of the liquid starts to rise slowly again. In this way the liquid can be kept near the lambda point for long periods of time. During this period the vapor pressure of the liquid is measured along with the temperature of the region surrounding the oil in the manometer. The vapor-pressure tabulations of the 1958 Temperature Scale[70] (where T_λ = 2.1720°K) were used to determine the density of the oil at a particular room temperature. It is estimated that the total error associated with the measurement of the oil density is ±0.02%. The two parallel curves in Figure 12 represent the uncertainty in the temperature of the liquid helium bath produced by the above-mentioned ±0.02% error and by the errors in measuring

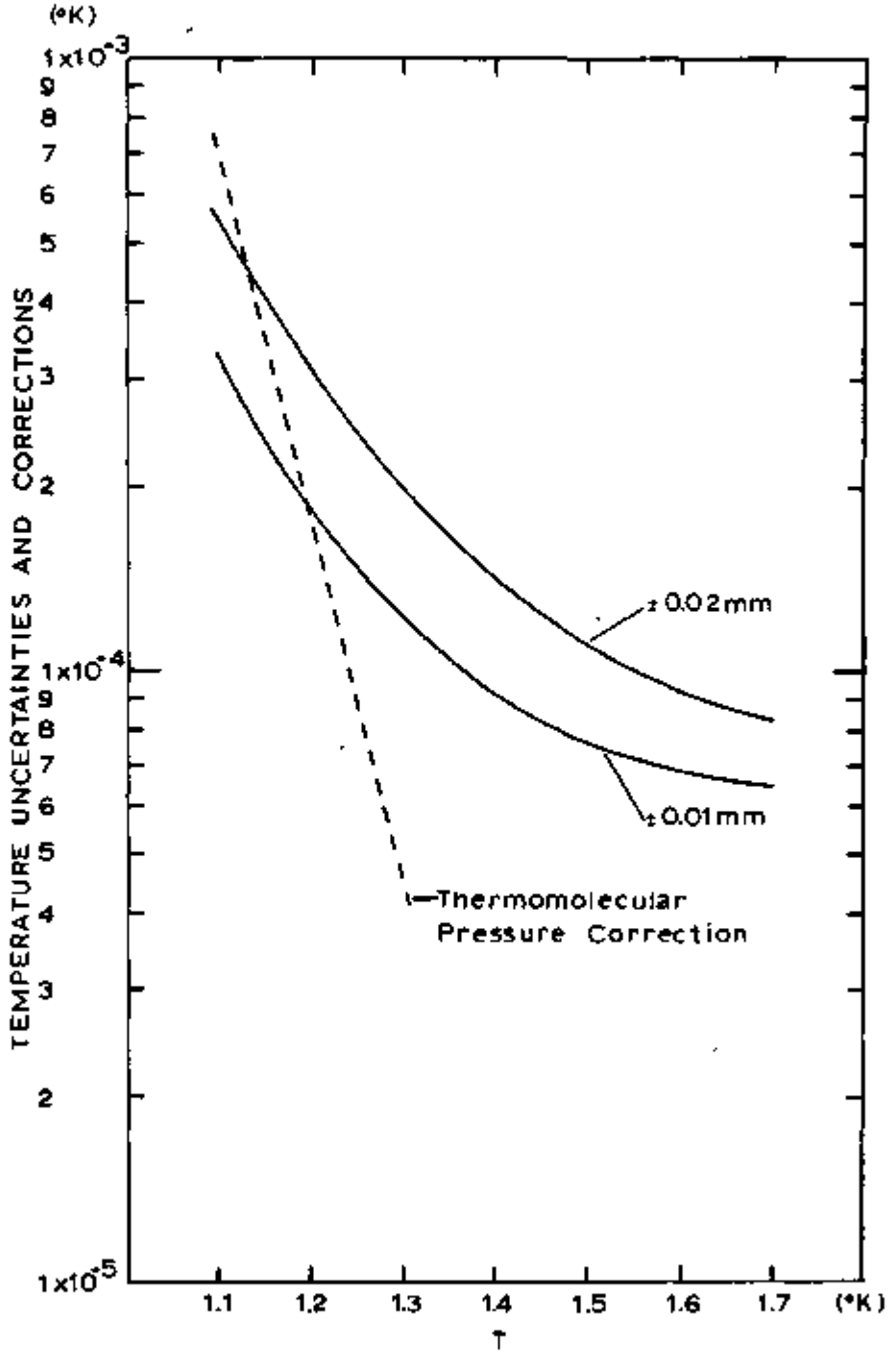

Figure 12: Temperature Uncertainties and Corrections

the oil levels in the manometer (±0.01 mm. to ±0.02 mm.) as a function of the temperature of the liquid.

There are two possible systematic errors. First, there may be a pressure drop between the liquid level and the top of the Dewar produced by the gas flow from the evaporating liquid. In order to check this, a 3/8" o.d. by 0.010" wall stainless steel tube open to the bath at the top of the pressure vessel and open to the top of the apparatus was attached to the 1" support tubes. A special coupling at the top of the inner Dewar made it possible to connect the manometer to the top of this tube when the apparatus was not rotating. At 1.6°K a pressure drop between the top of the Dewar and the liquid level of 1 micron of mercury was observed. At 1.1°K the drop was 21 microns of mercury. Thus all temperatures have been determined from the pressure measurements made with the manometer connected to the 3/8" tube. Second, there may be a significant thermomolecular pressure drop in this 3/8" tube at low pressures. The relevant parameters are tabulated by Roberts and Sydoriak, and the results are shown by the dotted line in Figure 12.[71] The indicated corrections are subtracted from the temperatures which have been determined from the pressure measurements made with the manometer connected to the 3/8" tube. It is these corrected temperatures which are tabulated in Appendix IV.

7. Experimental Procedure in Determining Lifetimes

As was mentioned at the beginning of this chapter, a sudden stop in rotation of a vessel containing superfluid liquid helium with trapped charge present brings about a release of this trapped charge. The released charge then moves in some manner under an applied electric field to the collector.

The experimental procedure for measuring the lifetime of the trapped ions consists of initially trapping in the rotating liquid a reproducible amount of charge. This is done by rotating the apparatus for 6 minutes at 60 rpm with negative ions travelling from the gate to the collector. A 6-minute rotation period appears to be long enough for the establishment of a stable vortex-line system with enough charge present to make lifetime measurements possible. During this period the low-speed chart recorder is monitoring the current to the collector. At the end of the 6-minute period the ion current is turned off by a reversal of the electric field between the source and the gate electrodes. After a variable waiting period during which the amount of trapped charge in the liquid is decaying exponentially in time according to $e^{-t/\tau}$ where τ is what we shall call the trapping lifetime, the rotation is suddenly stopped. Just before the rotation is stopped, the high-speed chart recorder is connected to the output of the electrometer; and the low-speed

chart recorder is connected to the output of the integrating circuit. The stop in rotation occurs in approximately 1/2 second. When the rotation speed control reaches zero rpm, the integrating circuit is activated. The charge remaining in the liquid is released, travels to the collector, and is measured by the integrating circuit. The above procedure is repeated several times with waiting periods of different lengths. The exponential decay of the trapped charge is measured out to a waiting time $t = 2\tau$.

The major source of error in determining the lifetime is the measurement of the trapped charge. The short lifetime measurements are the least accurate, for the amount of charge that can be trapped is less. Suppose for a current I going from the gate to the collector that ΔI is captured by the vortex lines. If no charge can leak out the ends of the vortex lines, then the amount of charge Q in steady state is

$$Q \triangleq \tau \Delta I \tag{59}$$

where τ is the lifetime of the trapped ion. Thus the final amount of charge is less for short lifetimes assuming that ΔI remains constant. The above expression is really only correct in the limit that the 6-minute rotation period is long compared to τ.

In Figure 13 are shown two plots of the experimentally-measured exponential decays of the trapped charge, representing the full range of lifetimes measured at saturated vapor

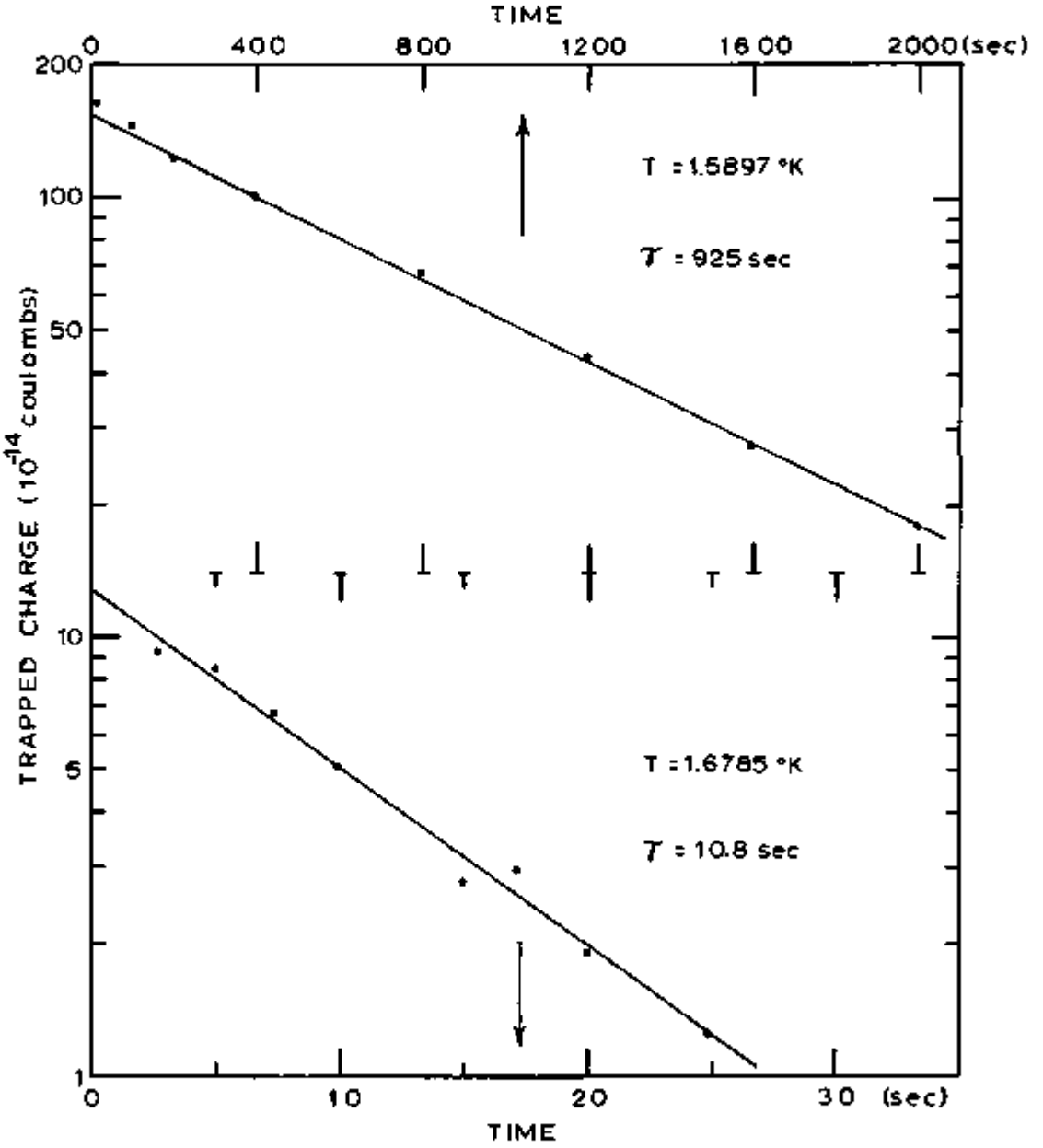

Figure 13: Decay in Time of Trapped Charge for Two Different Temperatures at Saturated Vapor Pressure

pressure. The larger errors associated with the shorter lifetimes is evident. The scatter of the data has two sources: First, one has the random-noise output of the electrometer. Second, occasionally when the rotating apparatus is suddenly stopped, the electrometer puts out a current pulse. This pulse appears to originate at the low-temperature end of the apparatus. It is thought to be either the result of a slight movement (during deceleration) of a conductor which is at a different potential than the electrometer input, or some piezoelectric effect associated with deceleration forces on the teflon insulators. These current pulses vary from day to day. During most of the runs, they were not observed. The high-speed chart recorder is used to check for these pulses. Finally, to miminize the effect of these pulses, the integrating circuit is not activated until the apparatus has come to rest. It is found that very little trapped charge is released from the liquid during the 1/2 second deceleration.

IV. RESULTS CONCERNING THE ROTATING STATE OF LIQUID HELIUM

Data which relate to some of the overall properties of charge trapped on an array of vortex lines are discussed in this chapter. Such overall properties include the build-up of trapped charge after the start of rotation, the decay in time of trapped charge after the stop of rotation, and the relationship between rotation speed and amount of charge trapped.

1. Trapped Charge Build-up

In Figure 14 a low-speed chart recording of the current to the collector as a function of time is presented. These data were taken at saturated vapor pressure with a measured lifetime for the trapped charge of 925 seconds and with a gate potential of -40 volts. The right-hand part of the recording represents the following sequence of events: First, the current between the gate and the collector was turned on. At the position of the arrow rotation at 60 rpm was suddenly initiated and maintained for 6 minutes. During this period the collector current began to decrease indicating that charge was being trapped in the liquid. At the end of the 6-minute rotation period, the current was turned off. (The low-speed chart recorder was kept connected to the output of the electrometer for these measurements.) After a 30-second waiting period the rotation was abruptly stopped. The trapped charge then ran out of the liquid with a characteristic pulse width

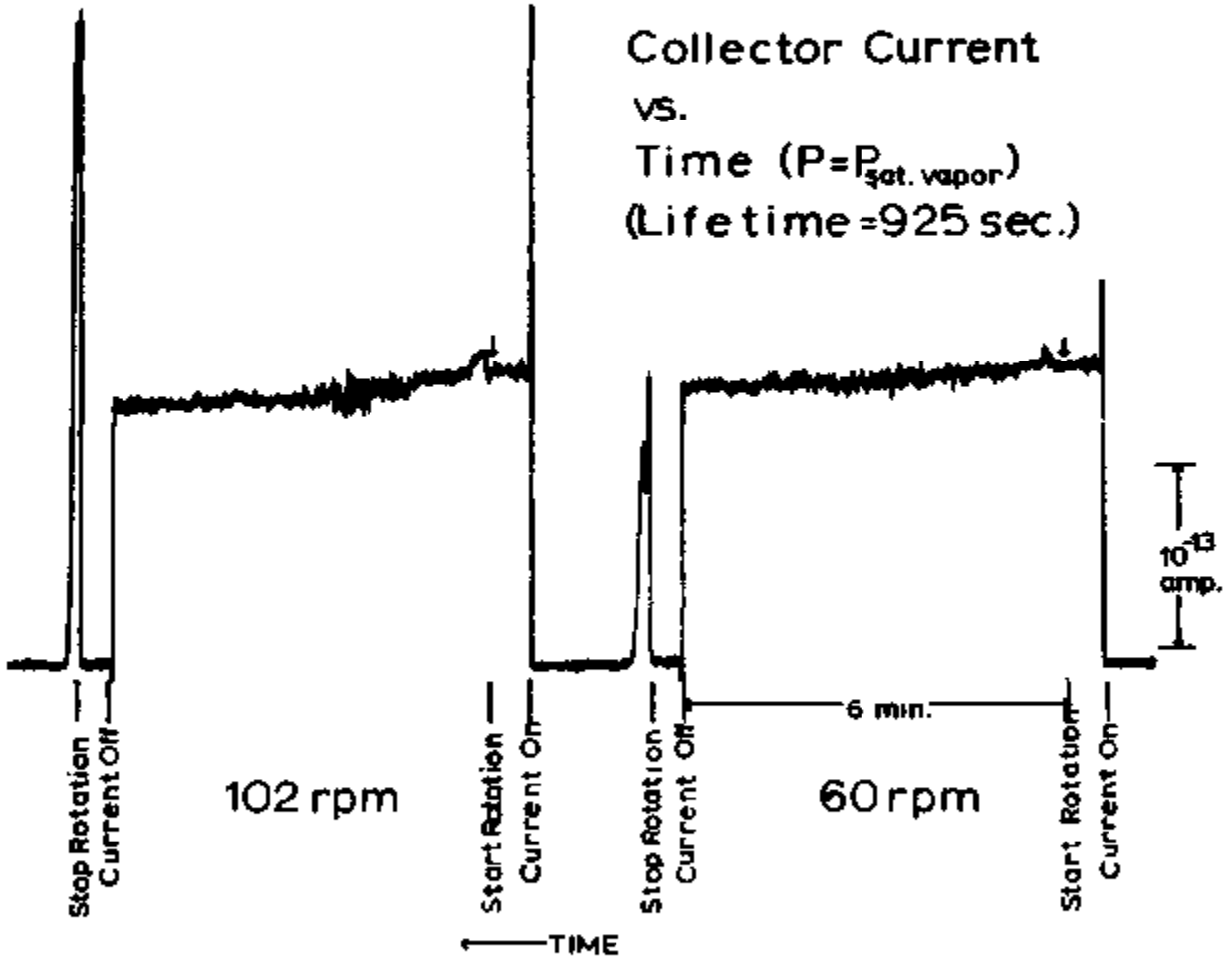

Figure 14: Collector Current as a Function of Time at Two Different Frequencies of Rotation

of approximately 15 seconds. The left-hand part of the recording is an exact repeat except that the rotation speed was 102 rpm instead of 60 rpm. In the left-hand chart trace the increased vortex-line density which is brought about by the increased rotation speed is evidenced by the greater decrease in the collector current and the larger amount of released trapped charge. Also note that the pulse width for the release of the trapped charge after rotation at 102 rpm is shorter than the pulse width after the 60-rpm rotation.

In Figure 15 the left-hand curve is a plot of the build-up of trapped charge in the liquid as a function of time after the start of the 60-rpm rotation. The measured lifetime at saturated vapor pressure was 925 sec and the gate potential was -40 volts. The build-up of the trapped charge was measured in the following way. The apparatus was set into rotation with the collector current turned on. After a certain length of time had elapsed, the current was turned off. A 10-second waiting period then followed at the end of which the rotation was abruptly stopped and the amount of trapped charge released was measured. The same procedure was repeated several times for different lengths of time between the starting of the rotation and the turning off of the collector current. The arrow along this curve points to the amount of trapped charge in the liquid after 6 minutes of rotation. The right-hand curve in Figure 15 is a plot of the trapped-charge build-up with the apparatus rotating for

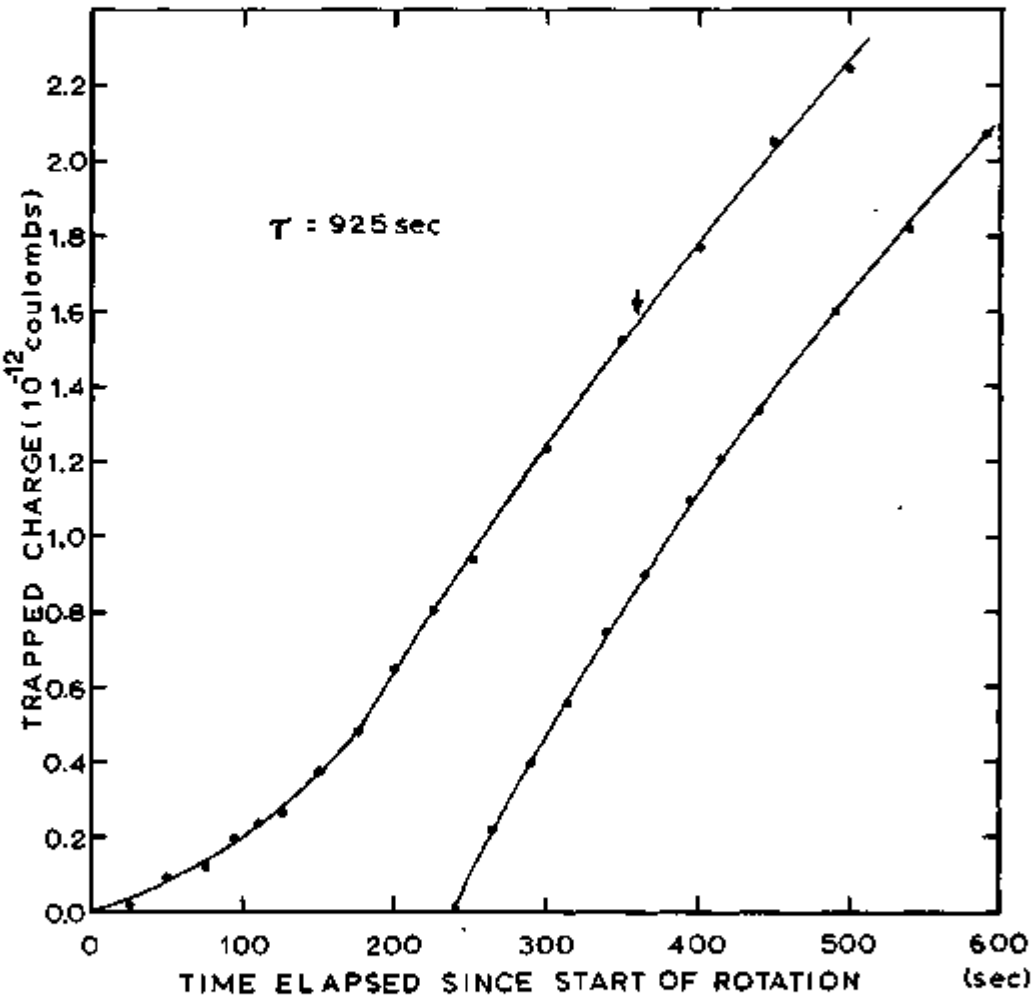

Figure 15: Trapped Charge Build-up as a Function of Time

4 minutes before the collector current was turned on.

If σ is the cross section for capture of an ion by a vortex line, N the vortex-line density (per unit area), J(r) the radial current density, and τ the lifetime of the trapped ion; the following equation describes the time development of the trapped-charge density for the case where charge is not leaking out of the ends of the vortex lines:

$$\frac{\partial \rho}{\partial t} = J(r)N\sigma(r) - \frac{\rho}{\tau} . \tag{60}$$

Assuming that during the early stages of the charge build-up ρ/τ can be neglected, we have

$$\frac{\partial \rho}{\partial t} = JN\sigma(r). \tag{61}$$

It is observed experimentally that σ depends upon the applied electric field strength.[72] In our cylindrical geometry we have $E \propto 1/r$, so σ depends upon position. Let a be the radius of the gate, and let b be the radius of the collector. The rate of the build-up of trapped charge can be expressed in the form:

$$\frac{dQ(t)}{dt} = 2\pi L \int_a^b rJ(r)N(t)\sigma(r)dr \tag{62a}$$

$$\cong I_{ave}\, N(t) \int_a^b \sigma(r)dr \tag{62b}$$

where L represents the effective length of the charge distribution along the z axis of the cylindrical-electrode system.

Thus we see that the rate of charge build-up in the liquid is a measure of both N and σ.

We interpret the region of positive curvature in the left-hand curve in Figure 15 as a period during which the density of the vortex lines is increasing. The curvature then becomes negative after approximately 175 seconds of rotation. This region of negative curvature appears to have the same shape as the right-hand curve which represents the case of a 4-minute rotation before the collector current is turned on. This similarity in shape suggests that the vortex line density may reach its maximum and stable value after approximately 175 seconds of rotation.

The following is offered as an explanation of the existence of a region of negative curvature: The rate at which charge is being trapped is constant once N is stable and is expressed by the term $J(r)N\sigma(r)$ in Equation (60). As the density of trapped charge builds up, the term ρ/τ can no longer be neglected. Therefore, as ρ increases, $\frac{\partial \rho}{\partial t}$ will decrease as is observed in Figure 15. At shorter lifetimes the establishment of a maximum charge density (where $\frac{\partial \rho}{\partial t} = 0$) has been observed experimentally.

The initial slope of the right-hand curve should provide an estimate of the cross section. This slope is 8.3×10^{-15} amperes. Tanner has recently measured σ and finds in the region of interest that $\sigma \propto 1/E$ where E is the applied electric

field.[73] For our geometry we have $E \propto V[r\ell n(b/a)]^{-1}$ where V is the potential difference between the gate and the collector. Hence, $\sigma \propto r$. This relation is now used in Equation (62b), and the result is

$$\sigma_{effective} \cong \frac{\frac{dQ}{dt}}{N(b - a)I_{ave}} \tag{63}$$

where σ_{eff} corresponds to a cross section measured at an effective field of

$$E_{eff} = \frac{2V}{(b + a)\ell n(b/a)} . \tag{64}$$

For a gate potential of 40 volts, E_{eff} is 33 volts cm^{-1}. Let us assume that the trapped-charge distribution is uniform. Then we have $\frac{dQ}{dt} = \frac{1}{y}\, 8.3\times10^{-15}$ amperes where y is the correction factor discussed in Section 4 of Chapter III and equals 0.34. With $I_{ave} = 1.55\times10^{-13}$ amperes (from the right-hand recording in Figure 14) we obtain $\sigma_{eff} = 1.1\times10^{-5}$cm. Tanner obtains at 1.6°K and 33 volts cm^{-1} approximately $\sigma \cong 1.3\times10^{-5}$cm. Our result is in reasonable agreement with Tanner's.

The assumption of a uniform charge density can be made plausible. For ρ/τ small we can use Equation (61). Now we have that $J(r) \propto 1/r$, $\sigma \propto 1/E \propto r$, and N is a constant. Hence, $\frac{\partial \rho}{\partial t}$ is very nearly a constant independent of r.

2. Charge Release Upon Cessation of Rotation

Presented in Figure 16 are high-speed chart recordings of the collector current upon cessation of rotation for various

rotation speeds at saturated vapor pressure with a measured lifetime of 925 seconds. The electrometer was adjusted to have a response time of approximately 0.2 seconds for the measurements. The experimental procedure for the upper four graphs consisted of rotating at the indicated frequency for 6 minutes with the collector current on and with a gate potential of - 40 volts. The collector current was turned off at the end of the 6-minute period. A 30-second waiting period then followed during which the high-speed chart recorder was activated. At the end of this 30-second waiting period, the rotation was abruptly stopped.

The general features of the upper four graphs are these:

1. The amount of charge released increases as the rotation frequency increases. This reflects the fact that the density of vortex lines is proportional to the rotation frequency.

2. The length of time it takes the charge to leave the liquid is longer at slower rotation speeds.

3. Superimposed upon the current pulses are oscillations the first few cycles of which have the same frequency as the rotation frequency. The two vertical lines on each graph have a separation equal to the period of rotation. The first line is placed opposite the first peak of this superimposed oscillation; the second line in all cases falls opposite the second peak of this oscillation. The

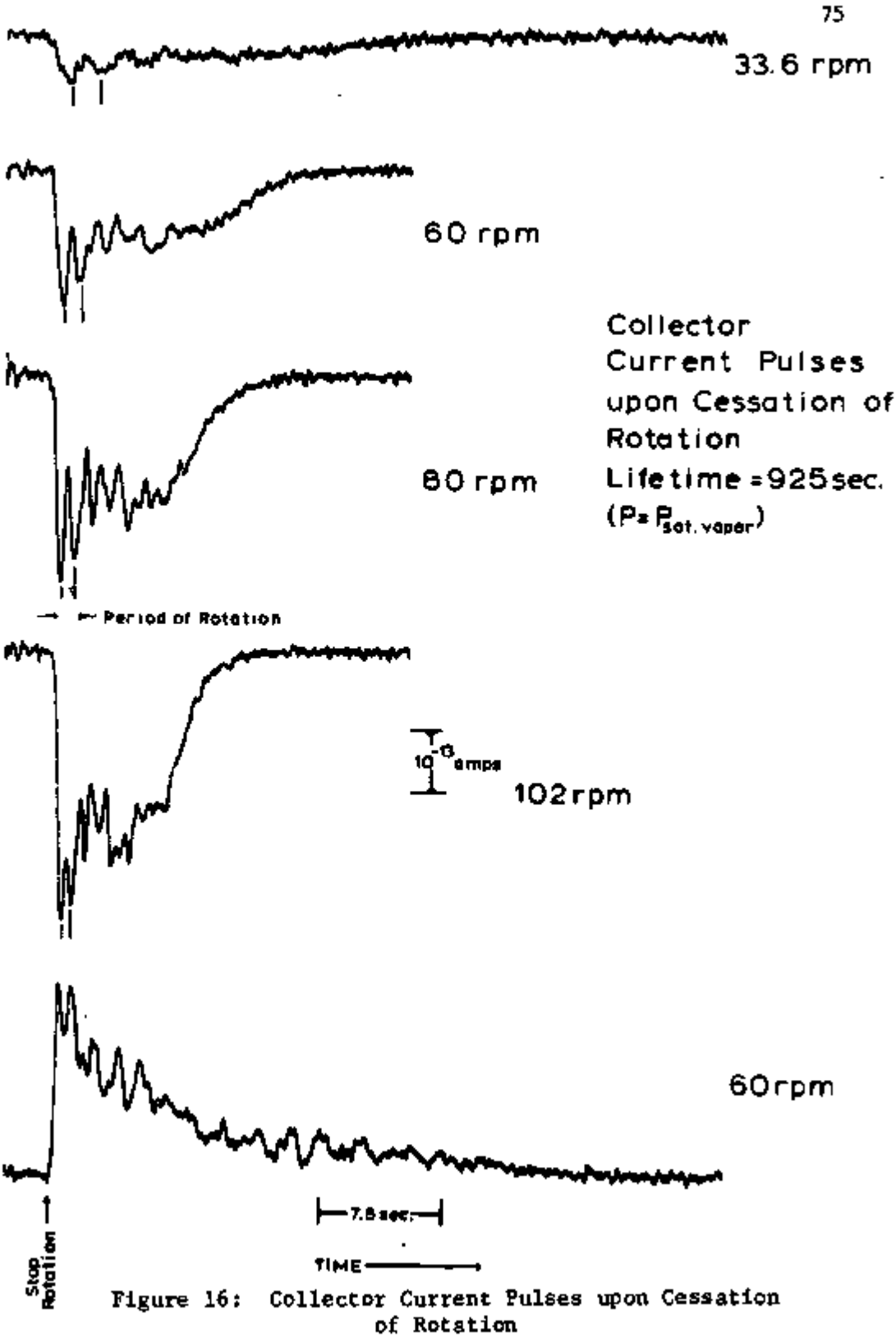

Figure 16: Collector Current Pulses upon Cessation of Rotation

origin of these oscillations is not known at the present time.

In connection with Item #2, experiments were performed at 60 rpm under the same conditions which apply to these graphs. However, approximately 5 seconds after the rotation had been stopped, the apparatus was suddenly set into rotation in the direction opposite to the original 60-rpm rotation. It was observed that the remaining charge in the liquid was released in a time period (2 to 3 seconds) which was shorter than the time it would have taken the remaining charge to leave the liquid had the rotation not been reversed. Another experiment performed in conjunction with these results consisted of rotating the liquid at 60 rpm (5 seconds after the stop in rotation) in the same direction as the original 60-rpm rotation. When this 60-rpm rotation was re-started, the rate at which charge ran out of the liquid was immediately reduced to a value smaller than the rate observed when the rotation was not re-started. This rate tapered off to zero in about 50 seconds. A stop in rotation about 20 seconds later showed that charge was still trapped in the liquid. Hence, rotation in the same direction kept some of the remaining trapped charge from leaving the liquid.

At the present time the mode of decay of the vortex line system with the release of trapped charge is not well understood. It is hypothesized that a sudden stop or reverse in

rotation causes vortex lines to be created at the walls of the container and fed into the liquid which, on the average, have circulations opposite to the circulations of the vortices already present in the rotating liquid. The normal fluid provides a dissipative medium in which vortex lines of opposite circulations can approach one another. The vortex lines of opposite sign, then, probably annihilate each other and release the trapped charge. In the case where rotation is re-started in the same direction as the rotation during the 6-minute charging period, it is probable that vortex lines are fed into the liquid whose circulations have, on the average, the same polarity as the vortex lines present in the liquid at the end of the 6-minute period. One would expect the rate of charge release to drop since this "new" vorticity would tend to destroy the vorticity of opposite circulation (produced by the stop in rotation) which is probably responsible for the charge release.

The velocity field of the normal fluid after stopping must also be considered, for any motion of the normal fluid relative to the vortex lines will produce forces on these vortex lines. In particular, during deceleration there may be secondary flow of the normal fluid produced by "end wall instabilities" due to the interaction of the normal fluid with the end plates of the electrode system. Such secondary flow of the normal fluid will produce forces on the vortex lines

which may affect the decay of the vortex-line system.

Our observation based on ion behavior that it takes much longer to set liquid helium into steady rotation (175 sec) than it takes to decelerate the liquid (≈15 sec) are in general agreement with those of others.[74]

The trace at the bottom of Figure 16 is a recording of the charge release upon cessation of rotation with the electric field between the gate and the collector reversed. This field reversal was performed at the end of the 6-minute, 60-rpm rotation period. The electrical forces on the negative ions, then, were directed toward the gate. In Figure 8b in the last chapter the electric field lines are shown for this configuration. The polarity of the trace in Figure 16 indicates that trapped negative ions appear to move along the field lines to the gate when they are released. The amount of charge which appears to pass through the electrometer during the release of the trapped charge to the gate with a reversed field is larger than the amount of trapped charge collected at the collector when the field between the gate and the collector is in its normal direction. This effect is expected since the electrometer "sees" only the change in the induced charge on the surface of the electrodes. In the previous chapter it was estimated that 34% of the induced charge would be on the gate and 66% on the collector for a uniform density of trapped charge in the liquid. The ratio of charge collected (as measured by

the electrometer) for the two directions of the electric field is then

$$\frac{\text{(charge collected at gate)}}{\text{(charge collected at collector)}} = \frac{66\%}{34\%} = 1.94 \ . \qquad (65)$$

The ratio experimentally is 1.7 for the 60-rpm traces in Figure 16. There are several plausible reasons why the above estimate might not be accurate. One is that the trapped charge distribution may not have been uniform. Another is that no account has been taken of the induced charge on the guard rings and on the end plates. Suppose that the charge distribution is uniform and that the amount of induced charge on the end plates is negligible. The collector electrode does not extend the full length of the electrode system. As the trapped charge builds up, some of the induced charge may appear on the guard rings. Let the ratio of the total induced charge on the guard rings and the collector to the induced charge on the gate be 1.94. The amount of induced charge on the guard rings need only be 4% of the total trapped charge to give the experimentally observed ratio of 1.7.

It is not understood why the length of time required for the release of the charge in the reversed electric-field case is over two times longer than the time required for the release of the charge with the field in its normal direction.

3. The Amount of Trapped Charge and the Rotation Speed

Measurements of the amount of charge trapped in the liquid

after 6 minutes of rotation are presented in Figure 17 as a function of the rotation speed. These measurements were made at T=1.6355°K and at saturated vapor pressure with a gate potential of -40 volts, and they were generally made 10 seconds after the collector current was turned off. The measured lifetime of 105 sec was used to extrapolate the measured amount of trapped charge back to time t=0 when the collector current was turned off. The measurements of the trapped charge for rotation speeds under 20 rpm include a reversal of rotation after the stop of rotation. As pointed out before, the length of time for release of charge becomes longer the slower the rotation speed. For speeds under 20 rpm these times were so long that the drifts in the electrometer circuit during integration caused large errors. The rotation was reversed in order to shorten the time for release of the trapped charge. The error bar on the 4-rpm measurement covers the range of three measurements at this speed; at higher speeds the scatter in repeated measurements was much less.

The linear relationship between the initial charge trapped in the liquid and the rotation speed is striking. Such a linear relationship is expected since the density of vortex lines is assumed to be a linear function of the rotation speed.

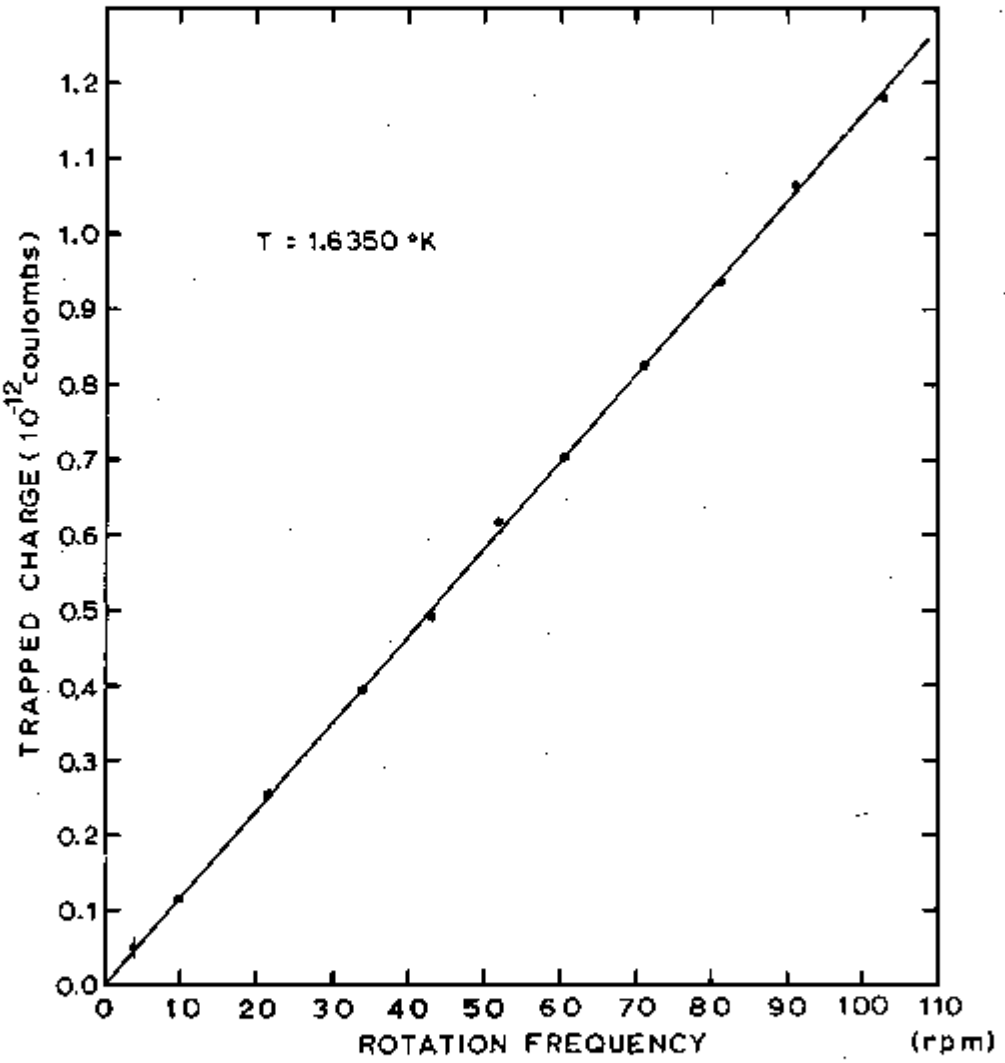

Figure 17: Charge Trapped in Liquid vs. Rotation Frequency

V. PRESENTATION AND DISCUSSION OF LIFETIME DATA AT SATURATED VAPOR PRESSURE

1. Presentation of Lifetime Measurements at Saturated Vapor Pressure

In Figure 18 the lifetimes are plotted logarithmically with respect to the reciprocal of the absolute temperature at saturated vapor pressure for various values of the gate potential. For the present we shall concentrate on the data taken at a gate potential of - 40 volts. The data are tabulated in Appendix II.

As predicted by Equation (54), the lifetime does depend exponentially upon 1/T. This equation is repeated here

$$\tau = \frac{F_o}{\rho_s(T)} e^{-\frac{\Delta}{T}} e^{\frac{f(R)\rho_s(T)}{T}} \qquad (66)$$

where $\Delta = 8.1°K$. One might be tempted to infer directly from the slope of the data on Figure 18 that $f(R)\rho_s(T) = 130°K$. However, over the temperature range indicated on this graph, ρ_s changes by about 7%. It is essential to take this temperature dependence of ρ_s into account in determining $f(R)\rho_s(T)$ from the slope of $\ln\tau$ vs. 1/T.

The slope of the data in the graph is expressed by the equation

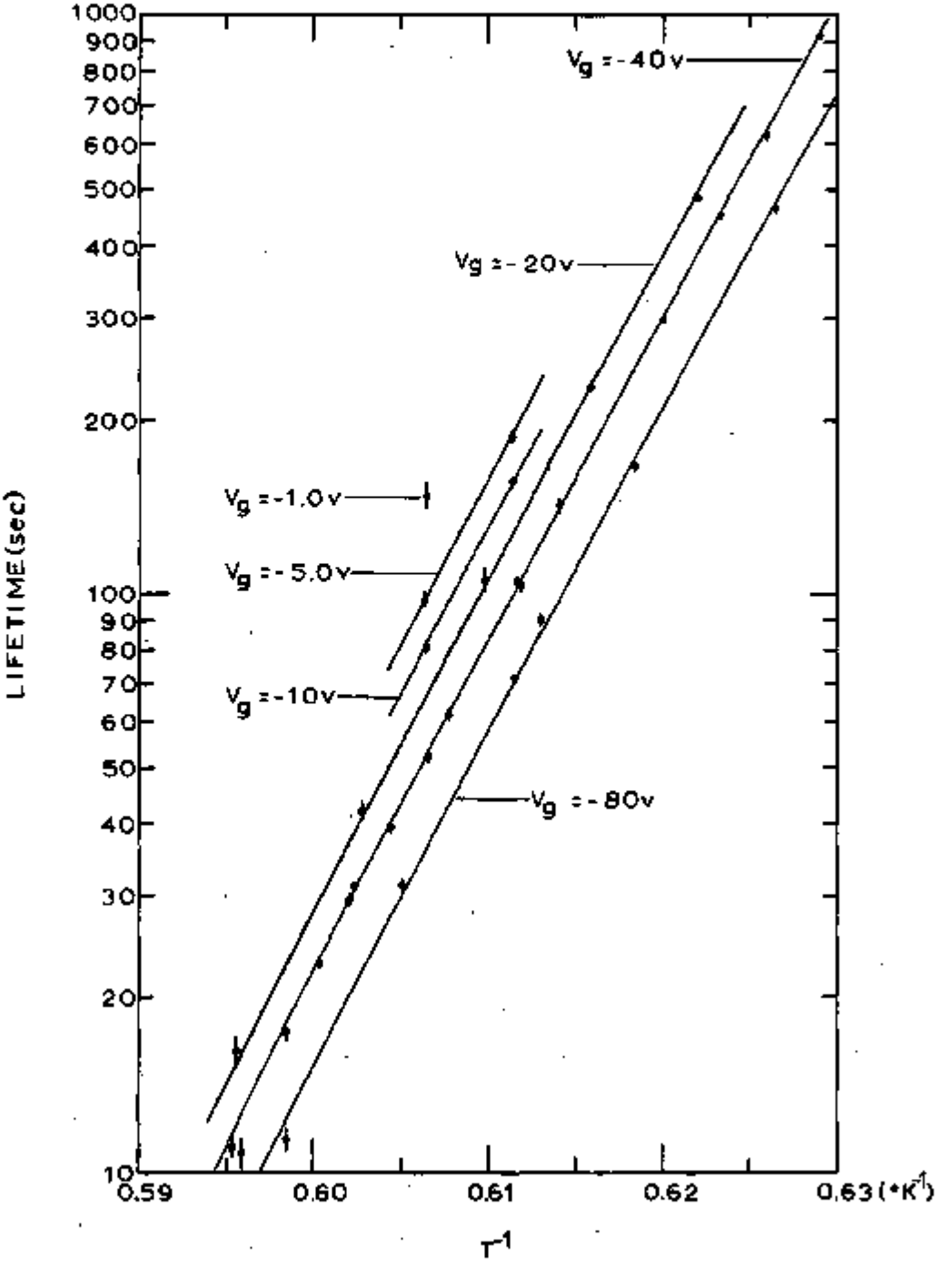

Figure 18: Lifetime of Trapped Negative Ions vs. 1/T at Saturated Vapor Pressure for Several Gate Potentials

$$\frac{d\ell n(\tau)}{d(1/T)} = f(R)\rho_s(T) + \frac{f(R)}{T}\frac{d\rho_s(T)}{d(1/T)} - \Delta - \frac{d\ell n[\rho_s(T)]}{d(1/T)} \qquad (67a)$$

$$= f(R)\rho_s(T)\left[1 + \frac{d\ell n[\rho_s(T)]}{d\ell n(1/T)}\right] - \Delta$$

$$- T\frac{d\ell n[\rho_s(T)]}{d\ell n(1/T)} . \qquad (67b)$$

Now experimentally at T=1.65°K [see Equation (73) at the end of this section] we have

$$\frac{d\ell n[\rho_s(T)]}{d\ell n(1/T)} \cong 1.2, \qquad (68a)$$

and therefore

$$f(R)\rho_s(T) \approx \frac{130°K+8°K+2°K}{2.2} \cong 64°K. \qquad (68b)$$

The curve drawn through the - 40-volt data in Figure 18 is the result of a least-squares computer-calculated fit of Equation (66) to the data where F_o and f(R) are the two adjustable parameters. The results are

$$f(R) = 507.4\pm1.9°K\ cm^3gm^{-1}$$

and

$$F_o = (1.78\pm0.25)\times10^{-13}sec\ cm^3gm^{-1}.$$

See Appendix II for discussion and tabulation of the computer calculations.

The - 40-volt data do not quite fall on a straight line.

Instead they have a slightly negative curvature. The computer-calculated curve also has a slightly negative curvature. It appears that this negative curvature is caused by the temperature dependence of the superfluid density.

Attempts were made to see if the least-squares fit could be improved by varying Δ over the range from 0 to 30°K. F_o and f(R) changed, of course, but unfortunately no statistically significant change in the fit occurred. For the reasons outlined in Chapter I, Δ has been chosen, then, to be 8.1°K.

Compared in Figure 19 are the lifetime measurements at saturated vapor pressure of R. L. Douglass and our computer-calculated curve for the - 40-volt data.[75] The slopes agree well, and it is the slope which determines the radius of the ion. This agreement provides an independent check of the validity of our sudden-stop-in-rotation technique. The disagreement in magnitude will be discussed in a later section.

Since the value of f(R) is extremely sensitive to the assumed temperature dependence of the superfluid density, it is quite important to state exactly what temperature dependence has been assumed. Some recent determinations of the normal fluid density ρ_n are presented in Figure 20. The natural log of ρ_n (in gm cm^{-3}) is plotted as a function of 1/T in this graph. In the Landau model for liquid helium the normal fluid density is expected to satisfy the relation

$$\rho_n \propto e^{-\frac{9°K}{T}} \tag{69}$$

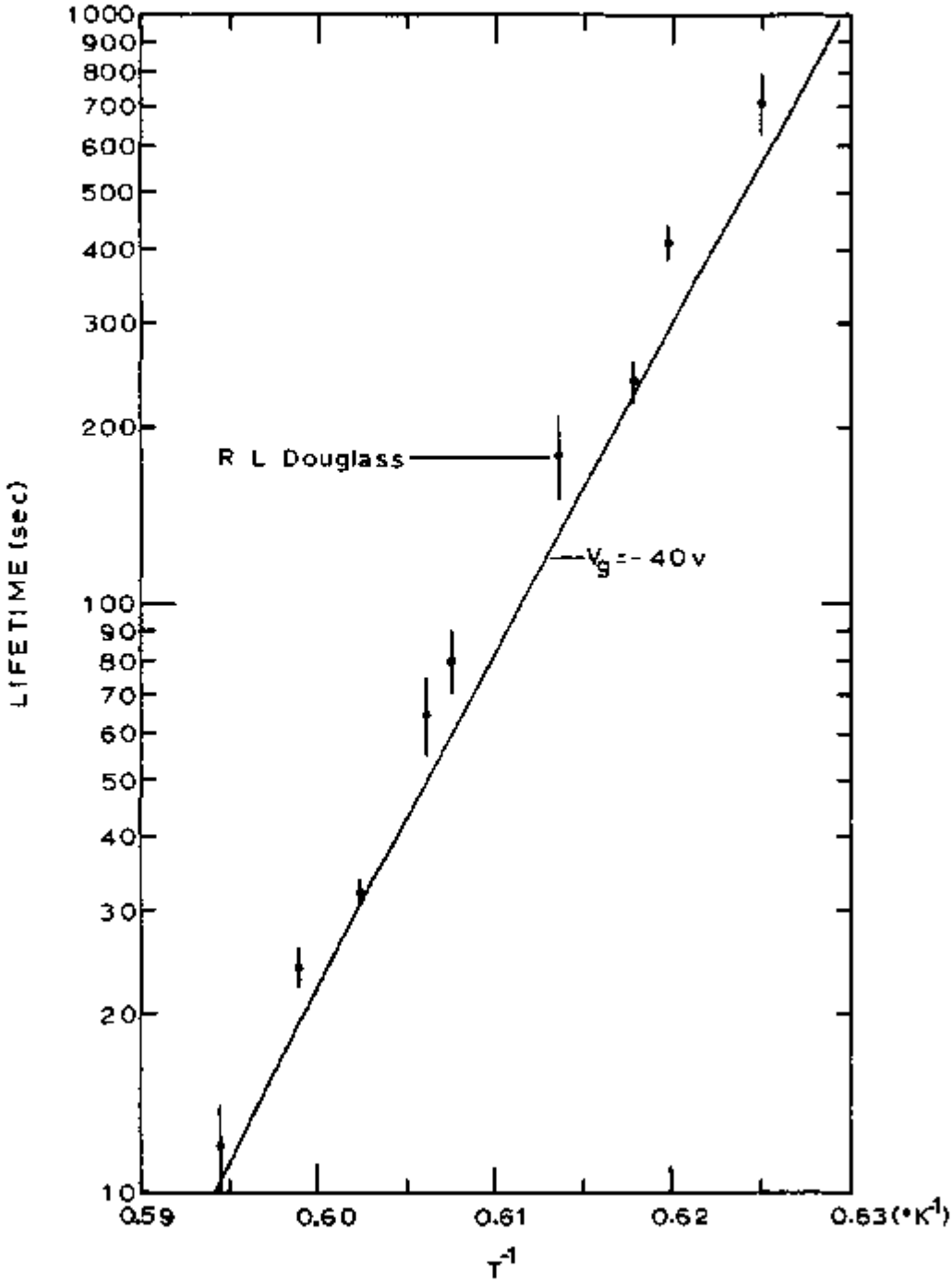

Figure 19: Comparison of Lifetimes for V_g = - 40 volts with Those of R. L. Douglass

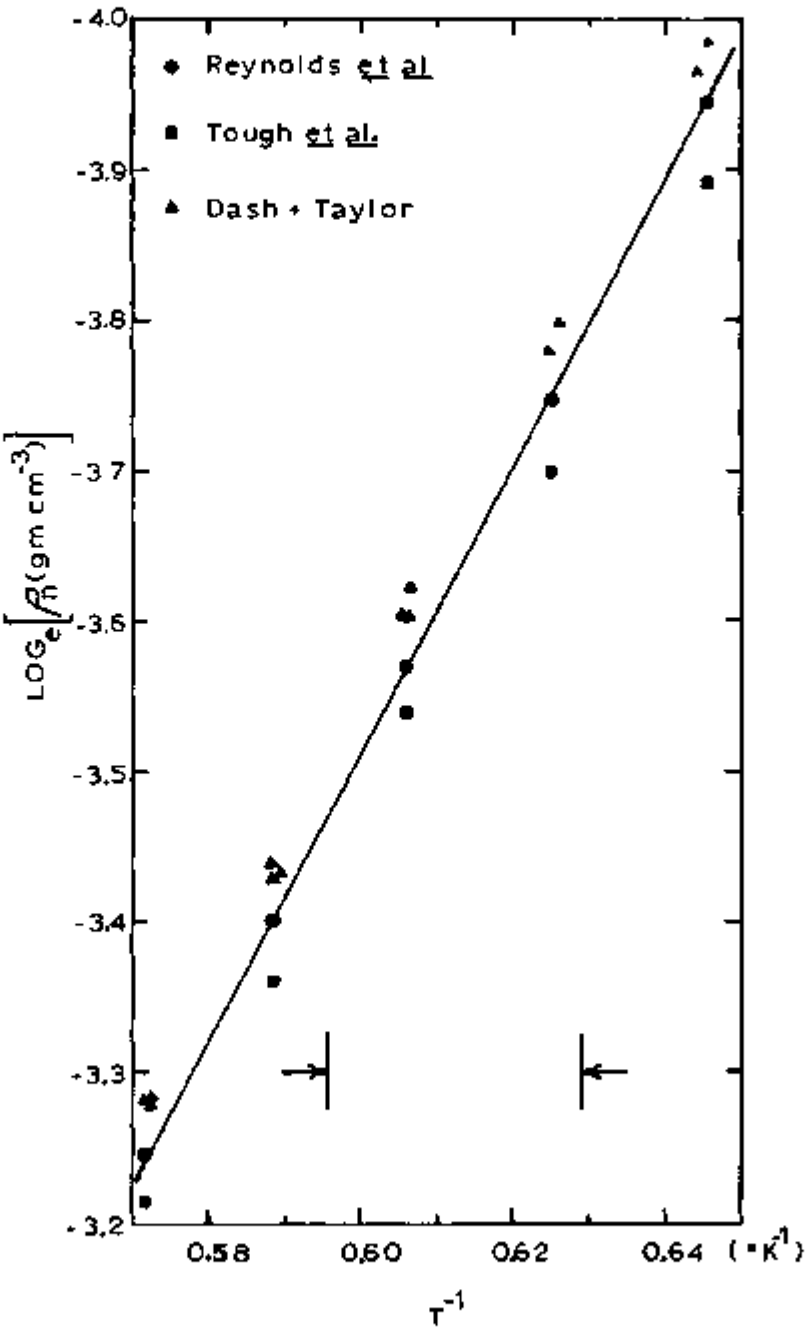

Figure 20: Natural Log of the Normal Fluid Density vs. 1/T

in this temperature range. The circles represent a recent calculation of the normal fluid density by Reynolds *et al.*[76] using the relation

$$\rho_n = \frac{\rho}{1 + \frac{C_V U_{II}^2}{TS^2}} \tag{70}$$

where ρ is the total density, C_V the specific heat per unit mass at constant volume, S the entropy per unit mass, and U_{II} the second sound velocity. The squares are the results of an earlier calculation by Tough *et al.* using Equation (70).[77] The triangles on the other hand represent a direct experimental measurement of ρ_n by Dash and Taylor employing the Andronikashvili-disk method.[78,79] All three results which are plotted on this graph, fortunately, have approximately the same temperature dependence.

The superfluid density ρ_s is defined to be

$$\rho_s = \rho - \rho_n. \tag{71}$$

Over the short temperature range of interest in this experiment, ρ does not vary appreciably. Thus most of the temperature dependence of ρ_s comes from the temperature dependence of ρ_n. The total fluid density is generally a factor of five larger than the normal fluid density in the temperature region of interest. Hence, the ±5% discrepancy between various determinations of ρ_n produces only a ±1% uncertainty in ρ_s. The data of Reynolds *et al.* have been adopted for the analysis

presented in this thesis.

The following formula falls on the line drawn through the data of Reynolds *et al.* in the region indicated between the arrows, which corresponds to the temperature interval over which the lifetime data was taken at saturated vapor pressure:

$$\rho_n = 8.75\, e^{-\frac{9.47^\circ K}{T}}\ \text{gm cm}^{-3}. \tag{72}$$

For the superfluid we have

$$\rho_s = 0.14520 - 1.6\times10^{-3}\left(\frac{1^\circ K}{T} - 0.6250\right) - 8.75\, e^{-\frac{9.47^\circ K}{T}}\ \text{gm cm}^{-3} \tag{73}$$

where ρ was interpolated from the data of Kerr and Taylor.[80]

2. Discussion of Lifetime Data at Saturated Vapor Pressure

Using the equation developed in Chapter II concerning the relationship between $f(R)\rho_s$ and the "depth of the well" $[U(0) - U_c]$ with an average applied electric field of 36 volts cm^{-1}, one obtains for $f(R) = 507.4^\circ K\ \text{cm}^3\text{gm}^{-1}$ that the radius of the ion is

$$R = 19.5\pm0.6\ \text{Å}.$$

Most of the assigned error of ±0.6 Å is due to the uncertainty in the healing length d of the core of the vortex line where $d = 1.46\pm0.14$ Å. Here, the average applied electric field is defined in the following way:

$$E_{ave} = \frac{V_g}{b - a} \tag{74}$$

where V_g is the gate potential (- 40 volts) and b - a is the distance between the gate and the collector in centimeters.

Using Equations (53), (33b), and (66) we can define the quantities $\tau_{experimental}$ and $\tau_{theoretical}$ to be

$$\tau_{ex} = \frac{F_o}{\rho_s} e^{-\frac{8.1°K}{T}} \quad \text{and} \quad \tau_{th} = \frac{2\pi\beta}{\omega_o^2\sqrt{3}} \tag{75}$$

At 1.6°K we have

$$\tau_{ex} = 9.4\times10^{-15} \text{ sec,}$$

and

$$\tau_{th} = 1.0\times10^{-10} \text{ sec.}$$

A difference of four orders of magnitude! That is, the lifetime of the trapped ions is four orders of magnitude shorter than would be expected theoretically for an ion of radius 19.5 Å. However, from the discussion of the trapping well in Chapter II it can be seen that the parameter ω_o is not well known. At 1.6°K the estimate for ω_o by Parks and Donnelly is 1.2×10^{10} sec^{-1}, which can be expressed in the form $\frac{\hbar\omega_o}{k} = 0.09°K$.

In order to decrease τ_{th} by four orders of magnitude, one could increase ω_o by two orders of magnitude; $\frac{\hbar\omega_o}{k}$ would then equal 9°K. This means that the ion would have a quantum-mechanical zero-point energy 9°K above the bottom of the trapping well. Thus, if one is to adjust the theoretical results by increasing ω_o, then quantum-mechanical corrections

must be taken into account. These corrections are calculated in Appendix III. Only the results will be presented here. They are that

$$\tau = \tau_{th} \frac{\left[\frac{\hbar\omega_o}{kT}\right]^2}{\left[1 - e^{-\frac{\hbar\omega_o}{kT}}\right]^2} e^{\frac{f(R)\rho_s}{T} - \frac{\hbar\omega_o}{kT}} . \tag{76}$$

In the limit that $\frac{\hbar\omega_o}{kT} \to 0$ this expression becomes equal to the the classical result, Equation (53). The temperature dependence of this equation can be expressed in the form:

$$= \frac{F_o}{\rho_s(T)} \left[\frac{\frac{\theta'}{T}}{1 - e^{-\frac{\theta'}{T}}}\right]^2 e^{\frac{f(R)\rho_s(T)}{T} - \frac{8.1°K}{T} - \frac{\theta'}{T}} \tag{77}$$

where $$\theta' = \theta'_o \left[\frac{\rho_s(T)}{\rho_s(T_o)}\right]^{\frac{1}{2}} = \frac{\hbar\omega_o}{k} . \tag{78}$$

T_o was chosen to be 1.63°K. This equation was fitted in the same way as before by a computer to our - 40-volt data where the adjustable parameters F_o and f(R) were determined for various values of θ'_o. In Appendices II and III the results of these computations are tabulated.

It turns out that $\theta'_o = 7.6°K$ brings τ_{th} into agreement with τ_{ex} and yields the values

$$f(R) = 525.0 \pm 1.9 °K\ cm^3 gm^{-1}$$

and $$F_o = (2.70 \pm 0.37) \times 10^{-13}\ sec\ cm^3 gm^{-1}.$$

For the above value of θ'_o, $\tau_{ex} = \tau_{th} = 1.41 \times 10^{-14}$ sec at 1.6°K.

Hence, we now have agreement between the theoretical and experimental factors in front of the exponent in Equations (76) and (77) for $\theta_o' = 7.6°K$. The radius of the ion for this value of θ_o' with an average electric field of 36 volts cm^{-1} is

$$R = 20.0 \pm 0.6 \text{ Å}.$$

If for some reason τ_{th} were increased by a factor of ten (say if β were made larger), the value of θ_o' at which $\tau_{th} = \tau_{ex}$ would be 14.1°K implying a radius of $R = 20.6 \pm 0.6$ Å. For all that has been considered above, the fit of Equation (77) to the data is statistically no better than the fit of the classical equation [Equation (66)] which gave R = 19.5 Å.

The use of this large value of ω_o is very much open to question. A large ω_o implies that a large force is needed to move the ion just a small distance off center on the vortex line. Unfortunately, we have found no strong physical reasons for such a large hydrodynamic force to exist.

3. Dependence of Lifetime Upon Applied Electric Field

The lifetime measurements for various applied electric fields are also presented in Figure 18. The potentials of all the electrodes were scaled according to the ratio of the actual gate potential to the - 40-volt gate potential. In this way the confining-field configuration was not altered; only the magnitude of the fields was changed. The curve drawn through the data for each gate potential is identical to the curve of best fit drawn through the - 40-volt data except for a scaling

factor. These curves seem to fit the data quite well.

According to the models already presented, an increase in the applied electric field should reduce the lifetime of the trapped negative ion. That is, an increase in electric field changes the shape of the lip of the trapping potential well in such a way as to make the depth of the well smaller. The data appear to be in qualitative agreement with this prediction. The exponential factor used in fitting the - 40-volt data has magnitude e^{30}. Small percentage changes in the depth of the well (for example 1/2%) produced by a change in the electric field will appear primarily as a shift in the magnitude of the lifetime ($e^{0.15} = 15\%$). This observation is offered as a partial explanation of why the curve of best fit drawn through the - 40-volt data need only be changed by a multiplicative factor and not in slope in order to fit the data taken at different voltages.

In Figure 21 the lifetimes are plotted as a function of applied electric field at 1.65°K. The data have been scaled by a common multiplicative factor for the purpose of comparison with certain theoretical predictions. The lifetime measurements at - 20 volts and - 80 volts were interpolated from the curves drawn through the data points for these two potentials in Figure 18. The applied electric field was chosen to be the average of the electric field between the gate and the collector [see Equation (74)].

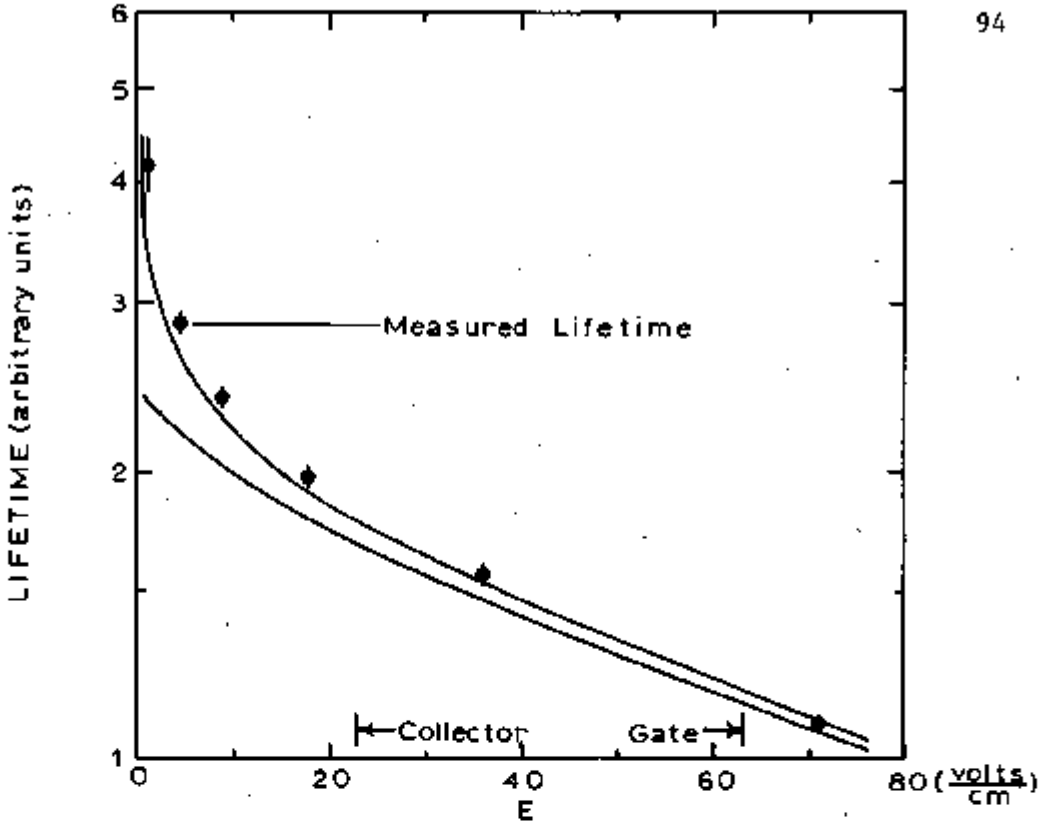

Figure 21: Lifetime vs. Applied Electric Field at Saturated Vapor Pressure

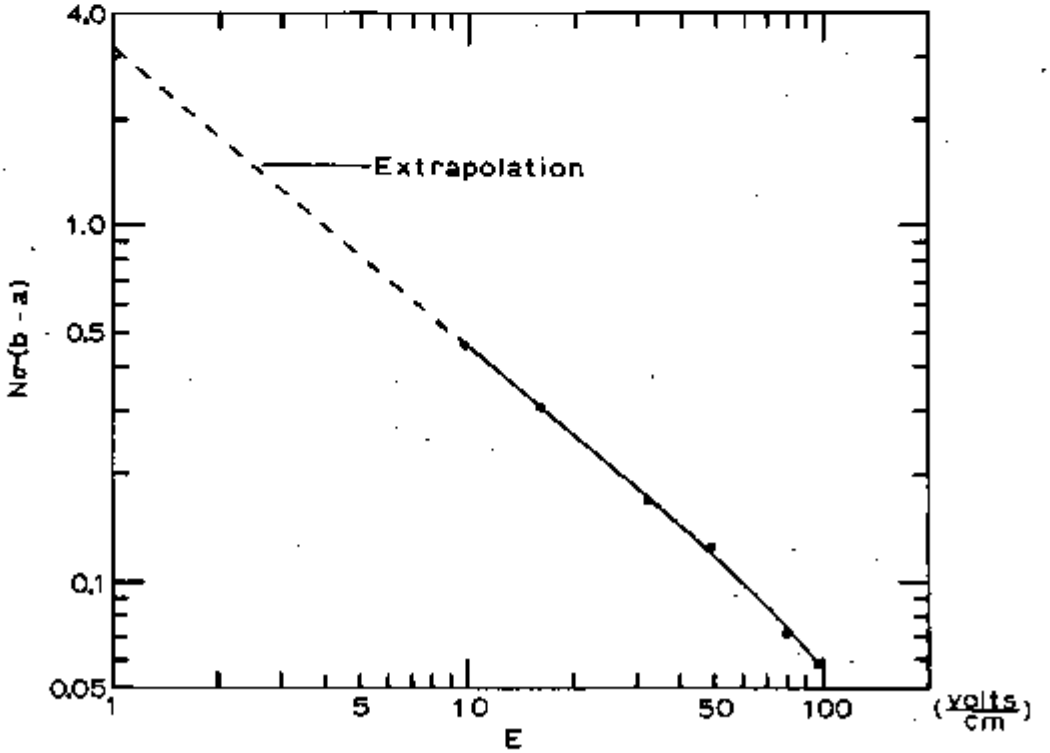

Figure 22: No(b-a) vs. Applied Electric Field

Referring back to Equation (53), one finds that the dependence of the lifetime upon electric field can be expressed in the form

$$\tau = A\, e^{\frac{U_c}{kT}} \tag{79}$$

where A is a constant independent of the field. U_c represents the electric-field-dependent potential of the lip of the trapping well. The lower curve in Figure 21 is a plot of this function at 1.65°K for R = 20.0 Å. A comparison of this curve with the data indicates that the change in shape of the potential well appears to be the major contributor to the electric field dependence of the lifetimes at large electric fields but not at small electric fields.

In Figure 22 the factor $N\sigma(b-a)$ is plotted as a function of applied electric field at 1.6°K using the data of Tanner[81] where N is the vortex-line density for a 60-rpm rotation speed and (b-a) is the distance between the gate and the collector in centimeters. No measurements of σ below 10 volts cm^{-1} were reported by Tanner. For the purposes of this discussion his data have been extrapolated to lower fields in the manner shown in Figure 22. This extrapolation probably under estimates the value of σ. The reciprocal of Nσ is an effective mean free path for capture of an ion by a vortex line. Hence, the factor $N\sigma(b-a)$ is the ratio of the apparatus dimensions to the mean free path. For low electric fields this

ratio is greater than one. For a mean free path on the order of apparatus dimensions, multiple capture of an ion by vortex lines becomes important. Multiple capture will tend to inflate the experimentally observed lifetimes because it takes longer for a given ion to escape from the liquid if it is recaptured several times. It is proposed that this enhanced recapture at lower electric fields is the cause of the rapid rise in the lifetime at low electric fields.

The differential equation concerning the capture and release of trapped charge which was considered in the last chapter is repeated here:

$$\frac{\partial \rho}{\partial t} = J(r)N\sigma - \frac{\rho}{\tau} \quad . \tag{80a}$$

The equation of continuity is

$$\frac{1}{r}\frac{\partial}{\partial r}[rJ(r)] = -\frac{\partial \rho}{\partial t} \quad . \tag{80b}$$

For the simplest solution assume that σ and τ are independent of r. By eliminating J(r) from these two equations, we get

$$\frac{\partial^2 q}{\partial r \partial t} = -N\sigma\frac{\partial q}{\partial t} - \frac{1}{\tau}\frac{\partial q}{\partial r} \tag{81}$$

where $q = \rho r$. We wish to set up a population of trapped charge and observe its decay for various values of $N\sigma(b-a)$. The following boundary conditions are imposed:

$$q(r,t=0) = q_o(r) \tag{82a}$$

and

$$q(a,t) = q_o(a)\, e^{-\frac{t}{\tau}} \tag{82b}$$

where a is the radius of the gate. The solution of Equation (81) with these boundary conditions is

$$q(r,t) = e^{-\frac{t}{\tau}} \int_a^r dr' q_o(r')\; No \sum_{n=0}^{\infty} \frac{(-1)^n}{n!} [No(r-r')]^n \times \int_0^{t/\tau} L_n(t')dt' + q_o(r)\, e^{-\frac{t}{\tau}} \tag{83}$$

where $L_n(t)$ is a Laguerre polynomial of order n. The decay of the total population of charge is

$$Q(t) = 2\pi\, e^{-\frac{t}{\tau}} \int_a^b dr' q_o(r') \left[1 + \sum_{n=0}^{\infty} \frac{(-1)^n}{(n+1)!} [No(b-r')]^{n+1} \int_0^{t/\tau} L_n(t')dt' \right] . \tag{84}$$

The decay in time of the above expression for various values of No(b-a) from 0 to 3 has been evaluated, assuming a uniform initial charge distribution $\rho(r,0) = \rho_o$. This decay in time, at least out to times on the order of 2τ, appears to be exponential over the indicated range of No(b-a). An "effective lifetime" which is proportional to τ and is a function of No(b-a) has been determined from this observed exponential decay of Q(t) in Equation (84). The upper curve

in Figure 21 is the result of this "effective lifetime" correction to the lower curve on this same graph. The agreement between the data and this upper curve is rather good considering the approximations made in calculating the recapture effects. For example, σ was assumed to be independent of r which is not the case; also the initial charge distribution may not have been uniform.

Thus it appears that the electric-field dependence of the lifetime is the result of two effects. First, the depth of the trapping well is electric-field dependent. Second, ion-recapture effects which are electric-field dependent make the experimentally observed lifetimes appear longer than the actual lifetimes. For the - 40-volt data this recapture process causes the measured lifetime to be 3 to 4% larger than the actual lifetime.

The capture cross section σ [in the factor $n\sigma(b-a)$] is expected to be a slowly varying function of temperature over the temperature range covered in Figure 18.[82,83] Thus the dependence of the ion-recapture effect upon the applied electric field is expected to appear in the form of a temperature-independent shift in the magnitude of the lifetimes in Figure 18 and not in the form of a change in the slope of the data in this graph. As was mentioned before, the dependence of the depth of the trapping well upon the electric field has an identical effect upon the temperature dependence of the

lifetimes. The sum of these two effects is offered as an explanation of why the curve of best fit drawn through the - 40-volt data need only be changed by a multiplicative factor in order to fit the data taken at other voltages in Figure 18.

The dependence of the measured lifetime upon rotation speed at a gate potential of - 40 volts at T=1.6355°K is presented in Figure 23. Since the density of vortex lines N depends upon the rotation speed, one would expect the lifetime to depend slightly upon the rotation speed because the recapture process is a function of N. The line drawn on this graph represents the rotation-speed dependence of the lifetimes calculated from Equation (84). Within the large error bars shown on this graph, the data and the theoretical prediction are in qualitative agreement.

It was shown in Figure 19 that our - 40-volt data and the data of R. L. Douglass agreed in slope but not in magnitude. R. L. Douglass stated that an applied field "exceeding 20 volts/cm" was used. His geometry, although cylindrical, is rather different from ours. Our applied field ranges from - 23 volts cm^{-1} at the collector to - 63 volts cm^{-1} at the gate with a gate potential of - 40 volts. We suggest that the shift in magnitude between our data and Douglass' could very well be due to a difference in electric-field configurations which can affect the lifetime measurements in the two ways previously stated.

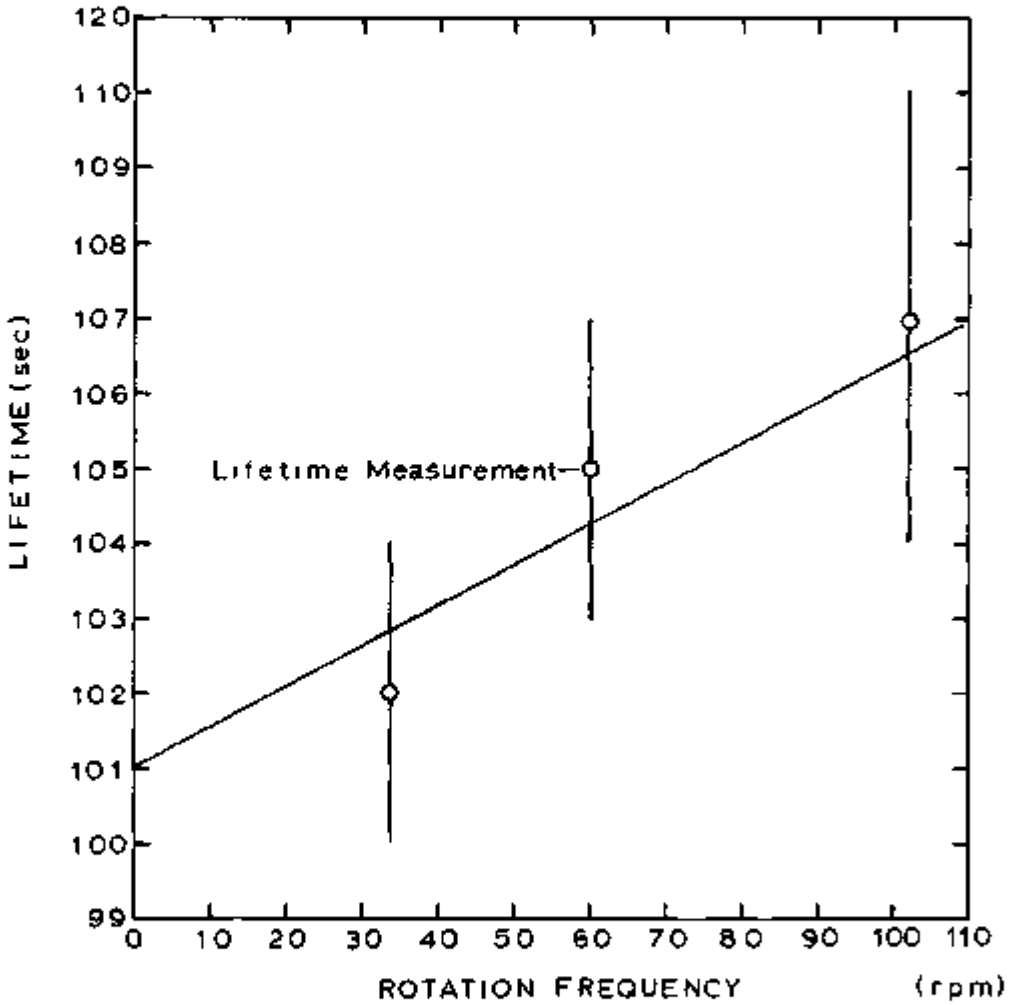

Figure 23: Lifetime vs. Frequency of Rotation at Saturated Vapor Pressure for V_g = - 40 volts

Also indicated in Figure 21 is the range of electric fields found between the gate and the collector with the gate potential at - 40 volts. Within this range the lower curve represents the spectrum of lifetime found between the gate and the collector. It is important to see if such a spectrum affects the experimentally observed exponential decay of the trapped charge in any observable way. The relevant equation is

$$Q(t) = 2\pi \int_a^b e^{-\frac{t}{\tau(r)}} \rho_o(r) r dr \qquad (85)$$

where $\tau(r)$ is the position-dependent lifetime and where recapture effects have been neglected. A numerical solution of this integral has been performed for T=1.65°K, r = 20.0 Å, and ρ_o = constant. This integral was evaluated by factoring out an exponential factor for a lifetime corresponding to an applied uniform electric field of 36 volts cm^{-1} [the average field as defined in Equation (74)] and then calculating corrections to this factor. In Figure 24 both the decay calculated for a uniform field of 36 volts cm^{-1} and the decay calculated for the actual nonuniform field are presented. The decay of the trapped charge presented in this graph for the actual electric field appears to be exponential out to times on the order of 2τ. The lifetime for the nonuniform field case is 3% larger than the lifetime for a uniform field of 36 volts cm^{-1} and corresponds to a lifetime of an ion in a uniform electric field of 33 volts cm^{-1}. This increase in

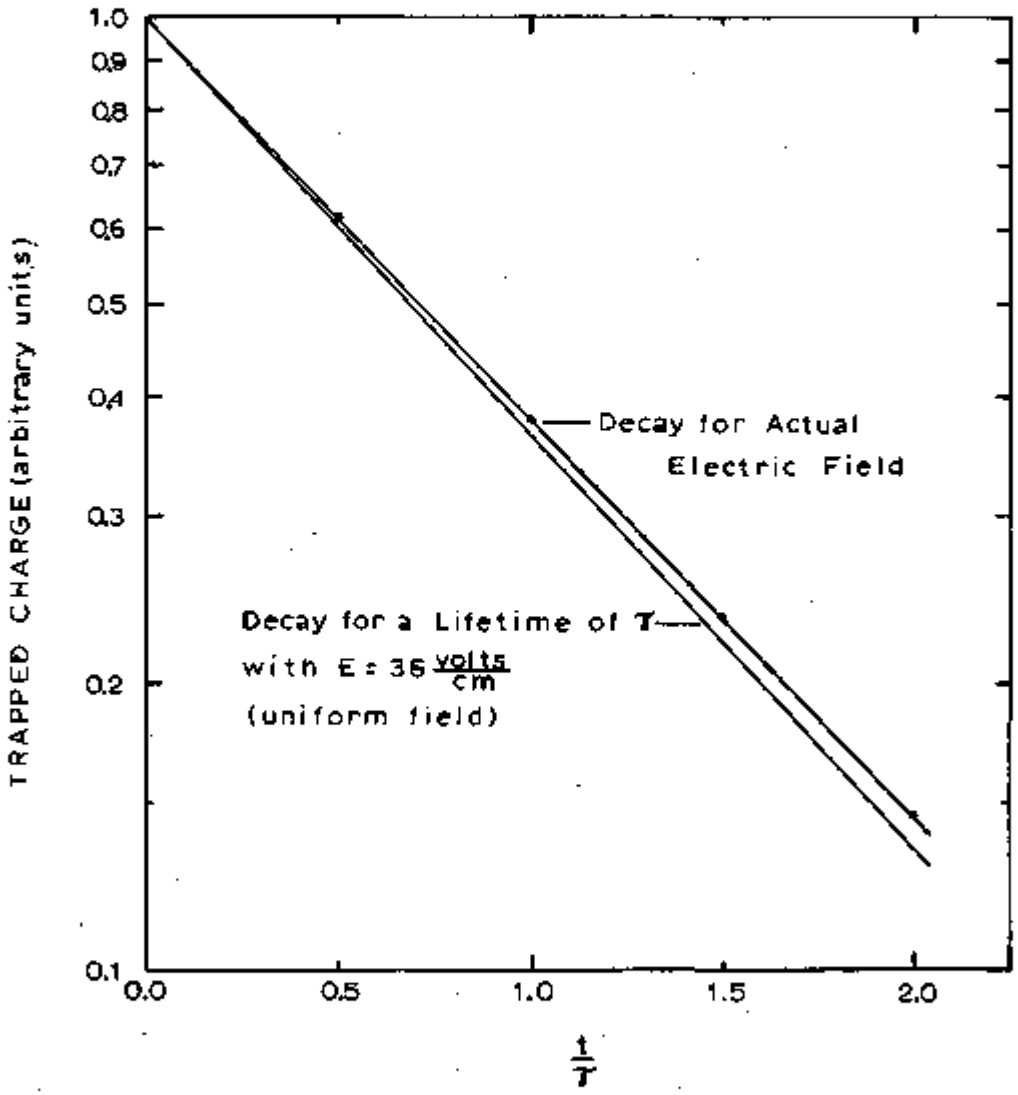

Figure 24: Influence of a Nonuniform Electric Field on the Decay in Time of Trapped Charge

the lifetime is expected for the nonuniform field case since there is more charge in the region of lower electric field where the lifetimes are longer for a uniform initial charge distribution.

Up to this point in the analysis, the charge distribution has been assumed to be uniform. In the last chapter it was shown that during the early stages of the charging of the vortex lines the density of trapped charge is expected to be nearly uniform. However, as the density of trapped charge builds up, charge will escape more rapidly from the liquid, the rate being ρ/τ. One then might expect the charge density to become nonuniform, the density being larger where the lifetime is longer. The ratio of the 6-minute charging period to the lifetime is a possible measure of this nonuniformity which might result. The proposed nonuniformity in the initial density of trapped charge has been evaluated in the limit of lifetimes which are short compared to the 6-minute charging period. In this limit one would expect the following: $\rho_o(r) \propto \tau(r)$. This initial condition has been applied to Equation (85). The resulting numerical solution appears to be an exponential decay in time at least out to times on the order of 2τ. The effective lifetime for this decay is approximately 1% longer than the lifetime for the actual electric field with a uniform initial charge distribution shown in Figure 24.

The possibility of a systematic error in the lifetime

measurements now arises. As shown above the initial charge distribution may depend upon the magnitude of the lifetime. Thus the averaging of the spectrum of lifetimes found between the gate and the collector, which determines the experimentally measured lifetime, may depend upon the magnitude of the lifetime being measured. This requires that a correction in the form of an increase in slope be made to the data in Figure 18. If our estimates are correct concerning the initial charge distribution (ranging from $\rho_o \approx$ const. at long lifetimes to $\rho_o \approx \tau(r)$ at short lifetimes), then the correction to be applied to the experimental data is on the order of 1%. This produces a negligible increase in the slope of the data in Figure 18.

VI. PRESENTATION AND DISCUSSION OF LIFETIME DATA UNDER PRESSURE

1. Presentation of Lifetime Data under Pressure

All the lifetime measurements at pressures between the saturated vapor pressure and the solidification pressure were made with the gate potential at - 40 volts and at a rotation speed of 60 rpm. The experimental procedure consisted of adjusting the applied pressure to some constant value. Lifetime measurements in the range 20 to 400 seconds were then made at four different temperatures while the pressure was held constant. This procedure was repeated at sixteen different pressures. The data are tabulated in Appendix IV.

At any given pressure the lifetimes were plotted logarithmically as a function of the reciprocal of the absolute temperature. It was found for most of these plots that the data fell along straight lines, as observed in Figure 18 for the data at saturated vapor pressure. The slopes of the data on this kind of plot are shown as a function of pressure in Figure 25. These slopes are also tabulated in Appendix IV. They are an indirect measure of the depth of the trapping well.

Since the data at any given pressure fell along straight lines in the previously mentioned log plot, it was easy to interpolate the data. In this way curves of constant lifetime in the pressure-temperature plane were calculated.

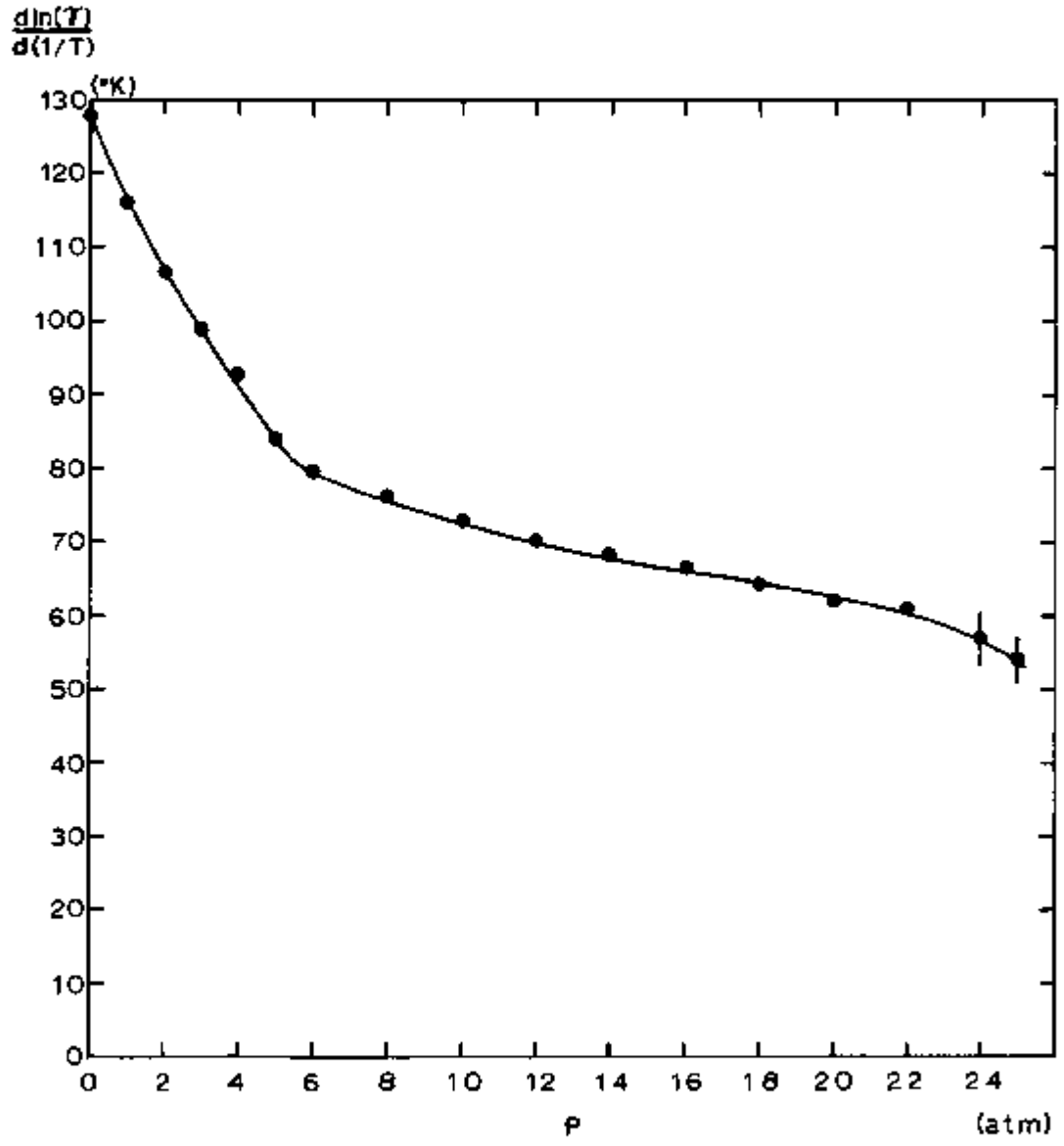

Figure 25: $\frac{d\ell n(T)}{d(1/T)}$ vs. Pressure

In Figure 26 three curves of constant lifetime, at 20, 85, and 350 seconds, are shown. The data are also tabulated in Appendix IV. At 24 atm and at the solidification curve, at least three measurements of the lifetime were made in the temperature interval between a lifetime of 20 seconds and the lowest temperature attainable, 1.095°K.

It is important to emphasize that lifetime measurements were actually made on the solidification curve with about 2 to 3% of the volume of the pressure vessel occupied by solid helium. There are two ways to check to see if one is on the solidification curve. First, one can add more helium to the pressure vessel and observe no increase in the final pressure. Second, if the pressure vessel is full of liquid helium, the temperature dependence of the density of the liquid is such that the pressure of the liquid will drop as the temperature is increased at constant density. If there is some solid helium in the pressure vessel, the pressure of the liquid-solid mixture will rise following the solidification curve until all of the solid helium has melted. Both of these techniques were used to insure that the lifetime measurements were made on the solidification curve.

Springett and Donnelly have performed a rotation experiment in which indirect measurements of the lifetime of the trapped negative ion were made as a function of pressure and temperature.[84,85] The cross section for capture of a

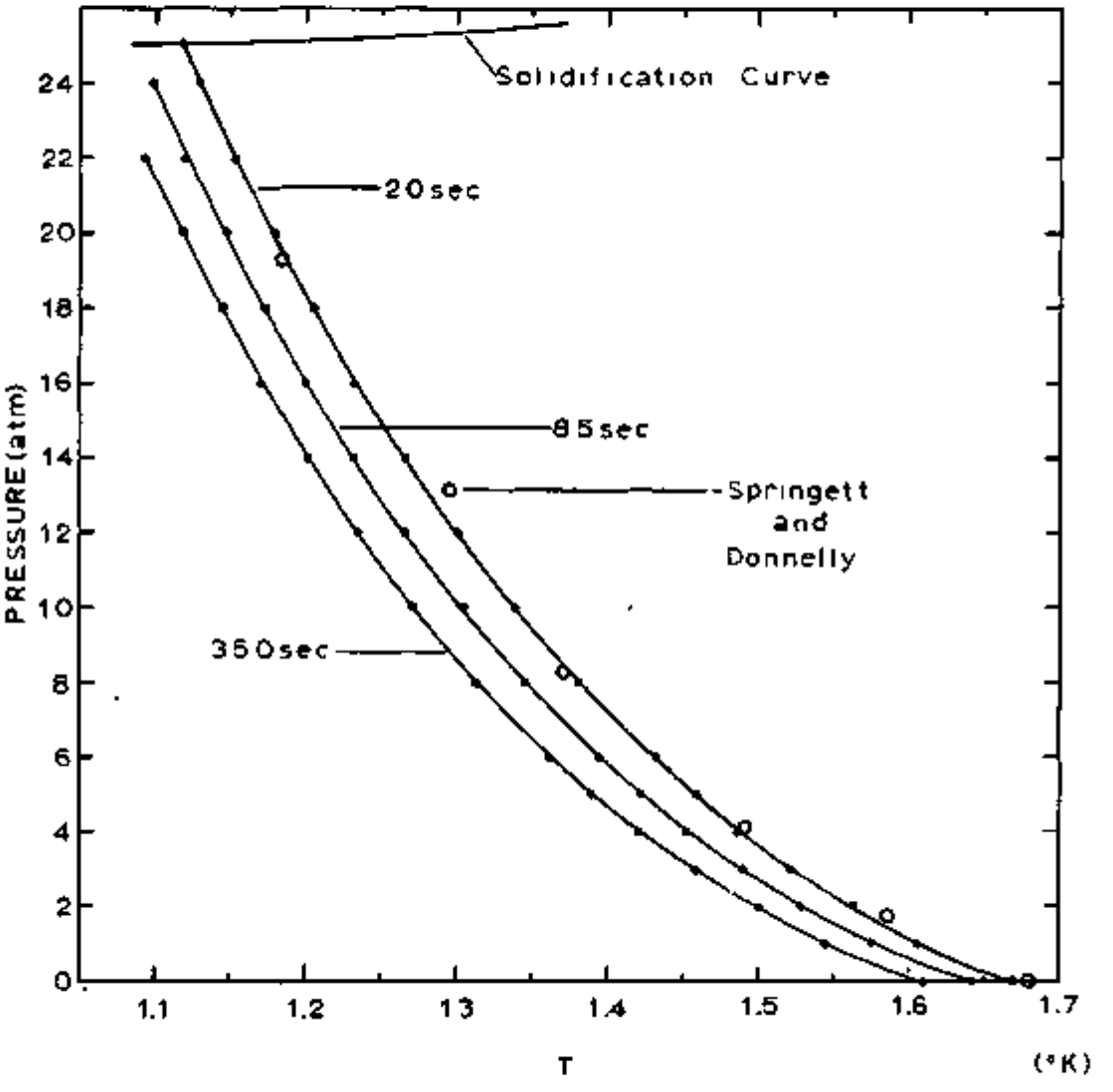

Figure 26: Curves of Constant Lifetime in Pressure-Temperature Plane

negative ion by a vortex line was determined as a function of temperature at several different pressures. A beam of negative ions was propagated in a direction perpendicular to the axis of rotation between two planar electrodes. From the observed attenuation of this beam during rotation the capture cross section was determined. Below a certain temperature which depended upon the applied pressure and which we shall call $T'(P)$, the cross section was observed to increase with increasing temperature at constant pressure. Above $T'(P)$ the cross section fell rapidly to zero. Springett and Donnelly were able to estimate the trapping lifetime of the negative ion from analysis of this region of rapid change in the cross section with temperature.

When an ion was captured by a vortex line in their apparatus, the ion would start to move along the vortex line away from the ion beam. The ion was driven by the electric field developed by the other trapped ions and by the ions in the beam. For very long lifetimes this trapped ion would eventually reach a position opposite one of the edges of the collector, the electrode to which the current measuring device was connected. Once this position had been reached, the ion was no longer able to reach the collector if escape from the vortex line occurred. This escape of the trapped ion beyond an edge of the collector was the cause of the attenuation in the ion beam. Let $t_o(T,P)$ be the average time for a trapped

ion to reach an edge of the collector. Springett and Donnelly pointed out that the region of rapid falloff in the cross section corresponded to the lifetime being on the order of t_o. They used the following equation, proposed earlier by Donnelly,[86] for their analysis of the region of rapid falloff in the cross section:

$$\sigma(T,P) = \sigma[T'(P),P]\, e^{-\frac{t_o(T,P)}{\tau(T,P)}} \qquad (86)$$

where σ is the capture cross section determined from the measured attenuation in the ion beam and where $\tau(T,P)$ is the lifetime of the negative ion.

Springett and Donnelly have determined the temperature at which $\frac{\sigma(T,P)}{\sigma[T'(P),P]} = 1/2$ for each pressure. Thus they have found the locus of points in the pressure-temperature plane which satisfy t_o/τ = constant. If t_o is also a constant independent of pressure and temperature, then the locus of points should follow a curve of constant lifetime in the pressure-temperature plane. The open circles in Figure 26 represent the locus of points for t_o = constant. Their data agree satisfactorily with ours, and the comparison indicates a t_o of approximately 10 seconds for their experiment.

2. Discussion of Lifetime Measurements under Pressure

Before the actual data are discussed, it is important to point out that a calculation of the superfluid density as a function of both pressure and temperature is needed for

this analysis. At present no direct and accurate measurements of the normal or superfluid density have been made at elevated pressures. The normal fluid density had to be calculated, then, from thermodynamic data. Equation (70) was used in connection with measurements of the second sound velocity, the entropy, the specific heat at constant volume, and the total density which have been made at elevated pressures by different investigators. The calculations and tabulations are presented in Appendix V. The normal fluid density is probably accurate to a few percent (2 to 5%); the total fluid density is known to ±0.1%.

The major temperature and pressure dependence of the lifetime is expressed in the following equation for the classical case, $\frac{\hbar\omega_0}{kT} \ll 1$:

$$\tau(T,P) = \frac{A\beta(P,T)}{\rho_s(P,T)} e^{\frac{f[R(P)]\rho_s(P,T)}{T}} \tag{87}$$

where A is a constant and radius R is assumed to be pressure dependent. The function $\beta(P,T)$ is inversely proportional to the mobility. The mobility of the negative ion under pressure has been measured by several investigators.[87-89] The experimental results are approximated in the following way:

$$\beta(P,T) \propto e^{-\frac{\Delta(P)}{T}} \tag{88}$$

where $\Delta(P) = 8.1°K$ for $0 \leq P \leq 5$ atm

and $\Delta(P) = [8.1 - 0.055(P)]°K$ for 5 atm $\leq P \leq 25$ atm.

Thus we obtain

$$\tau(P,T) = F_0 \, e^{\frac{f[R(P)]\rho_s(P,T)}{T} - \frac{\Delta(P)}{T} - \ell n[\rho_s(P,T)]} \tag{89}$$

where $\rho_s(P,T)$ in the denominator of Equation (87) has been placed in the argument of the exponent of this equation.

The curves of constant lifetime in Figure 26 and the above equation can now be used to determine $f[R(P)]$ where $f[R(0)]$ is chosen to agree with the previously determined radius of 19.5 Å at the saturated vapor pressure. For the 20-second curve of constant lifetime at saturated vapor pressure, we have $f(R)\rho_s/T \approx 37$, $\Delta/T \approx 5$, and $\ell n\rho_s \approx -2$. As one moves along this curve of constant lifetime from $P = 0$ to $P \approx 24$ atm, ρ_s/T increases by approximately a factor of two, Δ/T increases by 20% and $\ell n\rho_s$ increases by 10%. Then from Equation (89) we see that $f[R(P)]$ must decrease as the pressure is increased, which implies that $R(P)$ decreases as the pressure is increased. The slope of the 20-second curve of constant lifetime in the P-T plane does not change abruptly in the neighborhood of the solidification curve. The product $f[R(P)]\rho_s(P,T)$, then, is well-behaved in this region. This behavior probably indicates that the superfluid density and the radius of the ion do not change abruptly when the solidification pressure is reached.

The radii of the negative ion as a function of pressure, calculated from the curves of constant lifetime, are presented in Figure 27. In the calculation of R(P) from f[R(P)], changes in the superfluid density with pressure and temperature which affect slightly the shape of the lip of the well have been taken into account for the average applied electric field of 36 volts cm^{-1}. The healing length d has been arbitrarily chosen to be independent of pressure and temperature. The solid circles represent the pressure dependence of the ion radius for the classical case where $\frac{\hbar\omega_o}{kT} << 1$. The open circles represent the case considered earlier in this chapter in which $\theta_o' = 7.6°K$ and $R(0) = 20.0$ Å. For the latter case Equation (76) becomes

$$\tau(P,T) = \frac{A}{T^2} e^{\frac{f[R(P)]\rho_s(P,T)}{T} - \frac{\theta'}{T} - \frac{\Delta(P)}{T}} \qquad (90)$$

where $\theta' = \theta_o' \left[\frac{\rho_s(P,T)}{\rho_s(0,T_o)}\right]^{\frac{1}{2}}$, A is a constant, and $T_o = 1.63°K$. Equation (90) and the curves of constant lifetime are used to determine R(P) where, for simplicity, θ_o' has been assumed to be independent of R(P). The fact that the radii from the two cases differ by more than the ratio $\frac{20.0}{19.5}$ at high pressures is due to the pressure and temperature dependence of θ' in the argument of the exponent in Equation (90).

In calculating R(P) from the three curves of constant lifetime, we find at any given pressure that the calculated

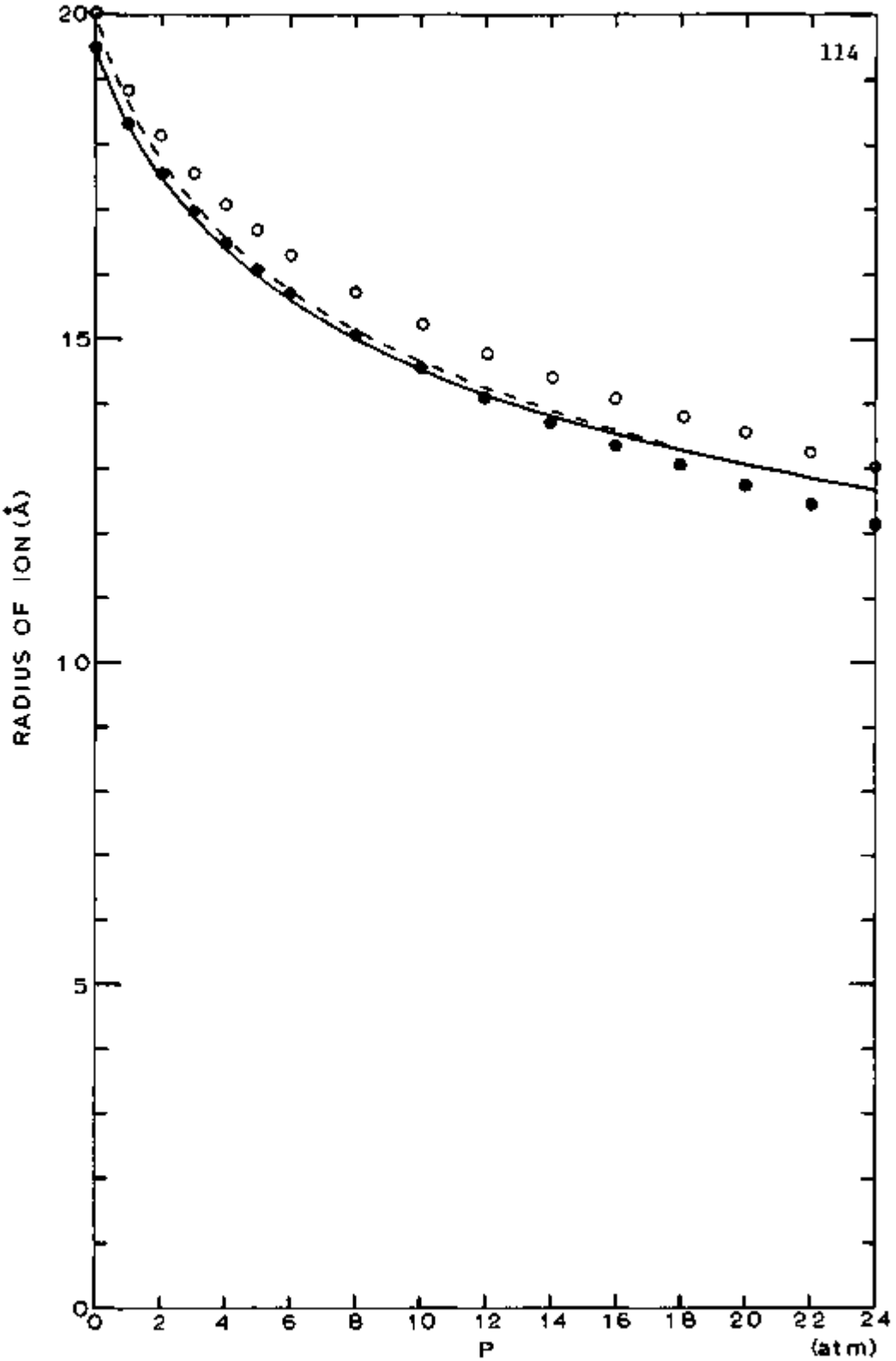

Figure 27: Negative Ion Radius vs. Pressure Calculated from Curves of Constant Lifetime

value of the radius depends only slightly upon which curve of constant lifetime is used. The magnitude of this disagreement is always less than 0.2 Å. The circles plotted in Figure 27 are an average of the radii determined from the curves of constant lifetime. The size of the circles plotted on this graph represent approximately the maximum value of this disagreement.

The solid and dashed curves in Figure 27 represent the predictions of the simple bubble model considered in Chapter I. The surface tension has been adjusted so that at the saturated vapor pressure R = 19.5 Å and 20.0 Å, respectively. Since the pressure dependence of the surface tension is not known, the surface tension has been arbitrarily chosen to be pressure independent.

Another way to determine the radius as a function of pressure is to make use of the data in Figure 25 where $\frac{d\ell n(\tau)}{d(1/T)}$ is plotted as a function of pressure. Of particular interest is the apparent "break" in this data at 6 atm. In Figure 27 the radius as a function of pressure, calculated from the curves of constant lifetime, shows no corresponding "break". For the case where $\frac{h\omega_o}{kT} << 1$ and R(0) = 19.5 Å we obtain from Equation (89)

$$\frac{d\ell n(\tau)}{d(1/T)} = f[R(P)]\,\frac{d}{d(1/T)}\left[\frac{\rho_s(P,T)}{T}\right] - \Delta(P) \qquad (91)$$

where the missing term $\frac{d\ell n[\rho_s(P,T)]}{d(1/T)}$ is small and can be

neglected. Using the superfluid densities tabulated in Appendix V and the data in Figure 25 together with Equation (91), we obtain the radius as a function of pressure shown in Figure 28. The solid curve represents the results from the curves of constant lifetime data. There is good agreement at 1 and 2 atmospheres between the two methods for calculating the radius of the ion. Above 2 atm a rather large disagreement occurs.

We suspect that the disagreement has its origin in the calculations of the normal fluid density. The slope method of determining the radius requires more accurate normal fluid data than the curves-of-constant-lifetime method. For the latter method the superfluid density along a curve of constant lifetime must be known. Along such a curve the superfluid density at 24 atm is 40% larger than the superfluid density at the vaporization pressure. The total density of the liquid is known to $\pm 0.1\%$, and this density is generally a factor of five larger than the normal fluid density in the region covered by the curves of constant lifetime. Thus percentage errors in the normal fluid density calculations produce one fifth that percentage error in the superfluid density. Only one third of the 40% change in the superfluid density along a curve of constant lifetime is produced by a change in the normal fluid density. For the former method the change in the superfluid density at constant pressure over a small temperature interval must be determined. The total density is a weak function of

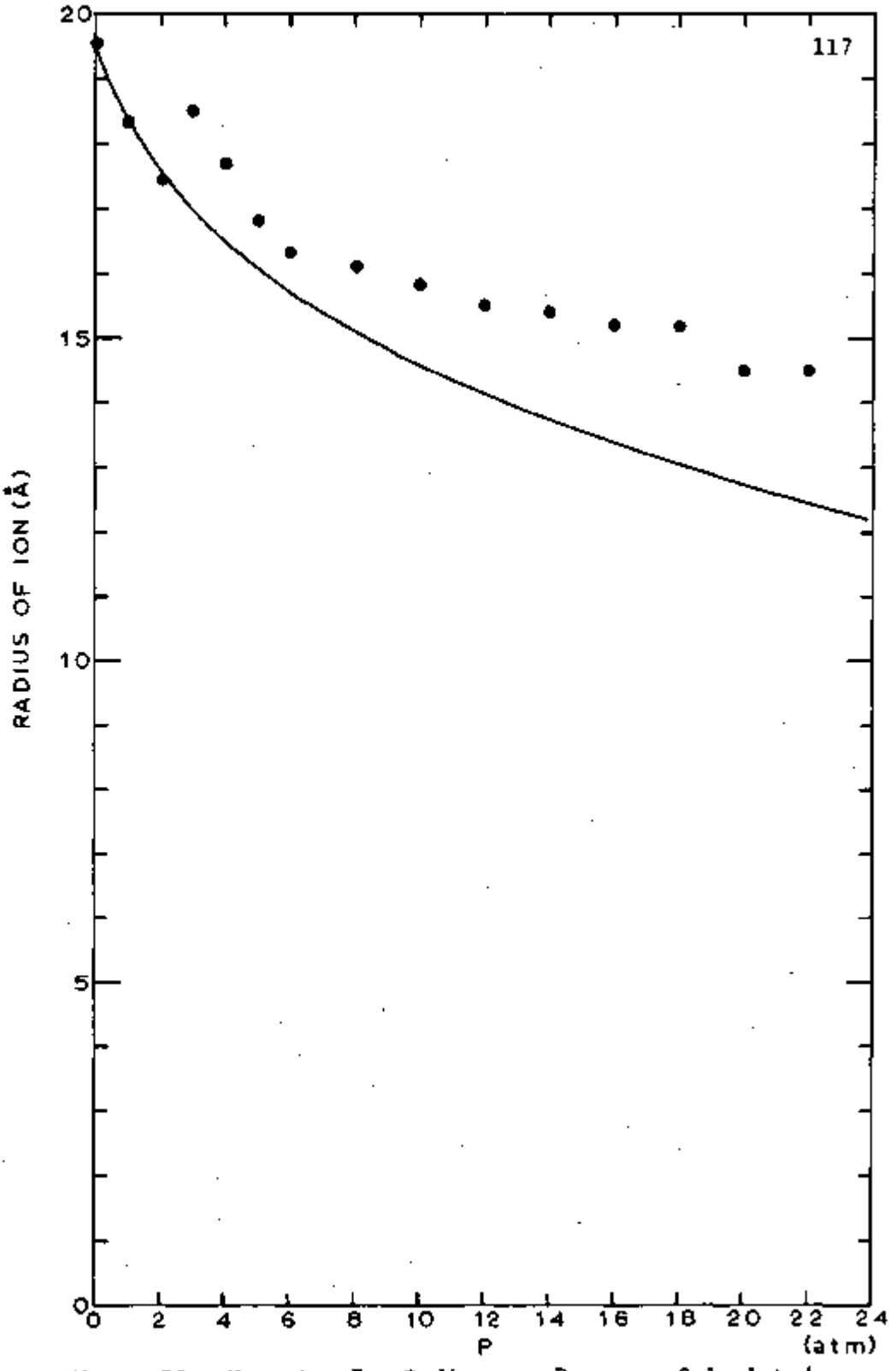

Figure 28: Negative Ion Radius vs. Pressure Calculated by "Slope" Method

temperature. The normal fluid density, then, makes the major contribution to the temperature dependence of the superfluid density over this small temperature interval. Thus larger errors are expected for the slope method of determining the radius of the ion as a function of pressure.

In Figure 29 the normal fluid density is plotted logarithmically as a function of the reciprocal of the absolute temperature over a wider range of temperature than was considered in Figure 20. The middle curve represents the calculations of Reynolds *et al.*[90] employing thermodynamic data measured at the saturated vapor pressure. The top curve represents our calculation of the normal fluid density at 3 atm pressure. An abrupt change in the slope of these two results at 1.52°K is quite evident. The lower curve is a plot of the direct experimental measurements of the normal fluid density by Dash and Taylor.[91] The lack of such an abrupt change in slope in the results of Dash and Taylor is quite startling and raises serious questions about the reliability of our normal fluid calculations using thermodynamic data.

It is now understood why a sudden upward jump in the radius of the ion occurs between 2 and 3 atm when the slope method is used. A careful look at the curves of constant lifetime will show one that the lifetime measurements at 2 and 3 atm fall on either side of 1.52°K. Below 1.52°K our

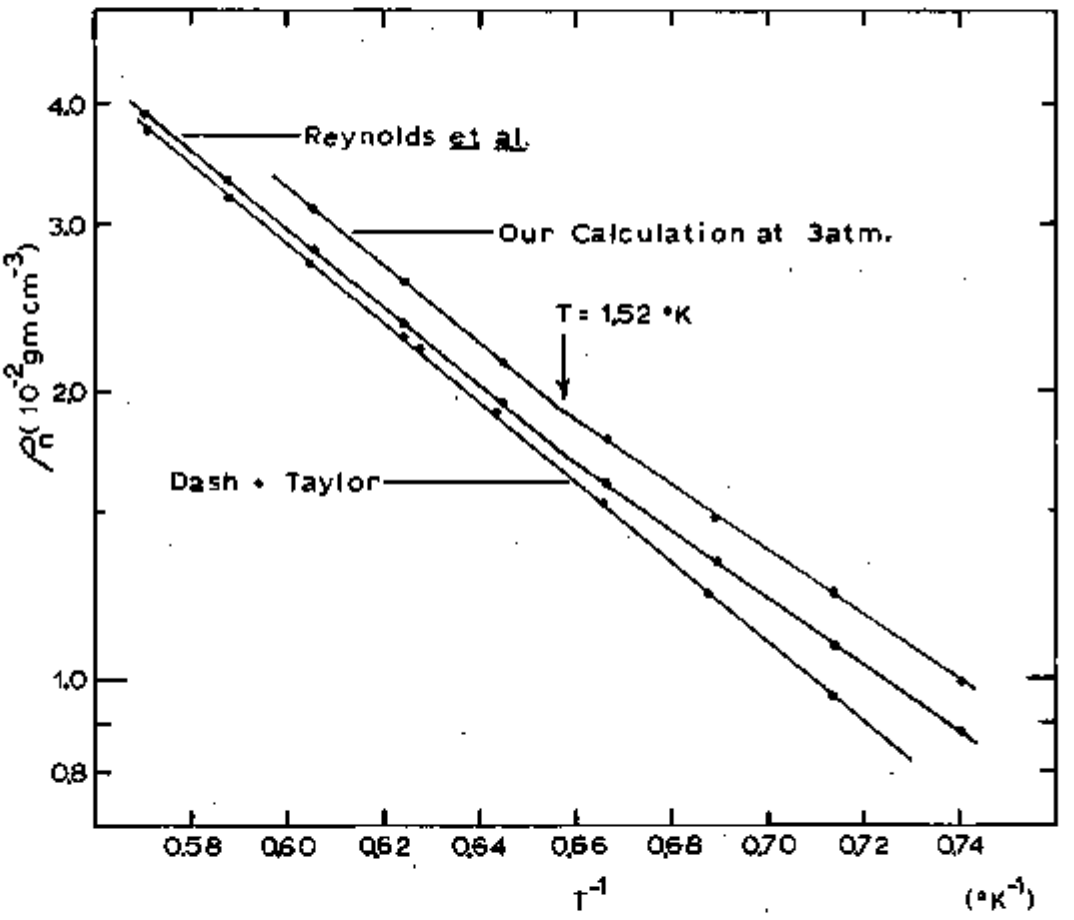

Figure 29: Normal Fluid Density vs. 1/T

normal fluid calculations produce a sudden drop in the quantity $\frac{d\rho_n}{d(1/T)}$. This means that $\frac{d}{d(1/T)}\left[\frac{\rho_s}{T}\right]$, too, will suddenly decrease at temperatures below 1.52°K, a behavior which will make the radius suddenly larger at these temperatures [see Equation (91)].

Until more accurate and direct measurements under pressure of the normal and superfluid densities are made, the curves-of-constant-lifetime method will have to be used. It is suspected that the "break" seen in the data shown in Figure 25 is a product of the temperature dependence of the normal fluid and is not related to any abrupt change in the pressure dependence of the ion radius.

Let us return to Figure 27. There have been a series of assumptions made in the calculation of the radius of the negative ion as a function of pressure from the curves of constant lifetime. Weaknesses in some of these assumptions will now be discussed.

The pressure dependence of the negative ion radius, calculated from the curves of constant lifetime, depends upon the assumed value of the radius at saturated vapor pressure. At saturated vapor pressure there are two values of the radius, $R(0) = 19.5 \pm 0.6$ Å and $R(0) = 20.0 \pm 0.6$ Å, which depend upon whether $\theta_o' = 0.09$°K or $\theta_o' = 7.6$°K. The relative strengths and weaknesses of these two results have already been discussed. Most of the 0.6 Å uncertainty in each radius is

produced by the uncertainty in the healing length of the superfluid near a vortex line. The value of the healing length used in our analysis was determined by Parks and Donnelly,[92] who analyzed the vortex ring experiments in terms of Fetter's[93] calculation for a vortex line in the Bose gas condensate [see Equation (5)]. The connection between the Bose gas condensate and the superfluid component of the two-fluid model is not well understood. Certainly a more careful analysis of how the superfluid density goes to zero at the core of a vortex line is needed. The general problem of the applicability of the two-fluid model in the region near the core of a vortex line where the superfluid velocity is large has not been considered in detail in the literature. It is not known at the present time what values the total fluid density and the normal fluid density have near a vortex line. If, for example, the result of such an analysis were to make the effective healing length of the superfluid larger than the presently used value, analysis of our data would result in a larger ion radius.

Also, at saturated vapor pressure the ion radius was assumed to be independent of temperature. We know that only a 7% change in the superfluid density over the temperature range covered at saturated vapor pressure affects the calculated binding energy by a factor of 2.2. Thus a very small change in the radius of the ion with temperature could have

a large effect upon the calculated value of the binding energy and hence on the ion radius. For example, the surface tension of liquid helium is experimentally known to be slightly temperature dependent.[94] If one includes this effect in Equations (11) and (12) of the simple bubble model, one obtains a temperature dependent ion radius which produces a 4% increase in our value of the ion radius calculated from the lifetimes at saturated vapor pressure. We have here an example of a possible modification in the experimentally determined radius of the ion which is dependent upon the model assumed for the negative ion.

For the calculation of the negative ion radius under pressure from the curves of constant lifetime, the healing length was assumed to be independent of pressure. In Fetter's calculation the healing length for a vortex line in the Bose gas condensate is inversely proportional to the square root of the fluid density. Thus the healing length of the superfluid may in fact be pressure dependent. If Fetter's result is applied to our calculation under pressure, a 0.6 Å reduction in our value of the radius of the ion at 24 atm results.

For our calculation of the negative ion radius under pressure, the dependence of ω_o upon the superfluid density was taken into account. However, the assumption was made that ω_o was independent of the radius of the ion R(P). In Equation (33) we see that ω_o is approximately inversely proportional to

R(P). If this dependence of ω_o upon R(P) is taken into account in our calculations of the negative ion radius, we obtain the following corrections: for $\theta_o' = 0.09°K$ our value of R(P) at 24 atm should be increased by 0.1 Å, and for $\theta_o' = 7.6°K$ our value of R(P) at 24 atm should be increased by 0.4 Å. Since there is some question about the validity of Equation (33) for the case $\theta_o' = 7.6°K$, the 0.4 Å correction should be viewed with some skepticism.

Also shown in Figure 27 are two curves representing the simple bubble model for R(0) = 19.5 Å and R(0) = 20.0 Å. Possible refinements in this model were considered in Chapter I and will not be repeated here. The two curves appear to agree better with the pressure dependence of the radius of the negative ion calculated from the curves of constant lifetime with $\theta_o' = 0.09°K$ than with $\theta_o' = 7.6°K$. However, the apparent agreement should not be taken too seriously since the simple bubble model is in need of refinements. Besides affecting the predictions of the bubble model, these refinements may also affect our experimentally determined radii through the temperature dependence of the radius of the ion, which has been previously discussed.

As mentioned before, Northby and Sanders have measured the radius of the negative ion at saturated vapor pressure and have found R = 21.2±0.5 Å.[95] They pointed out that there were certain aspects of their results which were not well understood.

They mentioned also that modifications of their apparatus were under way so that the radius of the ion under pressure could be measured. They said that these measurements under pressure should improve their understanding of their results.

Any serious comparison between our results and the results of Northby and Sanders should perhaps await the completion of their measurements of the radius of the negative ion under pressure. However, it is certainly encouraging that such different experiments have produced values for the radius of the negative ion which differ by only 6 to 8%.

Finally, it should be mentioned that an attempt was made during the measurements of the negative ion lifetime on the solidification curve to look for positive ion trapping on vortex lines. None was observed at the lowest temperature reached, 1.095°K, or above. This means that the radius of the positive ion is probably less than 12 or 13 Å at these pressures. Positive ion trapping was also looked for at lower pressures and higher temperatures; no trapping was observed.

VII. CONCLUSION

The lifetime of negative ions trapped on vortex lines has been measured as a function of temperature and pressure from the vaporization pressure to the solidification pressure between 1.1 and 1.7°K. On the average the accuracy of the lifetime measurements was ±2%. The temperature was measured to an accuracy of ±0.0001°K at 1.7°K and ±0.0004°K at 1.1°K. The pressures were measured to an accuracy of ±0.002 atm at 1 and 2 atm, ±0.03 atm between 3 and 14 atm, and ±0.1 atm above 14 atm. The analyses conducted in this thesis indicate that the lifetimes as tabulated for $V_g = -40$ volts and a 60-rpm rotation frequency may require the application of a maximum correction of -4%. This correction is needed to offset the effects of multiple capture of the ions by the vortex lines.

At saturated vapor pressure the temperature dependence of the lifetimes is fitted equally well by two theoretical curves based on different assumptions about the shape of the bottom of the trapping potential well. For one curve $R(0) = 19.5 \pm 0.6$ Å; for the other curve $R(0) = 20.0 \pm 0.6$ Å. However, the first curve involves a reasonable value of the curvature of the bottom of the well and yields lifetime values wrong in magnitude by a factor of 10^4 while the second curve yields the correct magnitude but requires the use of a questionably large curvature of the bottom of the well. These two results

are to be compared with the 21.2±0.5 Å radius of the negative ion measured by Northby and Sanders. The pressure dependence of the radius of the negative ion for R(0) = 19.5 Å appears to agree well with a simple bubble model of the negative ion. However, the resulting radii obtained from analysis of the lifetime results both at the vaporization pressure and at higher pressures are strongly model dependent. Further analysis of the lifetime measurements must await refinements in the bubble model of the negative ion.

Over the full range of pressures and temperatures covered in this experiment, no positive ion trapping has been seen. Modifications of the apparatus should be made so that positive ion trapping can be investigated in the temperature region from 0.6 to 1.1°K at different pressures. In this way a better understanding of the structure of the positive ion might be obtained.

APPENDIX I

Electrostatic Potential between Concentric Cylinders with End Plates

Let a be the radius of the inner cylinder, b the radius of the outer cylinder, c the distance between the end plates, and $\phi(r,x)$ the electrostatic potential. Two sets of boundary conditions are considered:

1.

$$\phi_1(b,z) = 0 \qquad \phi_1(a,z) = V$$

$$\phi_1(r,0) = 0 \qquad \phi_1(r,c) = 0$$

2.

$$\phi_2(b,z) = V \qquad \phi_2(a,z) = 0$$

$$\phi_2(r,0) = 0 \qquad \phi_2(r,c) = 0$$

where the origin of the z axis is situated at one of the end plates.

The general solution of the Laplace equation for either set of boundary conditions is

$$\phi(r,z) = \sum_{n=1}^{\infty} a_n \sin\left[\frac{n\pi z}{c}\right]\left[A_n I_o\left[\frac{n\pi r}{c}\right] + B_n K_o\left[\frac{n\pi r}{c}\right]\right]$$

where I_o and K_o are the modified Bessel functions.[96] Specifically,

$$\phi_1(r,z) = \frac{4V}{\pi} \sum_{n=1,3,\ldots}^{\infty} \frac{1}{n} \sin\left[\frac{n\pi z}{c}\right]\left[\frac{I_o\left[\frac{n\pi r}{c}\right] - K_o\left[\frac{n\pi r}{c}\right]}{I_o\left[\frac{n\pi b}{c}\right] - K_o\left[\frac{n\pi b}{c}\right]}\right]\left[\frac{I_o\left[\frac{n\pi a}{c}\right] - K_o\left[\frac{n\pi a}{c}\right]}{I_o\left[\frac{n\pi b}{c}\right] - K_o\left[\frac{n\pi b}{c}\right]}\right]$$

and

$$\phi_2(r,z) = \frac{4V}{\pi} \sum_{n=1,3,\ldots}^{\infty} \frac{1}{n} \sin\left[\frac{n\pi z}{c}\right] \left[\frac{I_o\left[\frac{n\pi r}{c}\right] - K_o\left[\frac{n\pi r}{c}\right]}{I_o\left[\frac{n\pi a}{c}\right] - K_o\left[\frac{n\pi a}{c}\right]} \cdot \frac{I_o\left[\frac{n\pi b}{c}\right] - K_o\left[\frac{n\pi b}{c}\right]}{I_o\left[\frac{n\pi a}{c}\right] - K_o\left[\frac{n\pi a}{c}\right]} \right] .$$

The two sets of boundary conditions applicable to the experimental situation are

$$\phi_t(b,z) = 0 \qquad \phi_t(a,z) = +V$$

$$\phi_t(r,0) = -2V \qquad \phi_t(r,c) = -2V.$$

The solutions of the two previously considered boundary conditions #1 and #2 can be combined to give solutions which satisfy the two boundary conditions shown above:

$$\phi_t(r,z) = -2V + \phi_1(r,z) + 2\phi_2(r,z),$$

and

$$\phi_t(r,z) = -2V + 3\phi_1(r,z) + 2\phi_2(r,z).$$

Note also

$$E_z(r,z) = -\frac{\partial \phi_t(r,z)}{\partial z} ,$$

$$E_r(r,z) = -\frac{\partial \phi_t(r,z)}{\partial r} ,$$

$$\frac{\partial I_o(x)}{\partial x} = I_1(x), \text{ and } \frac{\partial K_o(x)}{\partial x} = -K_1(x) .$$

The values of $E_z(r,z)$ shown in Figures 9a and 9b were calculated by computer from the tabulated polynomial

approximations to I_o and K_o.[97] For the field lines shown on Figures 8a and 8b, $E_r(r,z)$ was also calculated from the tabulated polynomial approximation to I_1 and K_1. The field lines were determined in the following manner: At an arbitrary point near a boundary of the electrode system, the direction and magnitude of the total electric field were calculated from E_r and E_z. The field point was then moved a short distance in the direction of the calculated electric field. The magnitude and direction of the electric field at this new point were evaluated, and the field point was again moved a short distance in the direction of the electric field; and so on. This calculation was repeated until another boundary of the electrode system was reached. The starting point was then changed, and the calculation repeated.

APPENDIX II

A. Lifetime Measurements at Saturated Vapor Pressure

T	1/T	τ	Error in τ	Computer Fit (non-QM)	Computer Fit (QM)
(°K)	($°K^{-1}$)	(sec)	(sec)	(sec)	(sec)
V_g = - 40 volts; speed at 60 rpm					
1.6796	0.5954	11.1	±0.4	11.7	11.7
1.6785	0.5958	10.8	0.7	12.4	12.3
1.6715	0.5983	17.5	0.7	17.4	17.4
1.6659	0.6003	22.8	0.6	22.9	22.9
1.6610	0.6020	29.5	0.8	28.8	28.8
1.6602	0.6023	31.0	0.7	30.0	30.0
1.6545	0.6044	39.5	0.8	39.8	39.8
1.6489	0.6065	52.5	1.0	52.6	52.7
1.6455	0.6077	62.2	1.5	61.7	61.7
1.6350	0.6116	105	2	103	103
1.6347	0.6117	103	3	104	104
1.6286	0.6140	143	4	140	140
1.6130	0.6200	300	5	302	302
1.6044	0.6233	455	5	456	456
1.5977	0.6259	625	20	630	630
1.5897	0.6290	920	20	922	921
V_g = - 40 volts; different rotation speeds					
1.6350	0.6116	102	2	33.9 rpm	
1.6350	0.6116	107	3	102 rpm	
V_g = - 80 volts; 60 rpm					
1.6715	0.5983	11.4	0.5		
1.6528	0.6050	31.3	1		
1.6355	0.6114	71	1		
1.6314	0.6130	90	2		
1.6170	0.6184	167	3		
1.5963	0.6264	470	10		

T (°K)	1/T (°K^{-1})	τ (sec)	Error in τ (sec)
V_g = - 20 volts; 60 rpm			
1.6792	0.5955	16.1	±1
1.6592	0.6927	42	1
1.6398	0.6098	107	5
1.6239	0.6158	230	5
1.6074	0.6221	485	10
V_g = - 10 volts; 60 rpm			
1.6490	0.6064	81	2
1.6355	0.6114	157	3
V_g = - 5.0 volts; 60 rpm			
1.6490	0.6064	98	3
1.6355	0.6114	187	5
V_g = - 1.0 volts; 60 rpm			
1.6490	0.6064	148	8

B. Least Squares Fit to Data

We wish to perform a least-squares fit of Equation (66) in Chapter IV to the data tabulated in this Appendix (V_g = - 40 volts). The two adjustable parameters are f(R) and F_o. This equation can be expressed in the following way

$$\text{lifetime} = g[F_o, f(R), T_k]$$

where the T_k are the temperatures at which the sixteen lifetime measurements were taken. Let τ_k be the corresponding lifetime measurements at T_k. We define δ_k to be

$$\delta_k = \tau_k - g[F_o, f(R), T_k]$$

where k = 1,2,.....16. The quantity we wish to minimize is

$$S = \sum_{k=1}^{16} \delta_k^2 .$$

However, since the various τ_k are not equally precise, the above sum should be weighted according to the accuracy of each data point. Let E_k be the error for each τ_k, and let W_k be the corresponding weight. We define

$$W_k = (E_k)^{-2}.$$

Thus S becomes

$$S = \sum_{k=1}^{16} W_k \delta_k^2 .$$

The equation for the lifetime is non-linear in the parameter f(R). The proper procedures for linearizing this equation and carrying out the least-squares analysis are discussed in Chapter 16 of Shchigolev's book.[98] A versatile computer program which could carry out these procedures, written by Dr. R. Stryk for his Ph.D. thesis, was available.[99] In this program a series of corrections to the values of f(R) and F_o are calculated repeatedly until S reaches a minimum. The minimum of S is defined to be that value of f(R) and F_o to which a further correction would change S by less than 1%. The mean square errors of f(R) and F_o are also calculated and can be represented by

$$(\delta x)^2 = h(x)\frac{S}{16 - 2}$$

where δx is the root-mean-square error in a parameter x, h(x) is a weighting factor dependent upon the partial derivatives of g with respect to all the parameters, and 16 - 2 = 14 is the number of degrees of freedom.

The results of this fit are

$$f(R) = 507.4 \pm 1.9\,^{\circ}K\ cm^3 gm^{-1},$$

$$F_o = (1.78 \pm 0.25) \times 10^{-13} sec\ cm^3 gm^{-1},$$

and $S = 12.1$

The computed values of τ from Equation (66) using these values of the parameters are tabulated with the data in Section A of this Appendix (see column "Computer Fit non-QM").

If we apply the chi-squared test, the probability for 14 degrees of freedom that χ^2 exceeds S = 12.1 is approximately 60%[100], a somewhat marginal level of confidence for the fit of Equation (66) to the data. However, the 10.8-second lifetime measurement is rather suspect. If this measurement is discarded, the probability that χ^2 exceeds S = 7.3 for 13 degrees of freedom becomes 90%. Until more accurate measurements of the lifetime are made around 10 seconds, this 10.8-second measurement should be kept.

APPENDIX III

Quantum-Mechanical Correction for a Narrow Well

As a first order correction to the lifetime, quantum-mechanical corrections to f_o in Equation (50) in Chapter II are considered. We are not considering possible quantum-mechanical corrections to the original Fokker-Planck equation. We start with Equation (50):

$$N_o = f_o \int^{\infty} e^{-\frac{M\omega_o^2 r^2}{2kT}} 2\pi r dr.$$

We let

$$V(r) = \tfrac{1}{2} M\omega_o^2 r^2.$$

We wish to include in the integral for N_o integration over all moments of the system. In deriving the Smoluchowski equation from the Fokker-Planck equation, Chandrasekhar made the following approximation

$$f(\vec{r},\vec{p}) \approx \left[\frac{1}{2\pi MkT}\right]^{\frac{3}{2}} e^{-\frac{p^2}{2MkT}} f(\vec{r})$$

which is valid for the case where the time intervals of interest are long compared to β^{-1}.[101] It follows that

$$f(r) = \iiint f(\vec{r},\vec{p}) d^3p.$$

Thus we may express N_o in the form

$$N_o = \frac{f_o}{2\pi MkT} \iiint e^{-\frac{p^2}{2MkT} - \frac{V(r)}{kT}} 2\pi r dr dp dp d\theta.$$

Therefore,

$$N_o = \frac{f_o}{2\pi MkT} \iiint e^{-\frac{E(S.H.O.)}{kT}} d^2r d^2p$$

where E(S.H.O.) is the total energy of a two-dimensional harmonic oscillator. In the quantum-mechanical limit we obtain

$$N_o = \frac{f_o}{2\pi MkT}(2\pi\hbar)^2 \sum_n e^{-\frac{E_n(S.H.O.)}{kT}} .$$

For a two-dimensional simple harmonic oscillator we have

$$E_n(S.H.O.) = \hbar\omega_o(n_x + n_y + 1)$$

where n_x and n_y are quantum numbers for one-dimensional simple harmonic oscillators in the x and y directions. Thus

$$N_o = \frac{f_o(2\pi\hbar)^2}{2\pi MkT} e^{-\frac{\hbar\omega_o}{kT}} \sum_{n_x=0}^{\infty} e^{-\frac{\hbar\omega_o n_x}{kT}} \sum_{n_y=0}^{\infty} e^{-\frac{\hbar\omega_o n_y}{kT}} .$$

This reduces to

$$N_o = \frac{f_o 2\pi kT}{\omega_o^2} \left[\frac{\frac{\hbar\omega_o}{kT}}{1 - e^{-\frac{\hbar\omega_o}{kT}}}\right]^2 e^{-\frac{\hbar\omega_o}{kT}} .$$

The above equation which relates N_o to f_o replaces Equation (51). The final result is Equation (76).

The least-squares fit of Equation (77), which exhibits the temperature dependence of the quantum-mechanical correction,

to the - 40-volt data has been performed for various values of $\frac{\hbar\omega_o}{kT}$. They are tabulated below:

θ_o' (°K)	F_o $(\frac{\text{sec cm}^3}{\text{gm}})$	f(R) $(\frac{\text{°K cm}^3}{\text{gm}})$	S	R (Å)
2.1	$(1.88\pm0.26)\times10^{-13}$	509.5±1.9	12.1	19.6±0.6
4.1	(2.01±0.28) "	513.8 "	12.0	19.7 "
6.1	(2.31±0.32) "	519.8 "	11.8	19.8 "
8.1	(2.87±0.39) "	526.7 "	11.6	20.0 "
10.1	(3.83±0.52) "	534.1 "	11.5	20.2 "
12.1	(5.45±0.74) "	541.5 "	11.4	20.4 "
14.1	(8.15±1.1) "	549.0 1.8	11.2	20.6 "
16.1	(12.6±1.7) "	556.6 "	11.1	20.8 "
18.1	(20.3±2.7) "	564.1 "	11.0	21.0 "
20.1	(33.2±4.4) "	571.7 "	10.9	21.2 "
22.1	(55.7±7.4) "	579.2 "	10.7	21.4 "

A series of computations with shorter intervals for θ_o' were made in the range $7.0 \leq \theta_o' \leq 8.0$°K. In this way the optimum value $\theta_o' = 7.6$°K was found, which is discussed in Chapter IV. The calculated values of τ are compared with the data for $\theta_o' = 7.6$°K in Appendix IIA (see column "Computer Fit QM"). For this value of θ_o', S = 11.7. Thus the fit of the quantum-mechanical equation to the data is really not much better than the fit of the classical equation where S = 12.1.

APPENDIX IV

A. Lifetime Measurements as a Function of Temperature and Pressure

V_g = - 40 volts; rotation frequency = 60 rpm

P	T	Error in T	τ	Error in τ	$\frac{d\ln(\tau)}{d(1/T)}$
(atm)	(°K)	($\times 10^{-4}$°K)	(sec)	(sec)	(°K)
0.997	1.5992	±1	27.5	±1	116±1
±0.002	1.5795	"	71	1	
	1.5595	"	182	4	
	1.5390	"	470	9	
1.995	1.5595	"	20.5	1	107±1
±0.002	1.5390	"	51.0	1	
	1.5203	"	122	3	
	1.4991	"	330	6	
3.00	1.5208	"	19.6	0.8	99±1
±0.03	1.4998	"	55	2	
	1.4799	"	131	2	
	1.4588	"	326	3	
4.00	1.4793	"	26	1	93±2
±0.03	1.4584	"	65	1	
	1.4399	"	147	2	
	1.4185	"	380	7	
5.00	1.4474	"	30.5	1	84±1
±0.03	1.4349	"	51	3	
	1.4240	"	77.5	1	
	1.4145	"	115	2	
	1.4042	"	181	2	
	1.3941	"	290	5	
6.00	1.4315	"	21	1	79.5±1
±0.03	1.4188	"	34.5	1	
	1.4078	"	51.5	1	
	1.3993	"	72	2	
	1.3880	"	114	2	
	1.3795	"	160	3	
	1.3675	"	277	5	
	1.3594	"	390	5	

P	T	Error in T	τ	Error in τ	$\frac{d\ln(\tau)}{d(1/T)}$
(atm)	(°K)	($\times 10^{-4}$°K)	(sec)	(sec)	(°K)
8.00	1.3739	±3	26	±2	75.5±1
±0.03	1.3542	1	58	2	
	1.3346	"	137	2	
	1.3140	2	320	5	
10.00	1.3339	1	23.5	1	73±1
±0.03	1.3143	2	54	2	
	1.2943	"	128	2	
	1.2753	"	285	5	
12.00	1.2936	"	26.5	1	70±1
±0.03	1.2749	"	57.5	1	
	1.2551	"	142	3	
	1.2353	"	325	5	
14.00	1.2579	"	26.0	1	68.5±1
±0.03	1.2384	"	62.5	1	
	1.2192	"	150	2	
	1.2012	"	345	7	
16.0	1.2355	"	17.3	0.5	66.5±1
±0.1	1.2151	"	43	1	
	1.1952	3	107	3	
	1.1747	"	285	5	
18.0	1.1996	2	23.5	1	65±1
±0.1	1.1786	3	65	2	
	1.1590	"	165	5	
	1.1383	"	455	10	
20.0	1.1713	"	27	1	62±1
±0.1	1.1487	"	82	4	
	1.1286	4	198	4	
	1.1090	"	530	10	
22.0	1.1484	5	22	1	61±1
±0.1	1.1283	4	60.5	1	
	1.1092	"	148	3	
	1.0946	"	310	6	
24.0	1.1283	"	19.5	1	57±3
±0.1	1.1071	"	56	2	
	1.0942	"	90	3	

P	T	Error in T	τ	Error in	$\frac{d\ln(\tau)}{d(1/T)}$
(atm)	(°K)	($\times 10^{-4}$°K)	(sec)	(sec)	(°K)
On solidification curve:					
25.1	1.1185	±4	18.5	±1	54±3
±0.1	1.1139	"	23.5	1	
	1.1041	"	34	2	
	1.0950	"	52	1	

Thermomolecular pressure corrections have been taken into account for the temperatures shown. Errors in $\frac{d\ln(\tau)}{d(1/T)}$ are only approximate.

B. Curves of Constant Lifetime in the P-T Plane

	20 sec	85 sec	350 sec
P	1/T	1/T	1/T
(atm)	($°K^{-1}$)	($°K^{-1}$)	($°K^{-1}$)
0.0	0.5990	0.6090	0.6212
1.0	0.6225	0.6348	0.6472
2.0	0.6401	0.6544	0.6677
3.0	0.6570	0.6717	0.6858
4.0	0.6730	0.6885	0.7037
5.0	0.6860	0.7030	0.7198
6.0	0.6984	0.7166	0.7343
8.0	0.7242	0.7433	0.7621
10.0	0.7473	0.7670	0.7867
12.0	0.7694	0.7900	0.8103
14.0	0.7912	0.8122	0.8327
16.0	0.8114	0.8331	0.8545
18.0	0.8299	0.8525	0.8745
20.0	0.8482	0.8718	0.8949
22.0	0.8687	0.8924	0.9158
24.0	0.8860	0.9114	
25.1	0.8949		

APPENDIX V

Calculation of Superfluid Density under Pressure

The following formula was used in determining $\rho_n(P,T)$:

$$\rho_n(P,T) = \rho\left[1 + \frac{U_{II}C_V}{TS^2}\right]^{-1} .$$

The thermodynamic quantities contained in this formula were obtained from:

ρ : Boghosian and Meyer[102]

Elwell and Meyer[103]

U_{II}: Mauer and Herlin[104]

C_V: Lounasmaa[105]

S : Van den Meijdenberg *et al.*[106]

The thermodynamic data were interpolated graphically . The normal fluid density was calculated at 0.05°K intervals between 1.20 and 1.65°K at the same pressures that the lifetimes were measured. Then $\ln\rho_n$ vs. 1/T was plotted at constant pressure. (According to the Landau model, $\rho_n \propto e^{-\frac{\Delta}{T}}$.) At all pressures the data fell reasonably well on straight lines. For 1.3°K and below the ρ_n calculations of Boghosian and Meyer were used (they used the same formula as we). In the region of overlap our calculations of ρ_n and those of Boghosian and Meyer agree reasonably well. The values of ρ_n along the curves of constant lifetime were interpolated from the $\ln\rho_n$ vs. 1/T plots. The value of ρ_s along the curves

of constant lifetime is tabulated below.

	20 sec		85 sec		350 sec	
P (atm)	1/T ($^\circ K^{-1}$)	ρ_s ($\frac{gm}{cm^3}$)	1/T ($^\circ K^{-1}$)	ρ_s ($\frac{gm}{cm^3}$)	1/T ($^\circ K^{-1}$)	ρ_s ($\frac{gm}{cm^3}$)
0	0.5990	0.1152	0.6090	0.1180	0.6212	0.1208
1	0.6225	0.1222	0.6348	0.1252	0.6472	0.1276
2	0.6401	0.1273	0.6544	0.1296	0.6677	0.1316
3	0.6570	0.1308	0.6717	0.1329	0.6858	0.1348
4	0.6730	0.1338	0.6885	0.1360	0.7037	0.1379
5	0.6860	0.1361	0.7030	0.1383	0.7198	0.1402
6	0.6984	0.1385	0.7166	0.1406	0.7343	0.1424
8	0.7242	0.1427	0.7433	0.1446	0.7621	0.1463
10	0.7473	0.1461	0.7670	0.1480	0.7867	0.1495
12	0.7694	0.1492	0.7900	0.1510	0.8103	0.1524
14	0.7912	0.1520	0.8121	0.1535	0.8327	0.1549
16	0.8114	0.1545	0.8331	0.1559	0.8545	0.1573
18	0.8299	0.1567	0.8525	0.1580	0.8745	0.1594
20	0.8482	0.1587	0.8718	0.1600	0.8949	0.1614
22	0.8687	0.1607	0.8924	0.1619	0.9158	0.1632
24	0.8860	0.1621	0.9114	0.1636		

REFERENCES

1. K. R. Atkins, *Liquid Helium*(Cambridge University Press, 1959).

2. G. Careri, Director, *Proceedings of the International School of Physics "Enrico Fermi", Course XXI, Liquid Helium*(Academic Press, New York, 1963).

3. I. M. Khalatnikov, *An Introduction to the Theory of Superfluidity*, translation by P. C. Hohenberg(Benjamin, New York, 1965).

4. C. T. Lane, *Superfluid Physics*(McGraw-Hill, New York, 1962).

5. F. London, *Superfluids, Vol. II*(Wiley, New York, 1954).

6. F. London, Nature 141, 643(1938); Phys. Rev. 54, 947(1938).

7. L. Tisza, Nature 141, 913(1938); Compt. Rend. 207, 1035, 1186(1938); J. Phys. Radium 1, 165, 350(1941); Phys. Rev. 72, 838(1947); and Phys. Rev. 75, 885(1949).

8. L. Landau, Phys. Rev. 60, 357(1941); J. Phys.(U.S.S.R.) 5, 71(1941); J. Phys.(U.S.S.R.) 8, 1(1944), J. Phys. (U.S.S.R.) 11, 91(1947); and Phys. Rev. 75, 884(1949).

9. L. Onsager, Nuovo Cimento 6, Supp. 2, 249(1949).

10. R. P. Feynman in *Progress in Low Temperature Physics, Vol. I*, edited by C. J. Gorter(North-Holland, Amsterdam, 1955).

11. W. F. Vinen, Proc. Roy. Soc.(London) 260A, 218(1960).

12. S. C. Whitmore and W. Zimmermann, Jr., Phys. Rev. Letters 15, 389(1965).

13. A. L. Fetter, Phys. Rev. 138, A429(1965).

14. G. W. Rayfield and F. Reif, Phys. Rev. 136, A1194(1964).

15. G. Gamota and T. M. Sanders, Phys. Rev. Letters 15, 949(1965).

16. D. V. Osborne, Proc. Phys. Soc.(London) A63, 909(1950).

17. H. E. Hall and W. F. Vinen, Phil. Mag. 46, 546(1956).

18. A. L. Fetter, Phys. Rev. 153, 285(1967).

19. A. L. Fetter, private communication.

20. E. L. Andronikashvili and Yu. G. Mamaladze, Rev. Mod. Phys. 38, 604(1966).

21. Reference 20, p. 604.

22. G. Careri in *Progress in Low Temperature Physics*, edited by J. G. Daunt(North-Holland, Amsterdam, 1961), Vol. 3, p. 58.

23. F. Reif and L. Meyer, Phys. Rev. 119, 1164(1960).

24. *Proceedings of the IXth International Conference on Low Temperature Physics*, edited by J. G. Daunt *et al.* (Plenum Press, New York, 1965), Part A, pp. 335-363.

25. K. R. Atkins, Phys. Rev. 116, 1339(1959).

26. R. A. Ferrell, Phys. Rev. 108, 167(1957).

27. C. G. Kuper, Phys. Rev. 122, 1007(1961).

28. R. C. Clark, Phys. Letters 16, 43(1965).

29. J. Levine and T. M. Sanders, Jr., Phys. Rev. Letters 8, 195(1962); see also, J. Levine, Phys. Rev. 154, 138(1967).

30. J. Jortner, N. R. Kestner, S. A. Rice, and M. H. Cohen, J. Chem. Phys. 43, 2614(1965).

31. K. Hiroike, N. R. Kestner, S. A. Rice, and J. Jortner, J. Chem Phys. 43, 2625(1965).

32. J. A. Northby and T. M. Sanders Jr., Phys. Rev. Letters 18, 1184(1967); see also J. A. Northby, Ph.D. Thesis, University of Minnesota, 1966(unpublished).

33. R. W. La Bahn and J. Calloway, Phys. Rev. 135, A1539(1964).

34. B. Burdick, Phys. Rev. Letters 14, 11(1965).

35. Reference 30

36. K. R. Atkins and Y. Narahara, Phys. Rev. 138, A437(1965).

37. H. Lamb, *Hydrodynamics* (6th ed.; Cambridge University Press, 1932, reprinted by Dover, New York, 1945), p. 124.

38. G. Careri, W. D. McCormick, and F. Scaramuzzi, Phys. Letters 1, 61(1962).

39. R. J. Donnelly, Phys. Rev. Letters 13, 79(1965).

40. D. J. Tanner, B. E. Springett, and R. J. Donnelly in *Proceedings of the IXth International Conference on Low Temperature Physics*, edited by J. G. Daunt, *et al.* (Plenum Press, Inc., New York, 1965), p. 346.

41. B. E. Springett, D. J. Tanner, and R. J. Donnelly, Phys. Rev. Letters 14, 585(1965).

42. D. J. Tanner, Phys. Rev. 152, 121(1966).

43. R. L. Douglass, Phys. Rev. Letters 13, 79(1964).

44. Sir William Thomson, Phil. Mag.(4) 45, 343(1873).

45. Reference 37, p. 54.

46. P. E. Parks and R. J. Donnelly, Phys. Rev. Letters 16, 45(1966).

47. S. Chandrasekhar, Rev. Mod. Phys. 15, 63(1943).

48. Reference 23.

49. W. P. Pratt, Jr., M.S. Thesis, University of Minnesota, 1965(unpublished).

50. Oil Seal #553545, National Seal Div. of Federal-Mogul-Bower Bearings, Inc., Detroit, Mich.

51. Model N30VM, Graham Transmissions, Inc., Menomonee Falls, Wisc.

52. #1400 Series Gauge, U.S. Gauge, Div. of American Machine and Metals, Inc., Sellersville, Pa.

53. #A431 needle valve, Hoke, Inc., Cresskill, N.J.

54. Reference 52.

55. Microvac #212-H-10 Vacuum Pump, F. J. Stokes Co., Division of Pennsalt Chemicals Corp., Philadelphia, Pa.

56. Porcelain insulated leads, ADVAC Products, Inc., Stamford, Conn.

57. Polymer is Epibond #100A, Furane Plastics, Inc., Los Angeles, Calif.

58. Cryoresistor S/N 42, Cryocal, Inc., Riviera Beach, Florida.

59. Source consists of "microspheres" prepared by the Nuclear Products Div. of Minnesota Mining and Manufacturing Co., St. Paul, Minn.

60. Reference 49.

61. #412AR Vacuum-Tube Volt Meter, Hewlett Packard, Pasadena, Calif.

62. Use was made of D.C. amplifier in Hewlett Packard VTVM, Reference 61.

63. Model Speedomax-G, Leads and Northrup Co., Philadelphia, Pa.

64. #680 Moseley Chart Recorder, Hewlett-Packard/Moseley Div., Pasadena, Calif.

65. H. V. Malmstadt, C. G. Enke, and E. C. Toren, *Electronics for Scientists* (W. A. Benjamin, Inc., New York, 1963), p. 346.

66. Reference 65, p. 356.

67. Consolidated Vacuum Corp., Rochester, N.Y.

68. Model 1402, Duo Seal Vacuum Pump, The Welch Scientific Co., Skokie, Ill.

69. H. Wild Surveying Instruments Supply Co. Ltd., Heerbrugg/ Switzerland.

70. National Bureau of Standards, Monograph 10(1960).

71. T. R. Roberts and S. G. Sydoriak, Phys. Rev. 102, 304(1956).

72. Reference 42.

73. Reference 42.

74. Reference 20, p. 604.

75. Reference 43.

76. J. M. Reynolds, R. G. Hussey, D. P. Thibodeux, B. E. Tucker, and R. F. Folse, "The Oscillations of Cylinders and Spheres in Liquid Helium II, Tech. Doc. Report ML TDR 64-314(Louisiana State Univ., 1964); see also R. G. Hussey, B. J. Good, and J. M. Reynolds, Phys. Fluids, 10, 89(1967).

77. J. T. Tough, W. D. McCormick, and J. G. Dash, Phys. Rev. 132, 2373(1963).

78. J. G. Dash and R. D. Taylor, Phys. Rev. 105, 7(1957).

79. E. L. Andronikashvili, J. Phys. (U.S.S.R.) 10, 201(1946); Zh. Eksperim. i Teor. Fiz. 16, 780(1946); Zh. Eksperim. i Teor. Fiz. 18, 424(1948).

80. E. C. Kerr and R. D. Taylor, Ann. Phys.(N.Y.) 26, 292 (1964).

81. Reference 42.

82. Reference 42.

83. Reference 39.

84. B. E. Springett and R. J. Donnelly, Phys. Rev. Letters 17, 364(1966).

85. B. E. Springett, Phys. 155, 139(1967).

86. Reference 39.

87. Reference 85.

88. L. Meyer and F. Reif, Phys. Rev. 123, 727(1961).

89. S. Cunsolo and P. Mazzoldi, Nuovo Cimento 20, 949(1961).

90. Reference 76.

91. Reference 78.

92. Reference 46.

93. Reference 13.

94. Reference 36.

95. Reference 32.

96. W. R. Smythe, *Static and Dynamic Electricity* (McGraw-Hill Book Co., Inc., New York, 1950), p. 196.

97. M. Abramowitz and I. Stegun, *Handbook of Mathematical Functions* (N.B.S. Appl. Math Series 55, Washington, D.C., 1964), p. 378.

98. B. M. Shchigolev, *Mathematical Analysis of Observations*, translated by H. Eagle (American Elsevier Publishing Co., Inc., New York, 1965), p. 236.

99. R. A. Stryk, Ph.D. Thesis, University of Minnesota, 1967 (unpublished).

100. *Handbook of Chemistry and Physics* (47th ed.; The Chemical Rubber Co., Cleveland, 1966), p. A157.

101. Reference 47, p. 41.

102. C. Boghosian and H. Meyer, Phys. Rev. 152, 200(1966).

103. D. Elwell and H. Meyer, private communication.

104. R. D. Mauer and M. A. Herlin, Phys. Rev. 81, 444(1951).

105. O. V. Lounasmaa, Cryogenics 1, 1(1961).

106. C. J. N. Van den Meijdenberg, K. W. Taconis, and R. de Bruyn Ouboter, Physica 27, 197(1961).

ACKNOWLEDGMENTS

The author wishes to express his gratitude to the following persons:

To his thesis advisor, Prof. William Zimmermann, Jr., for his helpful advice and criticism during the execution of this experiment and the preparation of this thesis.

To his colleague, Dr. Robert Stryk, for making available his computer program for the least-squares analysis conducted in this thesis.

To his colleagues, Stephen Kral and Brian Sabo, for their assistance in the execution of this experiment.

To his wife, Sally, for constant support during his graduate study and for a critical reading of this thesis.

The support of the Air Force Office of Scientific Research and more recently of the U. S. Atomic Energy Commission is gratefully acknowledged.

The author also wishes to thank the National Aeronautics and Space Administration for a fellowship during part of his graduate studies.